INNOVATING MATERIALS IN BRIDGE CONSTRUCTION. CONTRIBUTION TO CONSTRUCTION WITH COMPOSITE FIBER-REINFORCED MATERIALS

Teză destinată obţinerii
titlului ştiinţific de doctor inginer
la
Universitatea "Politehnica" din Timişoara
în domeniul INGINERIE CIVILĂ
de către

Ing. Lucian-Attila BLAGA

Conducători ştiinţifici:
        prof.dr.ing. Radu BĂNCILĂ
        prof.dr.ing. Sergio de TRAGLIA AMANCIO-FILHO

Referenţi ştiinţifici: acad.prof.dr. Dan DUBINĂ
                dr.ing. Jorge dos SANTOS

Ziua susţinerii tezei: 07.03.2012

BUPT

Cuvânt înainte

Teza de doctorat a fost elaborată pe parcursul activităţii mele în cadrul Departamentului de Construcţii Metalice şi Mecanica Construcţiilor al Facultăţii de Construcţii din cadrul Universităţii „POLITEHNICA" din Timişoara, precum şi în cadrul departamentului Solid State Joining Processes al Helmholtz Zentrum Geesthacht – Institute of Materials Research.

Mulţumiri deosebite se cuvin conducătorului de doctorat prof.dr.ing. Radu Băncilă pentru sprijinul, îndrumarea şi vorbele înţelepte de-a lungul perioadei de doctorat. De asemenea, mulţumiri considerabile se aduc prof. dr. ing. Sergio de Traglia Amancio Filho, pentru efortul susţinut şi ajutorul acordat, cât şi pentru acceptul de a coordona în cotutelă cercetarea doctorală de faţă. Îmi exprim aprecierea şi consideraţia pentru acad. prof. dr. ing. Dan Dubină şi dr. ing. Jorge dos Santos, care mi-au făcut onoarea de a accepta numirea ca referenţi ai lucrării mele de doctorat, pentru disponibilitatea lor şi ajutorul acordat. Totodată, aş dori să îmi exprim recunoştiinţa faţă de dr. ing. Heiko Trumpf şi Fiberline Composites A/S, pentru sprijin şi mai ales pentru iniţierea în lumea construcţiilor cu materiale compozite, cât şi prof. dr. ing. Martin Mensinger şi echipei sale de la Catedra de Construcţii Metalice a Universităţii Tehnice din München pentru sfaturile lor preţioase. De asemenea le sunt recunoscător celor de la Helmholtz Zentrum Geesthacht, fără de care această cercetare nu ar fi fost posibilă şi domnişoarei Daniela Benedini Junqueira pentru suportul în cadrul experimentelor efectuate.

Le sunt recunoscător colegelor mele drd. Anamaria Butişcă, dr. Ramona Gabor şi drd. Silvia Romînu, fără de care nu aş fi reuşit să mă descurc în problemele organizatorice. Nu în ultimul rând, le mulţumesc colegilor de la Departamentul de Construcţii Metalice şi Mecanica Construcţiilor (UPT) precum şi celor de la Solid State Joining Processes (HZG) şi prietenilor mei dragi pentru că am avut de învăţat câte ceva de la fiecare. Pentru susţinerea, încrederea şi înţelegerea lor, le sunt recunoscător părinţilor mei, Maria şi Constantin, şi iubitei mele Anca.

Dedic această lucrare memoriei bunicului meu precum şi ţării mele, în speranţa unui viitor desăvârşit.

Timişoara, februarie 2012   Lucian-Attila Blaga

Rezumat:

Teza de faţă prezintă problematica unor materiale structurale moderne, polimerii armaţi cu fibră în general şi cei armaţi cu fibră de sticlă în special, cu aplicabilitate în construcţia de poduri. În introducere sunt prezentate noţiuni de bază din domeniul materialelor compozite cu exemple de structuri existente. Scopul tezei este dezvoltarea unei noi metodologii de îmbinare pentru poduri din materiale compozite, având ca studiu de caz un pod pentru situaţii de urgenţă. Se trec în revistă metodele de îmbinare existente iar apoi se detaliază o nouă tehnologie – Fricriveting (nituirea prin frecare). Nituirea prin frecare este un proces nou, dezvoltat pentru polimeri termoplastici nearmaţi. În teză este testată fezabilitatea Fricriveting pe mai multe combinaţii de nituri metalice respectiv polimeri armaţi cu fibră de sticlă. După determinarea fezabilităţii, este testat comportamentul noilor îmbinări metal-polimer armat iar ulterior un design experimental este efectuat pentru optimizarea nituirii prin frecare pentru nituri din titan şi plăci compozite din polieterimidă armată cu fibră de sticlă. Rezultatele experimentelor şi măsurătorilor validează Fricriveting ca soluţie potenţială pentru îmbinarea profilelor structurale utilizate la construcţia de poduri.

Summary

1. INTRODUCTION

1.1. General aspects of fiber reinforced polymers.

Fiber reinforced polymer (FRP) composites proved their effectiveness during the last 50 years for the aerospace-, marine- and automotive industries. In the last two decades, FRP composites emerged as a material suitable also for civil engineering applications. They made their way initially from windows and doors, through facade elements and finally being integrated as load bearing elements for buildings and bridges.

FRP composites can be produced different technological processes, to be shown in the following chapters, such as molding, pultrusion, filament winding and autoclave cure or hand lay-up. The reinforcement fiber type appoints the name of the polymer composite, for example CFRP, GFRP or AFRP for carbon-/ glass-/ aramid fiber reinforced plastics. This thesis concentrates on glass fiber reinforced polymers (GFRP) used for bridge construction.

The first GFRP composites were used in the petro-chemical industry in the late 1940's for pipelines. Their good mechanical and chemical properties, such as high strength, low weight, durability, environmental and chemical resistance supported their selection and use in several industrial branches. Until the 1970's production costs were almost prohibitive for composites, leaving only niche applications available, such as in the aerospace and military industries [1].

Production optimization through the years and the gained experience contributed to the lowering of the costs of GFRP, making it more appealing for the public sector. Today, GFRP have impacted and revolutionized many industries and markets, from marine applications, processing and manufacturing industries, medical applications, sport equipment to automotive, architectural and civil engineering applications. Figure 1.1 shows some examples of current industrial applications of FRP.

Figure 1.1 –Current applications of FRP
(a – Visby class corvette [2], wind turbines, c – translucent composite facade [4], d – IAR 111 Excelsior supersonic aircraft [75])

1.2. Glass fiber reinforced plastics in civil engineering and bridge construction

The construction sector was perhaps one of the most conservative regarding the introduction of GFRP as a new structural material, for justified reasons, such as the high fabrication costs, lack of experience and gaps in knowledge regarding material properties and structural behavior. GFRP profiles can work together or even replace classical materials such as masonry, timber, concrete, steel or aluminum but its main purpose is not to replace classical materials, but to be applied as an efficient alternative where its properties could add value for the desired structural applications. The last two decades brought important innovations and improvements in the manufacturing and assembly of FRP profiles in general, while the industry and the governments invested considerable funding in research, development, testing and demonstration projects all which contributing to the enlargement of the FRP market worldwide [2]. Figure 1.2 shows an example of one of the first successful application of fiber reinforced plastics in civil engineering

Figure 1.2 – Example of selection of FRP as structural material: pavilion of the USSR at the Osaka World Trade Fair Expo 1970 [76].

The history of FRP bridges begins in the 1980's in Asia, the first vehicular bridge using FRP being erected in China in 1982 – the Miyun Bridge, Beijing [77]. The premiere is being disputed by the 12 m long Ginzi Highway bridge in Bulgaria (Figure 1.3), built also in 1982, from glass fiber reinforced polyester beams. Today, hundreds of pedestrian and vehicular bridges worldwide contain FRP as decks, beams, trusses, rebar / concrete reinforcement rods, cables, tendons, reinforcements and panels. FRP structures shall be divided into all-FRP structures (built entirely from reinforced composites) and hybrid structures (for example steel-

FRP). An estimated number of around 300 bridges worldwide are built entirely using FRP (all-FRP structures).

Figure 1.3 – Ginzi Highway GFRP- Bridge, Bulgaria

A milestone in FRP bridges has been made with the Aberfeldy Footbridge in Scotland (Figure 1.4) built in 1992. This bridge is today regarded as the world's first major advanced composite bridge. It still remains the longest span all-FRP bridge in the world with 120 m, with a middle span of 63 m. After 20 years in use, this cable stayed bridge structure is still in good condition, being a proof of the capabilities of FRP in bridge construction [3].

Figure 1.4 – All-FRP Aberfeldy Footbridge over the River Tay

Another important all-FRP bridge is the Fiberline Bridge (Figure 1.5) in Kolding, Denmark, built in 1997. The 40 m span cable stayed structure is a remarkable example of the advantages of using GFRP for infrastructure applications. The bridge was designed with three segments. The complete installation took only 18 hours, during three consecutive nightshifts, without disturbing the train traffic.

This all-FRP bridge structure crosses over a high speed railroad which uses a 25 kV overhead power line. The entire structure, with the 18,5 m high pylon, weights a total of only 12 t [4].

Figure 1.6, 1.7 and 1.8 show other examples of all-FRP bridges worldwide. The Lleida Bridge in Spain (Figure 1.6) is a 38 m span pedestrian bridge, with an arch structure. It was built in 2004 and weights a total of 19 t. The bridge was assembled on site in three months and the installation took only three hours, without disturbance of the traffic.

Figure 1.5 – The Fiberline Bridge in Kolding, Denmark
(Image courtesy of Fiberline Composites A/S [4])

Figure 1.6 – The Lleida Bridge in Spain
(Image courtesy of Fiberline Composites A/S [4])

Another important example is that of the Pontresina Bridge in Switzerland (Figure 1.7), a lightweight FRP construction showing excellent maneuverability. This bridge is dissembled and removed from its position and later reinstalled twice a year because of rising water levels. The whole process lasts less than 2 hours, for the whole 2x12,5 m span bridge with a total weight of three tones.

But FRP are not suitable only for pedestrian bridges. It is also applicable to road bridges, as it is the case of the Sugar Grove Bridge (Figure 1.8) in Virginia, US. It is a 12 m span experimental bridge built in 2001, implementing an innovative type of FRP beam.

Figure 1.7 - The Pontresina Bridge, Switzerland
(Image courtesy of Fiberline Composites A/S [4])

Figure 1.8 – The Sugar Grove Bridge, Virginia, US
(Image courtesy of Strongwell, Bristol, Virginia, US [5])

2. MOTIVATION AND OBJECTIVES

2.1. Motivation: emergency bridges

The worldwide climate changes in the last decades, as well as the growth of potential threats, such as war and terrorism, increased the need of bridge structures, having an adequate load bearing capacity, that are simple and fast to erect and at low costs at the same time. In emergency situations (flooding, earthquakes, accidents etc), interrupted transport connections must be restored as fast as possible, in order to re-establish traffic for rescue and humanitarian missions. Emergency bridges can also be used as temporary pedestrian, road or railway bridges. Typical prefabricated bridges can be erected much faster than a cast-in-in place structure, therefore are the optimal solution for emergency hazard cases.

For example, Romania has been the scene of floods at least once a year since 2005, causing several damages and collapses of bridge structures, not to mention life losses and other direct material and property damage. Some known examples of collapsed bridges in Romania are presented in Figures 2.1 and 2.2. In some cases, the traffic was re-established just months or even years after the catastrophes because of the lack of intervention methods of the authorities [20].

Figure 2.1 – Collapsed bridge in Marginea, Suceava County, Romania (Floods, July 2008)

The extraordinary loads that can affect damage or lead to the collapse of bridges are: rising of the water flow rate, explosions, earthquakes, avalanches, high

floods, cloudburst floods, torrents, debris flow or hitting of the infrastructure by ships or other vehicles.

Emergency bridges have to respect the following specifications:

- has to be compose of as less different standardized profile types as possible
- elements must be lightweight materials and relatively small clearance and therefore able to be transported with small vehicles
- modularity; static system and span should be variable through implementing additional modules
- simple and fast assembly, even with unskilled personnel
- life cycle of the structure should be similar to that of permanent bridges

The modular elements of emergency bridges are traditionally produced out of metallic alloys, such as steel (e.g. the D-Bridge and the Bailey bridge [79]. Recently, Sedlacek, Oppe and Trumpf have reported the use of fiber reinforced plastics to design emergencies truss bridges [78]. Although this structural concept resulted in a very flexible and lightweight bridge in comparison with metallic structures, there are still some technical limitations to be improved to make this design more competitive. Sedlacek and Trumpf have applied a hybrid metallic bolting/adhesive bonding approach to connect FRP-profiles with the addition of metallic shoe [25]. Although their selection of the hybrid joining technologies could accomplish the load requirements, assembly time was increased due to the complex preparation of the joining partners (i.e. drilling of holes for bolts and surface preparation for adhesive placement) and the long adhesive curing time (about 24hs). In case of emergency situations time is a crucial factor to save lives. Therefore emergency bridges should be fabricated, assembled and launched within very short time.

Figure 2.2 – Collapsed railway bridge near Giurgiu, Romania
(Floods, 2008)

2.2 Objectives of the thesis

Considering the recent developments in design of FRP emergency bridges reported in the literature, and the identified need to reduce fabrication and assembly time, without compromising mechanical performance, the scope of the thesis was to develop an innovative joining solution for GFRP structural profiles for truss bridges. Friction Riveting (FricRiveting), a new and fast mechanical fastening technology developed at Helmholtz-Zentrum Geestacht, Germany [80] was selected for this purpose. The technique presents a more efficient and material tailored joining solution, with regard of the properties of the polymers.

This work had the objective to evaluate the feasibility of the innovative FricRiveting technology for GFRP in bridge structures. For that, experimental research was conducted on different types of material combinations, including thermoplastic and thermoset GFRP laminates, aluminum junction plates and aluminum and titanium rivets. Design of experiments and statistical analysis were applied to optimize and understand the joining process in terms of joint mechanical strength and macrostructure, with the purpose of adapting the technology on a case study of a lightweight composite GFRP bridge. Finite element structural analysis was used to analyze the bridge structure aiming at the definition of geometry of the metallic/GFRP connectors produced by FricRiveting.

3. STATE OF THE ART

3.1. Fiber reinforced composites

In fact, the majority of the biological systems are built of polymers, performing mechanical functions (for example wood, bone, cartilage, leather) or containing chemical reactions (leaves, cells etc.). Wood and bone for example are natural composites, consisting of fibers embedded in a matrix of polymer [70]. By definition, composite materials are macroscopic combinations of two or more distinct materials being separated by a discrete and recognizable interface [6], as schematically shown in Figure 3.1. The properties of a composite material depend on the properties of each constituent material of the combination, they are heterogeneous and their properties cannot be achieved by one of their components individually. The most common natural composite material is wood. Nevertheless, the focus of this work is on synthetic fibrous polymeric composites.
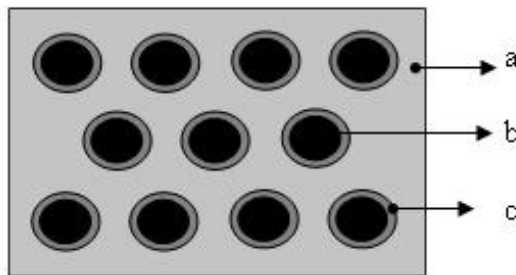
Figure 3.1 – The phases of a composite system:
a – continue phase (matrix) ; b – reinforcement (disperse phase)
c – interface [2]

3.1.1. Reinforcements

Regardless of the fibre material, reinforcements can be of multiple types: long, short aligned, woven fabric, mat, chopped or particulate [2]. This thesis discusses only the long continuous type of reinforcement. As shortly mentioned in Section 1.1, fibre reinforcement material may vary from glass fiber, carbon fiber, aramid or even nano-fibres. The main function of the fibre reinforcements in the composite material is to carry the loads and provide stiffness and strength.

The choice and orientation of reinforcement is highly important for the properties of the composite [32]; therefore, many combinations of various types of roving, weaves and mats are available and recommended, depending on the producer and on the customer's necessities [4]. Figures 3.2 and 3.3 show types of roving and mats available for continuous fiber reinforced polymer laminates. Such

composite materials are usually fabricated via ply-by-ply lay-up technique, resulting in a laminar profile (i.e. laminates) [6].

unidirectional   spun   mock

Figure 3.2 – Types of roving used in polymeric composites [4]
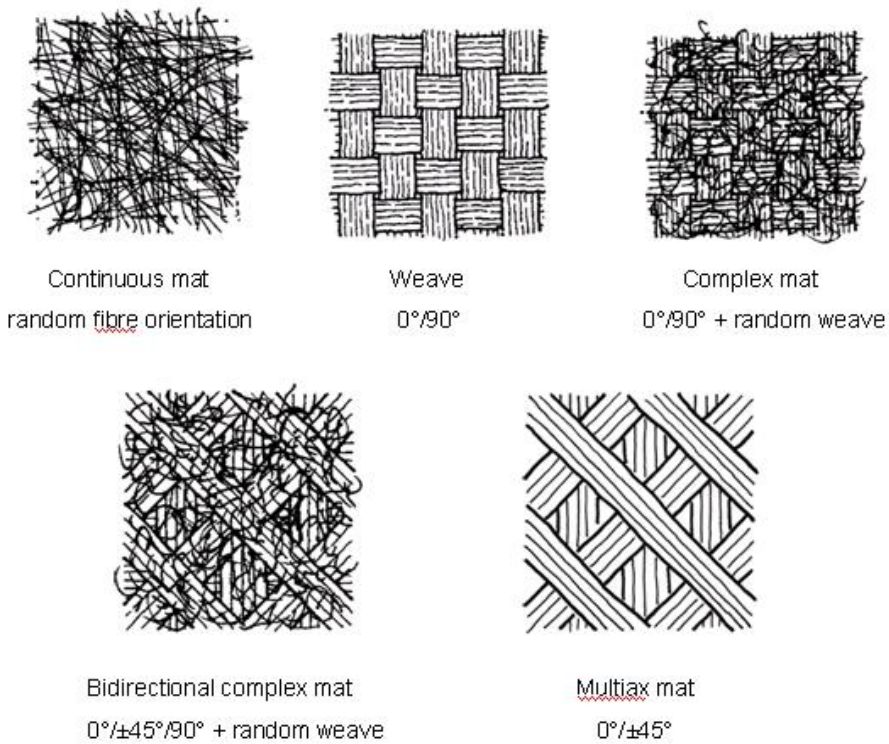
Continuous mat   Weave   Complex mat

random fibre orientation   0°/90°   0°/90° + random weave

Bidirectional complex mat   Multiax mat

0°/±45°/90° + random weave   0°/±45°

Figure 3.3 – Types of mat applied in polymeric composite [4].

The most common general purpose glass fibre used in the industry is E-glass (electrical grade glass). Starting from the initial use as insulator for electrical wiring, it was soon found out to have excellent fiber forming capabilities. E-glass is a low alkali glass, consisting of silicon dioxide (approx. 54%), aluminium trioxide

(14%), calcium oxide + magnesium oxide (22%), boron trioxide (10%), sodium oxide and potassium oxide (2%). The key properties of E-glass are [7]:

- relatively low cost
- high strength
- high stiffness
- low density
- heat and chemical resistance
- good electrical insulation

Another available type of glass fibers would be the much stiffer S-glass. S-glass has a tensile strength more than two times higher than that of E-glass, with higher stiffness and at a lower density; it is also far more difficult to process than E-glass, resulting in higher production costs. Consequently is only an option in more extreme cases, where improved mechanical performance is required under severe conditions. Other special purpose glass fibres are D-glass, A-glass, ECR-glass, ultrapure silica fibres and trilobal fibres [8]

3.1.2. Polymeric matrix

The polymeric resin compound in the reinforced composite is known as the matrix of the composite. The polymeric matrices have the following main functions in the composite [6]:

- provide interlaminar shear strength between the fibers
- even load distribution between the fibres
- protect reinforcement against abrasion
- provide resistance to fire, moisture and chemicals
- determine the overall service temperature of the composite
- keep the fiber reinforcements into the proper position
- provide resistance to crack propagation

The polymer composite matrices are divided into two types: thermoset and thermoplastic. Their main differences are addressed in the following sections.

3.1.2. a. Thermosetting polymeric matrices

In thermosetting polymers, generally referred to as thermosets, a chemical reaction cross links the material structure (i.e. the molecular chains) so that it cannot return to liquid form [9]. This means that, once cured, they cannot be re-melted or reprocessed. Thermosets are produced by mixing two components, a resin and a hardener, which react and harden at a specific temperature [9]. The very large number of available resin formulations, curing agents, fillers and other additives result in a large diversity of possible composite properties. Depending on the aimed properties, resins vary from general purpose, chemically resistant or heat resistant resins [6].

Thermosets undergo an irreversible chemical reaction, cross-linking or polymerization (the formation of strong chemical bonds between the polymeric chains, reducing chain mobility). The processing of thermosetting polymers consists of [11]:

1. resin formulation to a liquid state
2. shaping into the desired configuration through flowing the liquid into a cavity

3. heating the liquid in order to cause the chemical reaction until it reaches rigidity
4. Removing the resulting rigid part from the cavity.

Most common used thermosets are epoxy, polyester, vinyl ester and phenol. For the composite material, thermosets provide high rigidity and strength, electrical and chemical resistance, but are more brittle than thermoplastic polymers [6].

Epoxy resins

Epoxy resins are extreme versatile resin systems that can be formulated in order to meet a wide range of specific processing and performance requirements. Epoxy resins are used as adhesives, potting and moulding compounds [10]. Their main advantages are:
- very good adhesion to the fibres increasing compatibility and optimizing load transfer to reinforcements
- relatively low cure shrinkage
- high dimensional stability
- no volatile by-products of the curing reaction
- resistance to hostile environments, both humid or non-humid

Polyester resins

Polyester resins can be produced generally through self-condensation of hydroxyl acids, condensation of polyhydroxy compounds with polybasic acids or ester exchange [12]. Esters are formulated by the reaction of an organic acid with an alcohol. Thermosetting polyesters can be produced from phthalic or maleic anhydrides and polyfunctional alcohols with catalyzation with free radical-producing peroxides [13]. Most of polyesther matrices used in FRPs are thermosets while thermoplastic polyester matrices are less used.

Vinyl ester resins

Vinyl esters are unsaturated resins made from the reaction of unsaturated carboxylic acids with an epoxy [9]. Figure 1.13 shows the typical structure of a vinyl ester. There are two types of vinyl esters. The general purpose vinyl ester has good mechanical properties, heat and chemical resistance. The heat resistant vinyl ester displays the same properties as the general purpose material but offers higher thermal resistance [6].

Phenol resins

The two-stage phenolic-resin also known as Novolac, is the most widely used grade, because of its good property processability; this resin system can be moulded by almost all thermosetting moulding techniques. It is also one of the most cost effective compounds used to produce FRP parts [13].

3.1.2. b. Thermoplastic polymeric matrices

Thermoplastic matrix materials are generally tougher than most thermosets and have similar or better performances at high temperatures or under humid conditions [6]. They offer good ductility and toughness but lower stiffness, creep resistance and strengths. Thermoplastics are made by adding together sub-units to form long chains ("polymerising monomers") [70].

Thermoplastics are usually not cross-linked. This allows polymeric chains to gain mobility at heating, leading to melting. When molten, thermoplastics are highly viscous fluids. The viscous fluid can be processed in different shapes by using plastics processing techniques [14], such as injection moulding and extrusion [14]. Due to their ability to melt, thermoplastics can be recycled. Nevertheless, there are some few thermoplastics showing a trend of slightly cross-linking under higher temperature or that have isolated cross-linked chains, supplying therefore an elastic effect to thermoplastic elastomers.

.Figure 3.4 shows a schematic view with the main differences between thermosetting of thermoplastic polymers. Commonly used engineering thermoplastics are: polyamides ("nylons"), polycarbonate (PC), thermoplastic polyester, polyetherimide (PEI) and polyethylene (PE) [12].
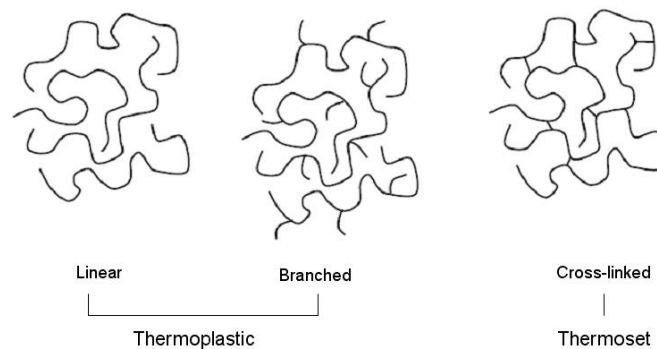
Figure 3.4 – Schematic representation of polymer structures [12]

Polyamide ("Nylon")

Polyamide, also known as nylon, is a semi-crystalline polymer with a high elastic modulus and strength, good impact properties and abrasion resistance. There is a large number of nylon grades available in the market. The number of carbon atoms in the polymeric chains determines the properties of the polyamide, such as mechanical resistance and thermal stability. Nylons are identified with a group of two numbers. Therefore, we have for example nylon 6, nylon 12, nylon 6/6, nylon 6/12 etc [14]. Polyamides are hygroscopic materials. Absorption of water reduces strength and creep resistance of nylons; therefore they are not normally used in humid environments.

Polycarbonate

Polycarbonate (PC) has very good properties, offering a good combination of toughness, high strength and high heat-deflection temperatures. Therefore it is one of the most used engineering thermoplastics. The structure of PC with its carbonate and bisphenolic chain groups contributes to its intrinsic properties. PC has a low density (around 1.20 g/cm³) but also presents some limitations, such as the need for drying or elevated processing temperatures and limited resistance to organic solvents, for instance benzene or toluene [14].

Thermoplastic polyester resin

Thermoplastic polyesters can have their properties tailored by using different combinations of diacids (phthalic anhydride, isophthalic acid etc) and glycols (ethylene glycol, propylene glycol etc). For example, from the reaction of terephthalic acid with ethylene glycol results the well known PET (polyethylene terephthalate used to produce soft drink bottles. Resins produced from isophthalic acid are characterized by higher strengths, toughness and heat resistance [12].

Polyetherimide

Polyetherimide (PEI) was introduced in 1982 by General Electric, under the commercial name of ULTEM. PEI, an amorphous thermoplastic, is characterized by high tensile strength, high impact strength and rigidity, creep resistance and high-temperature resistance. This thermoplastic is prepared by condensation polymerization of diamines and dianhydrides. PEI has a glass transition temperature of 215°C and processing temperatures up to 425°C. Taking into consideration its excellent properties, it is used in a large variety of applications from electrical applications to aerospace parts [14].

Polyethylene

Polyethylene (PE) is the highest-volume polymer available [12]. Its main advantages are high toughness, ductility, increased chemical resistance, low permeability and water absorption, high versatility and ease of processing. PE is limited by its low modulus, yield stress and melting point [14]. Polyethylene is also the commonest of thermoplastics [70].

3.1.3. General properties of glass fiber reinforced plastics

It is difficult to list up the entire mechanical, physical and chemical properties of GFRP in general. As it was shown in the previous chapters, composite properties may vary related to type and percent of reinforcement, resin or additives.

That is in fact one of the main advantages of composites, the incredibly wide range of potential combinations of constituent materials, all according to the specific needs of the designers, engineers and costumers. For example, E-glass fibres may be placed in a matrix of PEI for building a pedestrian bridge. In the case of a bridge located in a highly corrosive medium (for example coastal areas or a footbridge in a salt mine), then a PE additive could be used in the matrix on one hand. On the other hand, a phenolic additive can be selected in order to increase the chemical resistance, where an increased risk of fire is present [12].

GFRP composites for structural applications offer the following advantages [1].

- Low density (approx. 20% of steel)
- Optimal weight-to-strength ratio (specific strength)
- Electrical and thermal insulation
- Good noise and vibration absorption
- No electrochemical corrosion
- Electromagnetic transparency
- Easy machining and surface treatment
- High energy efficiency (in manufacturing)
- Minimal maintenance
- Fast installation
- Low environmental impact
- Sustainability

Regarding the above mentioned environmental impact of GFRP, recent studies by R.A. Daniel compared different structural materials for a pedestrian bridge in terms of energy efficiency and pollution [81]. Energy consumption on delivery and during maintenance, as well as water and air pollution were investigated for composites, structural steel, stainless steel, aluminum and reinforced concrete. It has been shown that building a GFRP bridge, would consume less than half of the energy consumed for the other classical materials while the volumes of air pollution were at a comparable level to steel; on the other hand, the critical water volumes polluted placed again GFRP composites as the most environmental friendly solution [81].

Tables 3.1 and 3.2 show selected material properties for two different GFRP composites. Composite laminates have an anisotropic character, so properties will be referred to as parallel or perpendicular (0° and 90°) to the main weave fiber direction (also known as warp and weft directions, respectively [6]).

The first example is a GFRP with a polyester based matrix, produced by Fiberline Composites A/S, used for GFRP structural profiles, especially in bridges. The second example consists of a GFRP-PEI composite normally used in transportation structural applications. By comparing both tables, it is possible to observe how highly the type of composite constituent materials can influence the final mechanical properties of composites laminates.

Table 1.1

Material parameters of a polyester matrix GFRP* [3]

Characteristic values	0°	90°	unit
Density	1,9		g/cm³
Elasticity modulus	23000-28000	8500	MPa
Shear modulus	3000	3000	MPa
Poisson's ratio	0,23	0,09	[--]
Bending strength	240	100	MPa
Tensile strength	240	50	MPa
Compressive strength	240	70	MPa
Pin-bearing strength	150	70	MPa
Shear strength	25	25	MPa

*) Material values stated are valid in dry condition, for temperatures ranging from -20°C to 60°C

Table 3.2

Material parameters of a PEI matrix GFRP* [15]

Characteristic values	warp	Weft	unit
Density	1,91		g/cm³
Elasticity modulus	26000	24000	MPa
Shear modulus	5000	5000	MPa
Poisson's ratio	0,36	0,36	[--]
Bending strength	669	585	MPa
Tensile strength	484	445	MPa
Compressive strength	727	676	MPa
Shear strength	130	130	MPa

*) Material values at 23°C and 50% relative humidity

3.1.4. Manufacturing of glass fiber reinforced plastics

There are different production processes available for GFRP, depending on the resin type, reinforcement and desired fibre placement. The main production process for GFRPs (schematically shown in Figure 3.5) are [6]:

- Transfer moulding
- Injection moulding
- Compression moulding
- Hand lay-up
- Vacuum infusion
- Filament winding
- Autoclave cure
- Press cure
- Oven cure
- Pultrusion

The following subchapters list some of the most used manufacturing processes for different types of composites. Later on, the experimental part of the thesis focuses mainly on pultruded polyester matrix GFRP profiles for bridge construction and compression moulded PEI matrix GFRP.
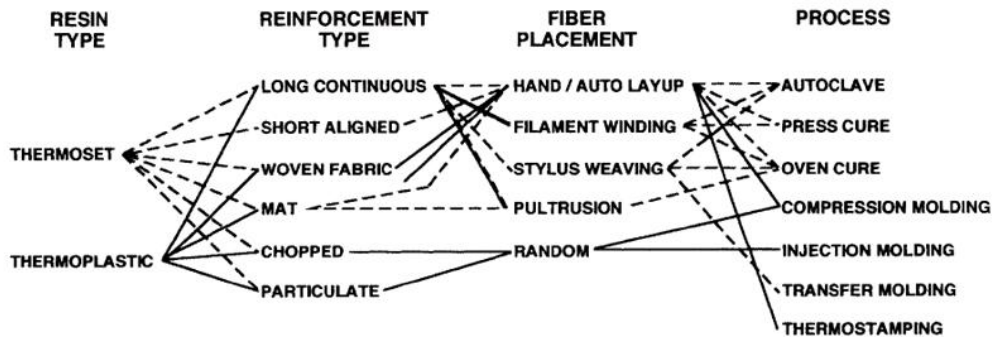
Figure 3.5 – Composite constituent materials and available manufacturing routes [6]

3.1.4. a. Pultrusion

Pultrusion is an automatic continuous process for manufacturing GFRP. It was patented in the early 1950's by W. Brandt Goldsworthy [82] and is somehow related to extrusion, used generally for manufacturing metallic or thermoplastic profiles. The pultrusion process consists of fibres being pulled through a pre-heated shaping tool, where they are infused with resins and additives through injection; in this phase pultruded profiles with constant cross sections are formed, finally being cured and cut to the desired lengths. The pultruded composite material is literally pulled through a precision die configured to the desired shape, hence the name of the process. Figure 3.6 presents the schematic overview of the process. The material is pulled at a controlled rate, in order to assure complete and homogenous curing [6].
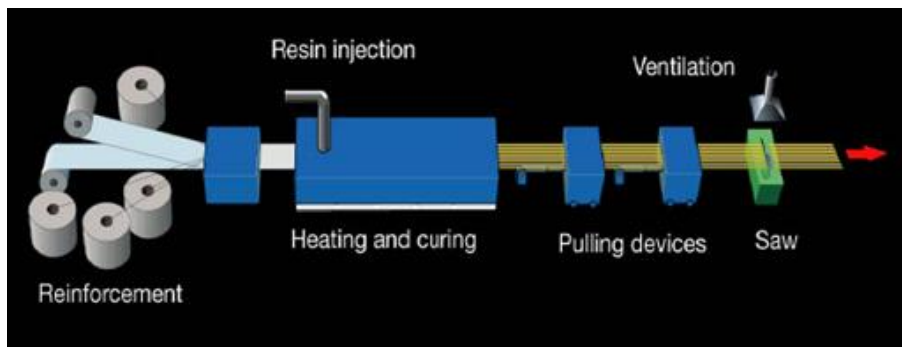
Figure 3.6 – Putrusion process
(Image courtesy of Fiberline Composites A/S [4])

The original process of pulling a bundle of unidirectional fibres through a curing die suffered many modifications and improvements throghout the years. Today, the process of adding strips or fabrics and fiber mats to the pultrusion process is a common procedure in order to provide transverse and shear strengths for more complex pultruded cross sections[16].

Generally, pultrusion offers the advantage of a high design flexibility, in terms of geometry, material properties (through the large variety of matrix and

aditives) and design. The limitations are mostly related to the dimensions of the pultrusion equipments (limited widhts and heights of the profiles) [16].

Applications of pultruded GFRP profiles may include: civil engineering (structural profiles, gratings, handrails, siderails, planks, walkways, bridge decks etc), automotive applications (panneling), electrical equipment (ducts), aircraft structures, wind turbine manufacturing, among others [4].

The properties of pultruded structural profiles are described by the European Standard EN 13706 [17], which specifies the minimum requirements for quality, tolerances, strength, stiffness and surface of structural profiles:

- EN 13706-1: selection of materials, surface treatment and labelling / designation;
- EN 13706-2: testing methods and tollerances.
- EN 13706-3: minimum values for material properties

The European standard divides pultruded structural materials into two classes,: the E17f for normal safety quality requirements and the E23 for severe safety quality requirements. Table 3.3 summarizes the main differences between these composite classes.

Table 3.3

Minimum requirements for characteristic properties of pultruded GFRP profiles [17]

Property	Test method	Minimum requirement E17	Minimum requirement E23	units
Elasticity modulus	Annex D, EN 13706-2:2002	17	23	GPa
Tensile strength - longitudinal	EN ISO 527-4	170	240	MPa
Tensile strength - transversal	EN ISO 527-4	30	50	MPa
Pin bearing strength – longitudinal	Annex E, EN 13706-2:2002	90	150	MPa
Pin bearing strength – transversal	Annex E, EN 13706-2:2002	50	70	MPa
Bending strength – longitudinal	EN ISO 14125	170	240	MPa
Bending strength – transversal	EN ISO 14125	70	100	MPa
Shear strength	EN ISO 14130	15	25	MPa

3.1.4. b. Hand lay-up

In the case of larger composite parts or when more complex geometries are needed, the hand-lay up process might be an option. The fibreglass reinforcements, in form of fabrics or mats, are places into a mould, after which a liquid resin is poured over the reinforcement system. Later on, as the composite hardens, the obtained shape is being removed from the mould. The process can be automated and adjusted depending on the requirements [11].

The advantages of the hand lay-up technique include: process simplicity, low cost tooling (rollers, brushes etc.), feasible for a large variety of resins and fiber, high fibre contents possible. On the other hand, the limitations and disadvantages of this simple process are [83]:
-    Skill-dependent quality of the products
-    Health and safety considerations
-    Suitable mostly for low-viscosity resins

A schematically display of the hand lay-up process can be seen in Figure 3.7:
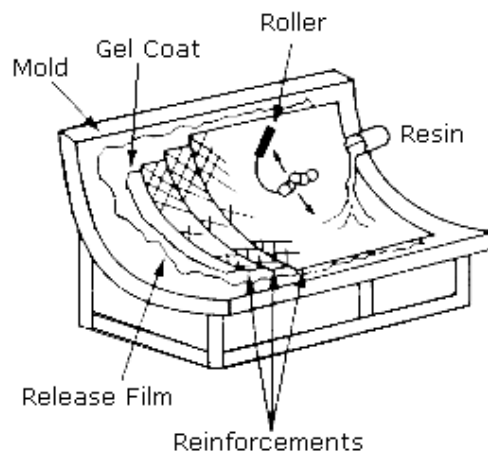
Figure 3.7 – Hand lay-up process [84]

3.1.4. c. Compression moulding

In this process, as shown in Figure 3.8, the thermosetting prepreg material (i.e. the thin plies of uncured matrix and fibers) is placed into the lower half of a pre-heated mould; following that, the heated upper mould half is placed on top and pressed down closing the mould. Prepegs harden together under continued heat and pressure forming the composite part. The applied pressure may vary depending to the type of polymer used in the composite [11].
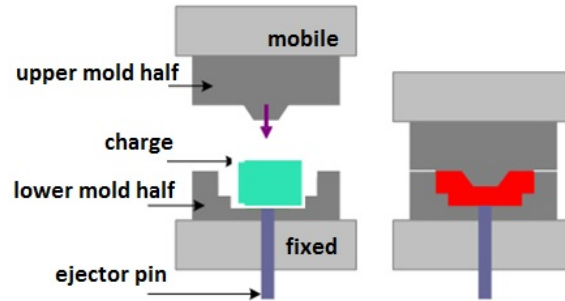
Figure 3.8 – Compression moulding (adapted from [11])

3.1.4. d. Resin transfer moulding

In the resin transfer moulding (Figure 3.9), fiber reinforcements (e.g. fiber woven) are placed in a matched male- female mould system to form composite components. The resin mix is transferred through injection ports into the cavity at relatively low pressures. Vacuum is applied during the curing step to avoid or reduce voids. Resin transfer moulding generally has the advantage of low production costs, allowing the fabrication complex composite structural shapes [18].
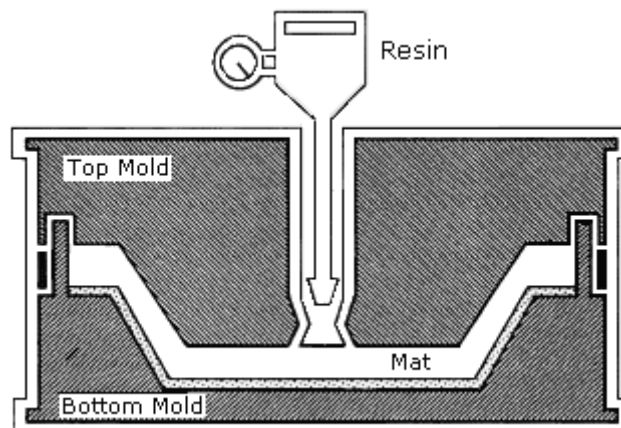
Figure 3.9 – Resin transfer moulding [84]

3.1.4. e. Filament winding

Cylindrical composite shapes can be achieved through filament winding, as displayed in Figure 3.10. Basically, an uncured preform of pre-impregnated filaments, tapes or fabrics are wound layer by layer with controlled tension onto a mandrel. The angle of the reinforcement fibres within one layer can be controlled by varying the angle of the filament placement. During filament winding, pressure is generated between the different layers of uncured composite because of the fibre tension, which contributes to a better compaction of the composite part (reduction

of the amount of consolidation voids) obtaining so a better utilization of the strength and stiffness of the reinforcements [19].
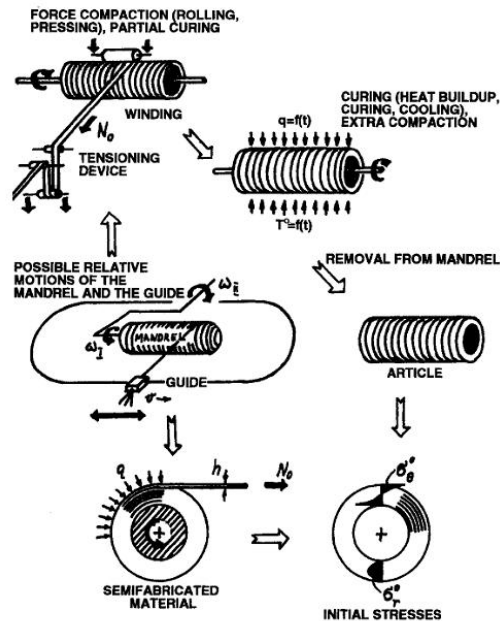
Figure 3.10 – Stages of the filament winding process [19]

3.2. Design standards

Design guidance for structural engineers working with GFRP is currently available mainly through design codes published by different manufacturers or few technical handbooks. From the current knowledge of the author, there are no official design codes covering all aspects of GFRP or FRP civil engineering structures.

The industry is still fragmented and protective and there is still lack of experience in working with GFRP. Another important aspect to take into consideration is the large variety of GFRP and FRP profiles and laminates generally, meaning that a one-structural-material FRP design code would cover only a particular niche on one hand and on the other that a general design code would have to cover all the matrix and reinforcement combinations used in civil engineering [87]. A short overview on some available design guidelines is presented in Table 3.4:

Table 3.4

Examples of currently available guidelines on structural design of FRPs

Designition	Type of Guideline, Code or Manual	Description	Reference
EUROCOMP	Design Code and Handbook	Design guide for structural FRP, based on the safety concept of EN 1990	[85]
Fiberline Design Manual	Manufacturer's Design Manual	Tool for architects, engineers and technicians working with pultruded GFRP structural profiles, based on the safety concept of EN 1990 [73]	[86]
EN 13706	European standard	European standard which specifies the minimum requirements for quality, tolerances, strength, stiffness and surface of pultruded structural profiles	[17]
Extern Design Manual	Manufacturer's Design Manual	Based on a global safety concept	[88]
ASCE Structural Plastic Design Manual	Manual of practice	Practical design criteria and guidelines for structural engineers engaged in the design of plastics and reinforced plastics structures	[89]
BÜV Empfehlung – Tragende Kunststoffbauteile im Bauwesen	German standard	Standard for design of plastics and reinforced plastics structures based on EN 1990 [73] and DIN 18820 [91]	[90]
Composites for Construction. Structural Design with FRP Materials	Design Handbook		[32]

3.3. State of the art in connections for glass fiber reinforced polymers

3.3.1. General aspects of GFRP connections

Joining is undisputed a major issue in structures. Generally speaking joints are a big design challenge for civil and structural engineers. Therefore, the joining of profiles in the case of GFRP construction elements has also a special significance in the design of structures. This new class of materials with its advantages (high strengths, chemical and corrosion resistance, low weight etc) and disadvantages (high initial costs, limited experience and knowledge, absence of design standards, potential durability problems, low shear strengths, different failure modes, etc.) altogether, plays currently a central role in the research and development activities of the structural design community.

Currently, the available joining techniques for structural GFRP applications are adhesive bonding, mechanical fastening, mechanical interlocking and hybrid bonded-bolted connections. Welding may also be an option, but only in the case of thermoplastic polymers. Although there are no published work on welding methods applied in GFRP bridge structures, one can assume that welding (e.g. friction-based technologies) would be a potential candidate to join thermoplastic composite structures [27].

In the design of GFRP connections, several factors must be taken into consideration, such as:
- the large number of constituent materials in composites
- selection of appropriate joining procedures for the available techniques
- possible occurrence of different types of failure modes
- decreased material ductility comparing to metals
- lack of design codes and standards
- design recommendations of composite manufacturers (e.g. guidelines and manuals)

A priori there are only three ways of joining materials and parts: by using and relying on mechanical and/or chemical forces, or by making use of and to depend on physical forces [41]. In the case of mechanical forces, materials remain separate and distinct at atomic or molecular level; no chemical bonds are formed. The parts are held together by the physical interlocking or interference of either macroscopic or microscopic characteristics. While relying on chemical forces, one material or part is held to another by the formation of chemical bonds, usually formed as a result of chemical reactions. When the joint relies on physical forces, the bond is being produced by the natural tendency of molecules, ions and atoms to attract one another, without the necessity of any chemical reaction. Mechanical forces are the basis for mechanical fastening techniques, while chemical forces are the basis for adhesive bonding and physical forces for welding. Joints based on mechanical forces can virtually always be disassembled; chemical-based joints are, with a few exceptions, permanent while joints based on physical forces can virtually never be re-opened without damaging the joining partners [41].

3.3.2. Adhesive bonding

Adhesive bonding is the most common and most material adapted joining technique used in structural applications for composite structures. The joining partners are held together by chemical forces, resulted from chemical bonding (chemical reaction); in the case of rough-surfaced or porous adherents, some mechanical interlocking forces can contribute to the bonding mechanisms between the adhesive and the adherents at microscopic level [41]. Adhesive joints can be highly effective when large surfaces are available and the joining partners are relatively thin. Stress concentrations and peeling stresses have to be minimized through proper design [28]. Using adhesives, mostly one- or two-component epoxy based, provides advantages such as lower stress concentrations, good joint stiffness, low weight, minimal alteration of the chemical composition and microstructure of the adherents and the possibility of joining dissimilar materials.

On the other hand, there are some design implications and disadvantages related to adhesive bonding which have to be taken into consideration and solved:

- Non-uniform stress distribution in the adhesives: extending the overlapped area of the joint, for example, beyond a certain length does not increase its strength, although it may provide safety against creep rupture [28]. Limiting the minimum strain to 10% of the maximum at ultimate load in a lap joint is more important than limiting the maximum strain, according to Hart-Smith [29]
- Prediction of the bond failure is difficult
- Temperature, chemical, ultraviolet and moisture sensitivity of the adhesive layer
- Bonded connections cannot be disassembled
- Need of complicated surface preparations: cleaning, solvent degreasing, pH neutralizing, abrasion [28]
- Curing times: two component epoxy bases adhesives require curing times of up to 24 hours in order to achieve the expected mechanical properties
- Adhesives can transfer only shear stresses
- complex inspection and repair procedures

According to ASTM D 5573-99 [30] six distinctive failure modes and one combined failure mode have to be taken into consideration:

a. adhesive failure (ADH): rupture of the adhesively bonded joint, separation appears at the interface between adhesive and adherent
b. cohesive failure (COH): separation within the adhesive layer
c. thin-layer cohesive failure (TLC): similar to COH, failure very close to the adhesive-substrate interface, characterized by a thin layer of adhesive on one adherent and a thick layer on the other substrate
d. fiber-tear failure (FT): failure occurs exclusively in the FRP matrix, characterized by the appearance of reinforcing fibers on both ruptured surfaces
e. light-fiber-tear failure (LFT): failure occurring within the FRP substrate, near the surface, characterized by a thin layer of the FRP matrix visible on the adhesive, sometimes with few glass fibers transferred from the substrate to the adhesive

f. stock-break failure (SB): characterized by a break of the FRP substrate outside the adhesively bonded joint region

g. mixed failure mode: any combination of two or more of the six distinctive classes of failure mentioned

Figure 3.11 schematically shows the ASTM D 5573-99 failure modes (a) to (f).
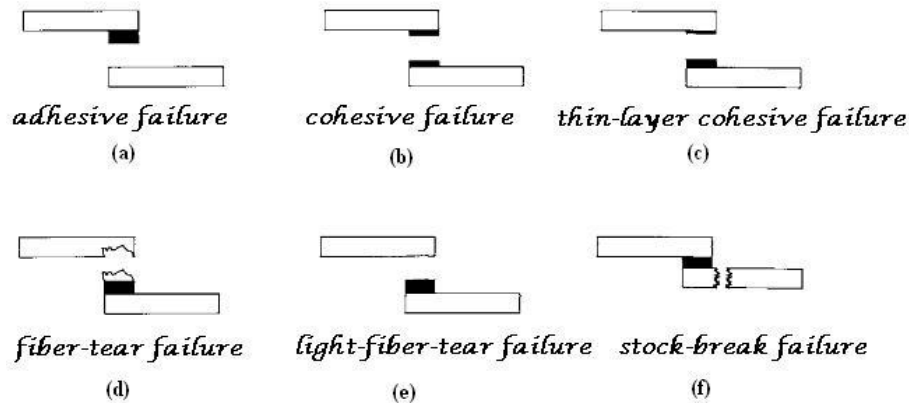
Figure 3.11 – Failure modes of adhesive bonded FRP [30]

3.3.3. Bolted connections

Mechanical fastening is an effective method for joining FRP members generally and GFRP particularly, although it was originally developed for isotropic materials. Research in the field of FRP bolted connections throughout the years has developed appropriate design methods for FRP and showed that, although mechanically fasted FRP joints share the same basic failure modes with metals, the mechanisms by which damage initiates and propagates can be fundamentally different, therefore classical metal failure criteria are not always applicable [28]. Depending on the application, bolts can be metallic (steel, stainless steel, aluminum, titanium) or even FRP (mostly CFRP) [31]. Besides bolting, other mechanical fastening types are available: self-tapping screws, rivets, connectors, embedded fasteners, dowels or pegs and mechanical interlocks (mostly together with adhesive bonding) [31].

Bolted connections offer multiple advantages, such as disassembly ability, simple surface preparation, easy predictability of joint failure, simple inspection, easy handling and machining, fast assembly and joining times. Two of the most important advantages of mechanical fastening are that it can be achieved without changing material structure or composition and it allows intentional separation of joining partners [41].

Bolted FRP connections are similar to steel or timber bolted connections and they reach straight away their full strength and stiffness. But these advantages come at the expense of disadvantageous issues:

- augmented stress concentrations
- reduction of the net cross sections
- increased joint weight
- torque limitations
- uneven distribution of the load to multiple rows of fasteners

- creep and stress relaxation
- notch sensitivity
- temperature and moisture sensitivity
- possibility of accidental disassembly [41]

Mechanical strength in bolted joints will be affected by a number of factors, like fiber orientation, lateral constraint, stacking sequence, joint geometry (width, hole size, clearance, interaction between holes). Previous studies have shown that temperature has a significant effect on the bearing strength of bolted FRP joints, much more than moisture [28].

According to Hart-Smith (1987) [64], the following failure modes (Figure 3.12) of mechanically fastened FRP connections can occur [28]:

    a) Tension failure: caused by the average net stress across the section. Because of the linear elasticity of FRP upon failure, stress concentrations are not decreased by yielding. Thus, stress concentrations will often cause failure to initiate at the hole. Tensile strength depends highly on the fiber orientations. The fibers parallel to the load (0°) will carry the most of it, while failure will initiate at the stress concentration at the edge of the hole perpendicular to the loading axis

    b) Shear-out failure: as in the case of tension failure, fiber orientation is also critical in determining the shear strength. The best shear performance is usually achieved in 0°/45° joints

    c) Pull-out failure: associated mostly with rivets

    d) Cleavage failure: failure will initiate in a single shear mode followed by failure of the net section on one side of the laminate

    e) Bearing failure: the determining factors for the bearing strength are the compressive strength of the 0° fibers and the clamping pressure. Bearing will cause compression on the loaded half of the bolt hole

    f) Bolt failure: the bolt material fails by shear

Most design guidelines recommend joint geometries that support bearing and tension failure. For obvious reasons, since the fibers are the determining strength factor in the composite material. There is actually no definitive method for predicting the strength of bolted joints; the methods used are generally based on boundary stresses and the failure theories underestimate the joint strength [65].

As mentioned previously, creep and stress relaxation is an important issue for mechanical fastening of FRP. Composites with polymeric constituents manifest often viscoelastic behavior, especially under the influence of moisture and high temperatures [66]. Fastener type and torque have also an important effect on stress relaxation performance of bolted joints [67, 68]. The influence of clamping effect on stress relaxation in E-glass/epoxy beams has also been investigated by Zhao and Gibson [69]. They observed the higher the clamping forces, the lower the effect of stress relaxation will be. Vibrations induce also stress relaxation because wear and hammering take place during vibration [66].
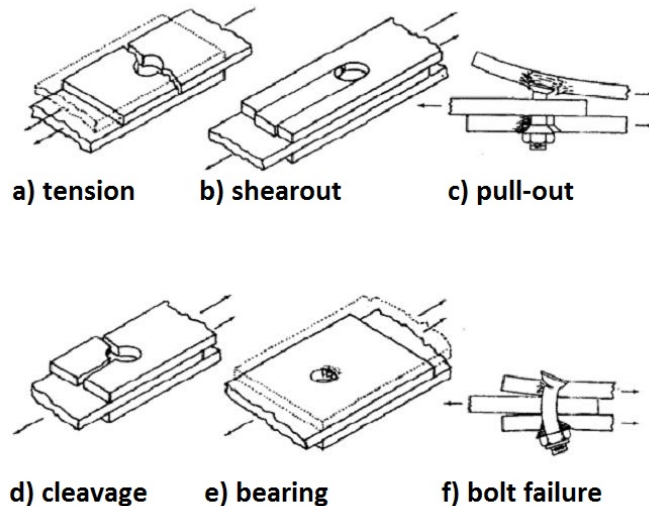
Figure 3.12 – Failure modes of bolted FRP according to
Hart-Smith [29]

3.3.4. Hybrid joining methods and other connection types

Hybrid joining methods consist mostly of a combination of adhesive bonding together with bolting. Current information in the field of hybrid joining of composite-metal structures available in literature is very limited. Some of the actual know-how comes usually from practical experience and is normally unavailable for copyright reasons. It is well known that the use of adhesive bonding in addition to bolting can improve the joint stiffness, but does not necessarily increase its mechanical performance [32]. Mottram and Zheng [33] demonstrated in their work, that this increased joint stiffness leads to the decrease of the connection ductility, followed by a brittle failure of the bonded-and-bolted joints. By the failure of the adhesive, the entire load is suddenly transferred to the bolts, which will not be able to withstand loading, leading to premature joint failure

While the previous three presented connection types are basically designed to transmit in-line forces, civil engineers must also concentrate on connections that can transfer moments as well as in-line forces and shear. Design guidance offer recommendations also for FRP frame connections (beam-to-column, pinned connections, semi-rigid connections), interlocking connections (mostly combined with adhesives, for connecting tubes and panels) or the so-called "SNAP" joints and different other inventions protected by patents [92].

3.4 FricRiveting

3.4.1. Principles of the technique

Friction Riveting, hence the name Fricriveting, is an innovative joining technique for polymer-metal hybrid structures, developed and patented by the Helmholtz Zentrum Geesthacht in Germany [80]. In this process, the polymeric parts are joined by a metallic rivet, while the joining is achieved by mechanical interference and adhesion between the metallic and polymeric joining partners.

The basic configuration of the process (Figure 3.13) consists in rotating a cylindrical metallic rivet and inserting it in a polymeric base plate. Heat is generated by the high rotational speed and the axial pressure. Due to the local increase of temperature, a molten polymeric layer is formed around the tip of the rotating rivet. By the end of the heating phase, the heat input rate increases to a higher level than the heat outflow, due to the low thermal conductivity of the polymer. The local temperature increases leading to the plasticizing of the tip of the rivet. While the rotation is being decelerated, the axial pressure is increased, the so called forging pressure is applied and the plasticized tip of the rivet is being deformed. As a result there will be an increase of the original rivet diameter, whereby the deformed rivet tip will assume a parabolic pattern due to the opposite reactive forces related to the colder polymeric volumes [34].

In first instance, it was developed to unreinforced thermoplastic by join metallic rivets; by now the FricRiveting technology has the potential to fulfill the needs of the market of the polymer-metal multi-material structures by offering strong joints obtained in a simple, fast and more environmentally friendly way [34]. The process is based on the principles of mechanical fastening and friction welding; the joining energy is supplied by the rotation of one of the joining partners (metallic rivet), in form of frictional heat.

The equipment used for Fricriveting consists of a commercially available friction welding system. Different joint geometries and material combinations are possible, including hermetic lap configurations on aluminum, titanium, polyetherimide, polyetherketone, polycarbonate and different polyolefins, among others. FricRiveting can be used in the production of metallic inserts in plastic products [27].
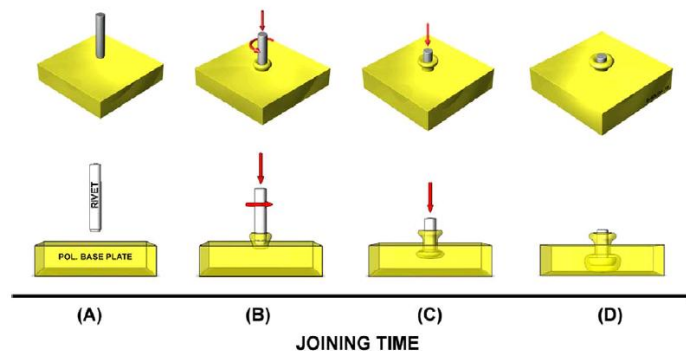

Figure 3.13 – Schematic view of the Fricriveting process. (A) Positioning of the joining partners, (B) Feeding of the rivet into the polymer (Friction), (C) Rivet forging, (D) Joint consolidation [35]

3.4.2. Process parameters and process variables

The controllable input data of the process represents the process parameters. The main parameters of Fricriveting are the Rotational Speed (RS), Joining Time (JT) and Joining Pressure (JP).

The Rotational Speed represents the angular velocity of the rotating cylindrical rivet and is the main parameter affecting the temperature development. It also controls the viscosity of the molten polymer and the formation of thermal defects and degradation. The Joining Time has two components, both controlled by the operator: Friction Time (FT) and Forging Time (FOT). The joining time influences the level of volumetric defects related to the thermo-mechanical processing (controls the amount of heat energy supplied to the molten polymeric film). The Joining Pressure has also two components, related to the ones of the joining time: Friction Pressure (FP) and Forging Pressure (FOP). Therefore, the friction time is the interval the friction pressure is applied while the forging time is the interval the forging (supplementary axial pressure) takes place. The main role of the Joining Pressure is to control the rivet forging and consolidation phases and is related to the normal pressure distribution on the rubbing surfaces of the joining partners [35].

The process variables are the outputs of the Fricriveting process: Heating Time (HT), Burn-Off (BO), Burn-Off Rate, Temperature and Frictional Torque. The heating time is the interval related to the initial contact between the rotating rivet and the polymeric base plate and the moment when the rotation stops. It represents the heat input regime of the process and provides an estimate of the material plasticizing level. The Burn-Off is obtained from the axial displacement monitoring curve, being associated with the insertion level of the rivet into the polymeric base plate and its consumed length. Therefore, the burn-off provides a good estimate of the plasticizing level of the rivet. The Burn-Off Rate represents actually the average joining speed of the process. It is calculated as the ratio between the burn-off and the heating time, thus providing a good approximation of the real joining speed.

The Average Process Temperature gives a proper estimation of the changes in viscosity of the softened or molten polymer. It is therefore a key-variable for explaining the microstructural and property changes within the joint area. Finally the frictional torque estimates the rheological behavior of the molten polymer and the plasticized metallic rivet. It can also help identifying process anomalies or equipment malfunctions [36].

Figure 3.14 shows the FricRiveting process parameters and variables discussed above in a schematic experimental monitoring diagram.
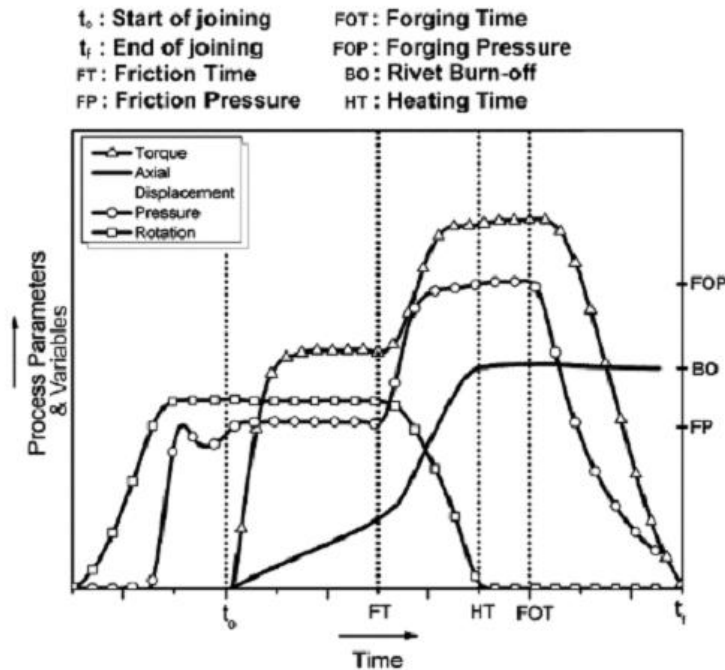
Figure 3.14 – Process parameters and variables of the
FricRiveting process [36]

3.4.3. The phases of the Fricriveting process

In analogy with other friction-based joining techniques, Fricriveting can be divided in process steps of phases related to the different stages of heat generation and axial rivet displacement over the joining time [36]:

- Phase I: the Coulomb Friction (solid friction), when the harder asperities of the metallic material penetrate the softer polymer. By this phase, the rivet axial displacement is virtually zero. When the frictional heating is enough to soften the polymer in the faying surfaces, the friction regime changes from the solid to the molten state (beginning of Phase II);
- Phase II: Unsteady State Viscous Dissipation – the frictional heating is mainly due to internal shearing in the molten polymer. The rivet starts penetrating the polymeric base plate while axial displacement increases (non-linearly) with time [38];
- Phase III: Steady State Viscous Dissipation – in this phase, there is a balance between the melting rate of the polymer underneath the tip of the rotating rivet and the outflow rate of the molten material, which is expelled as flash. The axial displacement of the rivet increases linearly and by the end of

this phase, the desired level of plasticizing of the rivet tip is achieved, thus the process is ready for the next phase (forging);

- Phase IV: Rivet Forging Phase - during this phase, the rotation of the rivet is decelerated and the axial pressure is increased. Consequently, the thickness of the molten polymer layer is considerably reduced below the rivet tip, causing the increasing of the expelled flash volume. An abrupt increase of the axial rivet displacement takes place and the plasticized rivet tip is deformed, following a paraboloidal pattern;

- Phase V: Consolidation Phase – in this phase, the joint solidifies under constant pressure, while the displacement reaches a maximum and becomes constant. In the same time, the molten polymer consolidates around the rivet tip, creating a bonded surface. Hereby, the anchoring zone is being created.

3.4.4. Advantages and limitations of Fricriveting

Friction Riveting combines the advantages of mechanical fastening and welding and with an adequate design of the joint the benefits of this innovating process are [38]:

- little or no surface preparation needed
- no obligatory pre-holes in the polymeric plates, leading to less stress concentrations
- hermetic sealed joints can be created
- joining is independent of position (horizontal / vertical)
- reduced number of process steps and short joining cycles, providing the potential of cost savings
- a wide range of materials can be joined
- simple and low cost commercial available machinery
- robotic applications are possible
- good joint tensile and shear mechanical performance

On the other hand, like every new technology, Fricriveting has its limitations, which may be overcome after further research. The process is directly applicable to thermoplastic polymers only; a minimum working thickness of the joining partners is needed; fricriveted connections cannot be disassembled and only spot-like joints can be achieved.

3.4.5. Previous research

As discussed, by the times of this work, Fricriveting was developed mainly for unreinforced thermoplastic polymers and no previous investigations on thermoset polymers were conducted. Also, there was no previous published work on joining fiber reinforced polymers through FricRiveting, either in thermoplastics or thermosets FRPs.

Several material combinations have been tested and went under thorough investigations, relating feasibility, influence of the parameters, temperature and heat generation and optimizations for tensile and lap-shear strength. For example, Amancio and Dos Santos [39] have studied the influence of the rotational speed on the process temperature, the number of flaws in the consolidated polymer layer and tensile strength of non-reinforced PEI/Aluminum 2024 friction riveted joints. They

concluded that, the higher the rotational speed, the higher the process temperature was. Furthermore, they also realized that, although the process temperature appears to be directly proportional to the rotational speed, the amount of thermo-mechanically degraded polymer did not follow any clear pattern [36]. This is probably associated to the high thermal resistance of the PEI, which did not present high level of degraded material in the investigated range of parameters [40]. Figure 3.5 shows an example of the macrostructure of an aluminum / unreinforced thermoplastic joint (A); and the influence of joining parameter (B) on the formation of the anchoring zone (the deformed tip of the rivet) of Fricriveting, by Amancio.

PEI/AA2024-T351[1]
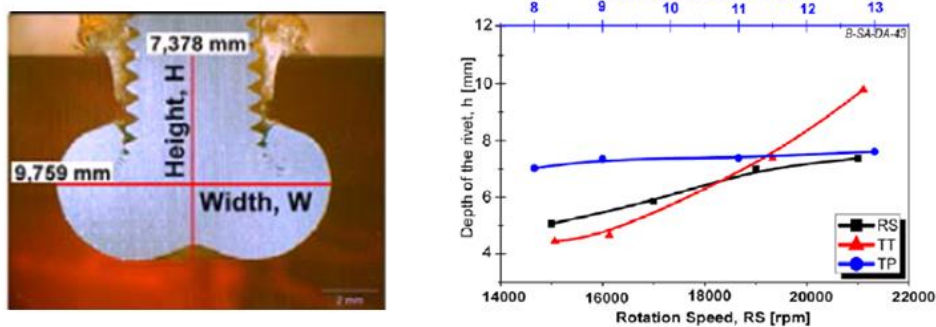
Figure 3.15 – Example of a friction riveted PEI/Aluminum 2024 joint. (A) cross-sectional view. (B) chart showing the influence of joining parameters on the penetration depth of the rivet [35].

Other investigated material combinations include Polyethylene/Titanium, PC/Aluminum and PEI/Titanium [95].

Amancio and dos Santos [93] and Rodrigues [94] investigated the dependency of tensile strength to the aspect ratio (H/W, as shown in Figure 3.5) in PEI/Al 2024 and PC/Al 2024 joints, by evaluating the ultimate tensile force and measuring the width and penetration depth (height) of the rivet anchoring zone. The authors tensile testing revealed the occurrence of five different failure types, as shown in Figure 3.16:

- Type I: Through the rivet failure: the final failure takes place in the metallic rivet portion located outside the joined area. The joints failing through this mode have high tensile strength similar to the rivet material
- Type II: Rivet pullout with back plug: Cracking initiates at the deformed tip of the rivet, which will be pulled out of the polymeric element, leaving behind pieces of the cracked anchoring zone ("the back plug"); this failure type normally leads to good tensile strengths
- Type III: Full rivet pullout: this type of failure was observed in polymers with high ductility (e.g. PC and Polyethylene) or in cases where the tip is not highly deformed. The crack initiates around the anchoring zone in the polymer; the rivet is

completely removed from the polymeric element leaving a hole in the polymer with an approximate diameter equal to the deformed tip of the rivet. Here the tensile strength is usually smaller than in Type I and Type II joints

- Type IV: Rivet pullout: This failure is normally observed in joints with highly deformed anchoring zones but in the proximities of the upper surface of the polymer. Cracks nucleate in the polymer at the borders of the anchoring zone, finally propagating to surface; a conical pattern of polymeric material stays attached around the rivet
- Type V: Rivet pullout with secondary cracking: This mixed failure mechanism appears to involve a complex stress distribution; however it is still not well comprehended. Multiple crack nucleation sites are normally observed around the rivet in the polymer. Crack propagation seems to initially follow the same pattern as in Type IV specimens, but rivet is pulled out in a similar way as in Type III specimens. Together with Type IV, Type V specimens   generally display medium to poor tensile strengths
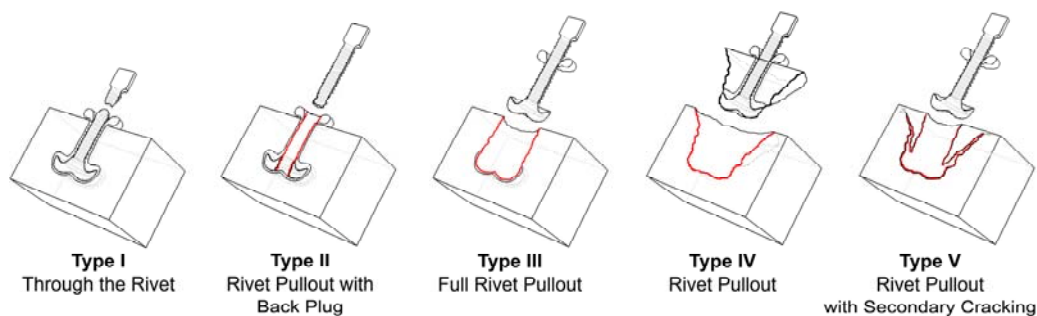
Figure 3.16 – Failure modes of Fricriveting under tensile loading. The thicker red lines indicate the crack propagation path upon final failure (Image courtesy of HZG, Germany).

3.5 Current examples of Emergency Bridges

3.5.1. The D-bridge

The D-Bridge was developed in Germany in the in the 1960s by the steel giant Krupp together with the truck producer MAN [79]. The D-Bridge is a transportable and dismountable structure, made by several individual components. Its name comes from the German word „Dreieck", meaning „triangle", which is also the shape of the individual components. The D-bridge consists of two main steel truss girders connected by cross girders on which a steel deck is present, having also the role of assuring the necessary transversal global rigidity of the structure. The bridge is launched into its place, while the connections of the elements are made through fitting bolts [79].

The structure can carry the load of a 30 tonne truck and reach a maximum span of 90m. The triangular elements can form trusses up to 3 storey and 3-wall configuration. Regarding the installation time, for example, a 9 m span D-Bridge can be launched with service personnel of 10 people in about 6 hours. Figures 3.17 and 3.18 show the launching and installation and of D-Bridges, respectivelly.

Figure 3.17 – Launching of a D-Bridge
(Image courtesy of Austrian Armed Forces [21])

Figure 3.18 – Installation of a D-Bridge
(Image courtesy of Austrian Armed Forces [21])

3.5.2. The Bailey bridge

The Bailey bridge is a modular transportable structure developed by Donald Coleman Bailey of the British Royal Army in the 1940s [22]. It was in the beginning a military purpose bridge, providing sufficient load bearing capacity to sustain the back then newly introduced 40 tonnes Churchill Tank in its combat missions. The bridge is built by manpower only, made entirely from prefabricated parts or segments (panels) and is very versatile. Several different types of bridge truss structures (single or double lane, single to triple trusses and story) can be assembled using the Bailey Panels. One Bailey Panel weights 300 kg and can be transported by five persons. The paneling configuration gives also the important possibility of standardizing the transport of the bridge parts. The chords of the panels have males lugs at one end and female lugs at the other. Bailey Panels are connected though panel pins which are inserted through the engaged lugs of two adjacent panels, while the whole structure is launched on rollers. Transoms act as cross girders and support for the bridge deck. Figure 3.19 shows the main assembly components of the Bailey Bridge truss [22].
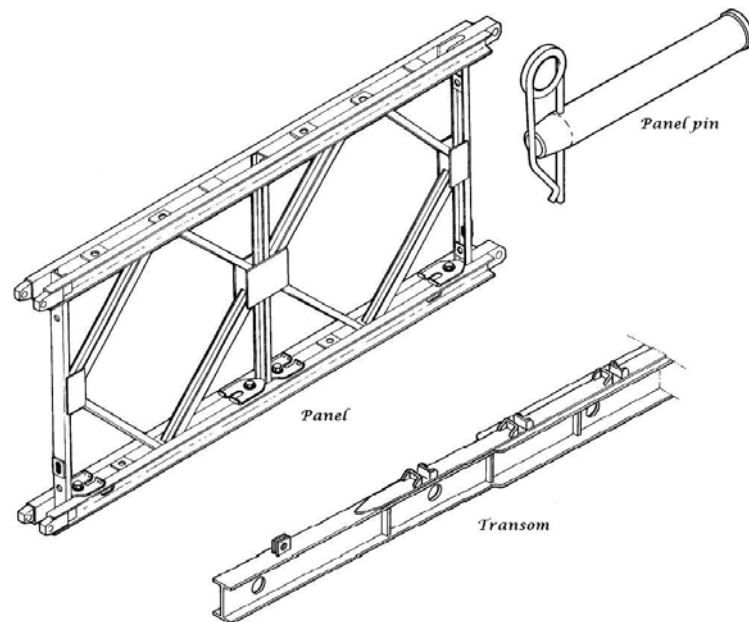
Figure 3.19 – Main assembly parts of a Bailey truss [22].

Each unit of the bridge consisting of single section of panels, transoms and stringers has a length of 3 m. The success of the system is proven by the fact that, 70 years later, a large number of temporary bridging systems currently in use around the world continue to borrow heavily from the Bailey Bridge concept [23]. Figure 3.20 shows the assembly of a Bailey Bridge.

Figure 3.20 – Assembly of a Bailey Bridge [24]
(Image courtesy of the Oregon Military Department, US)

3.5.3. A new lightweight GFRP-Truss-Bridge

In 2004 an inovative concept of GFRP-truss bridge was developed at the Technical University in Aachen, Germany [25]. The proposed 30 m all-GFRP emergency truss bridge was subject of detailed research, especially regarding the selection of joining techniques for the pultruded GFRP profiles. A prototype has been constructed and tested successfully. The 30 m span structure consists of two main GFRP Warren trusses, a construction height of 2600 mm and a single lane width of 3330 mm. The lightweight bridge is modular, each module having a length of five meters and used only four different standard cross sections for the pultruded profiles. The dismountable connections were made with M24 stainless steel bolts, using stainless steel shoes for reinforcing the connection area. The bridge deck was also made of GFRP, the whole structure weighting a total of 16 tonnes, from which 8,5 tonnes was the weight of the truss structure including all connection elements. The bridge was designed for the load of a 40 tonne truck (according to standard MLC40) [25, 96].

Because of the low shear resistance of pultruded FRP profiles, a hybrid joining approach (adhesive bonding/bolting) was identified as the most adequate the solution for transmitting the high shear forces in the connection areas of the truss. Bonded stainless steel plates have been additionaly used for strengthening the bolted areas [25, 26]

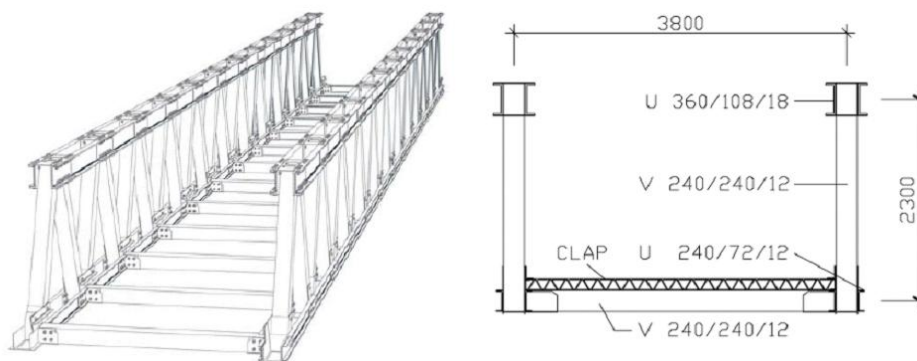Figure 3.21 presents the structural details of this GFRP-truss bridge:

Figure 3.21 – Isometric and cross sectional views of the GFRP-lightweight-emergency-bridge [25]

4. EXPERIMENTAL PROGRAM

4.1. Experimental approach

The experimental program of the thesis is focused on the joining of fiber reinforced polymers with metallic rods (rivets) using FricRiveting. Starting from the previous acquired experience and published results, other new joint material combinations were selected and analyzed, related to the objectives of the thesis stated in Chapter 2.

Taking into consideration the previous research on unreinforced PEI / Aluminum joints, glass fiber reinforced PEI (PEI-GF) composite was selected for a **feasibility study** by FricRiveting. Point-on-plate joints- a joint geometry where the rivet is anchored in a single polymeric piece – were investigated. Rivets produced from two different metallic alloys (aluminum AA 2024-T351 and titanium grade 2) were used to join PEI-GF laminates. Preliminary feasibility studies were additionally conducted on friction riveted joints of thermoplastic glass fiber reinforced polyester (P-GF) with different titanium alloys (Ti grades 1, 2, 3 and 5) rivets in order to investigate the process on thermosetting composites.

The **feasibility study** was based on following qualitative evaluation criteria: optical microscopy analysis of the cross-sectional joint area (i.e. geometry of the deformed tip of the rivet, anchoring of the rivet into the composite, visual amount of volumetric flaws and burned matrix) and visual observation of smoke evolution, ashes, sparks or even fire generated during FricRiveting (an indicative of extensive composite thermal degradation).

After the process feasibility has been proven, the three best point-on-plate joints for each material combination (PEI-GF / aluminum, PEI-GF/titanium and P-GF/titanium) were selected for tensile testing based on: reduced amount of volumetric flaws, burned matrix, good rivet anchoring, reduced/absent level of smoke and ashes, and absence of sparks or fire. **T-pull testing and evaluation of the aspect ratio** of the anchoring zone – a simple mathematical methodology to evaluate the influence of the geometry of the deformed rivet tip on the anchoring performance – were utilized to select the **most adequate combination of GFRP and Rivets** for the next experimental phase.

The following phase consisted of analyzing metal/composite overlap joints on the selected rivet/GFRP combination. Design of Experiments (DOE) and statistical analysis were utilized to **evaluate the influence of FricRiveting's joining parameters on lap shear strength and temperature evolution. DOE was additionally used to optimize the process aiming at achieving the highest joint lap shear strength for emergency bridge structural calculation**.

Finally the optimized friction riveted overlap connections were implemented in a **bridge structural model**. Structural stresses were calculated with a computational model for a case-study emergency bridge with GFRP-truss elements assembled by FricRiveting. Optimized GFRP profile/metallic gusset friction riveted connections were calculated and suggestions for best-practice on FricRiveting of GFRP profiles for emergency bridges were proposed. Figure 4.1 summarizes the main phases of the experimental approach:
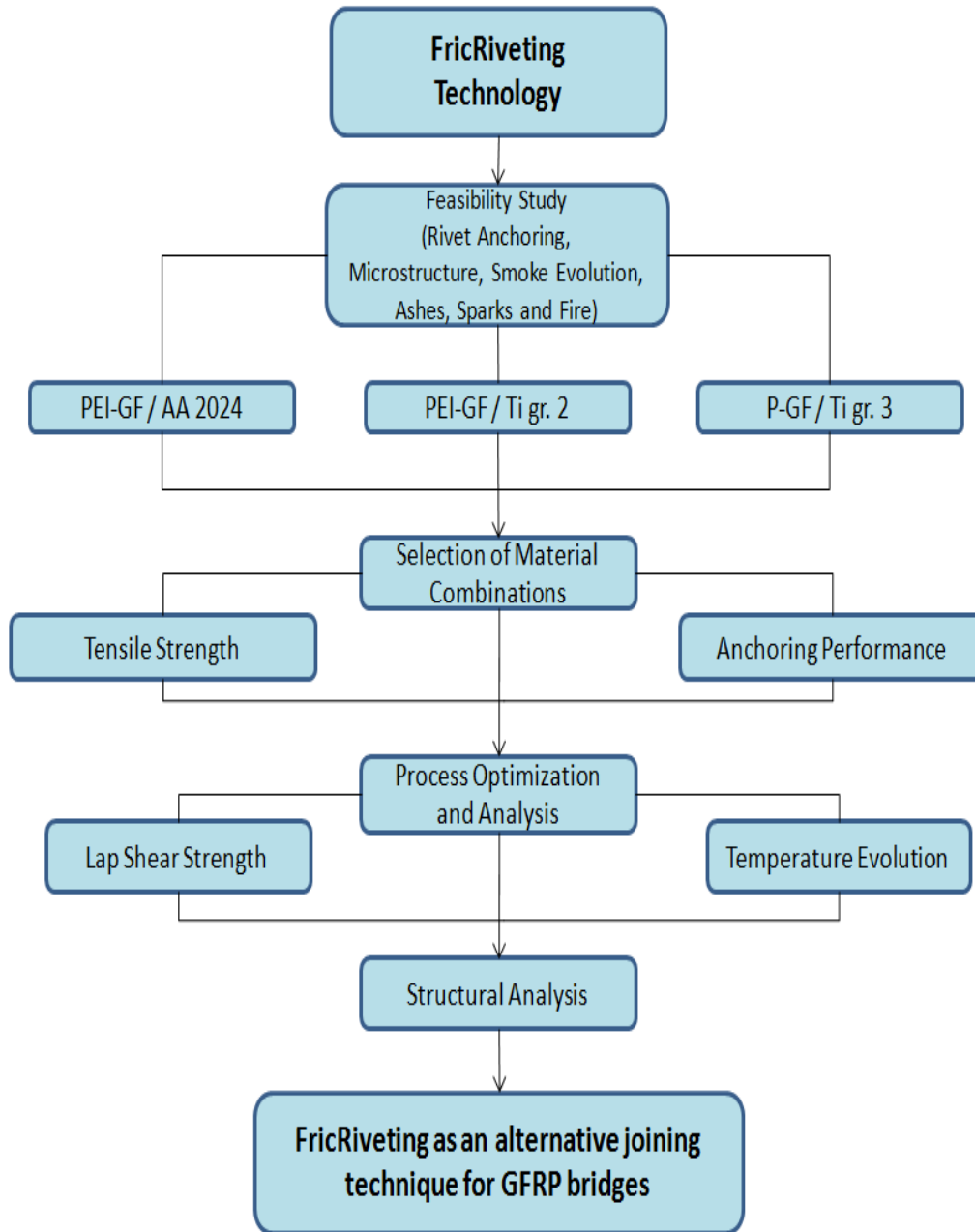
Figure 4.1 – Summarized experimental approach of the current work

4.2. Equipment and materials

4.2.1. Friction riveting joining equipment

The friction riveting equipment used at the Helmholtz Zentrum Geesthacht (HZG) consists of a friction welding system RSM 400 manufactured by Harms & Wende GmbH & Co. KG, Hamburg, Germany. The welding head was developed for joining steel, aluminum and non-ferrous alloys. The welding system is fully automatic equipped with pneumatic operated chuck to clamping the rivets [42]. Technical data regarding the friction riveting system RSM 400 used in this work is presented in Appendix 1.

The modular friction welding system consists mainly of three components: the modular welding head RSM 400, the switch cabinet and the control panel. An experimental setup aluminum frame was designed by Witte GmbH, Germany, for the HZG (formerly GKSS Forschungszentrum), previously for an earlier RSM 200 welding head [35]. The frame is used also for the RSM 400. The welding head is placed horizontally in a fixed position, while the clamping-table can be moved forwards and backwards in 20mm steps. Additionally to the welding system, a force measuring system was used for recording the frictional torque during the joining process [35] so possible process anomalies could be identified by variations during joining. Figure 4.2 show the whole ensemble of the welding system together with the experimental frame.
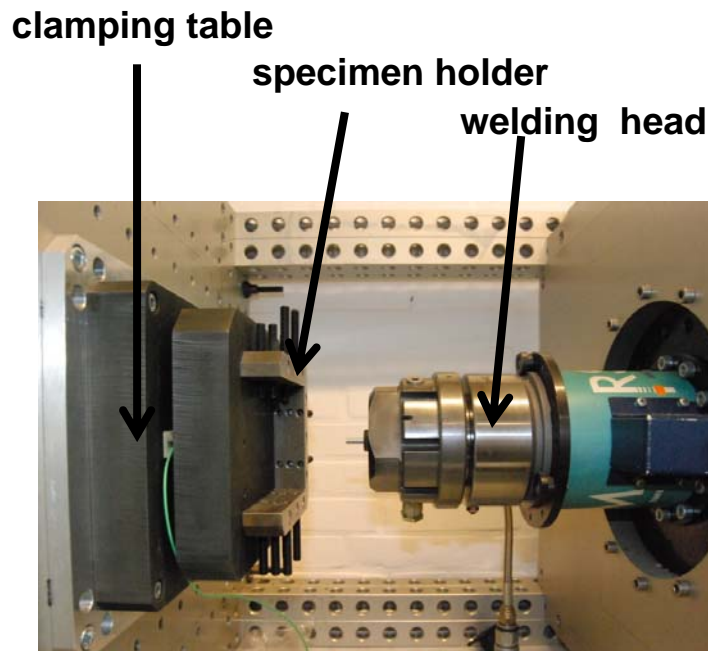

Figure 4.2 – RSM 400 welding system used for FricRiveting

The joining parameters are controlled by the RQ-Fuzzy software (Harms & Wende), which graphically records four analogue variables: rotational speed, joining time, pressure and axial displacement. For further statistical analyses, the experimental data can be exported as ASCII-files. Together with the torque measurement data, the joining system can supply the complete set of process information, important for identifying possible process issues or equipment mal-function [35].

4.2.2. Joining procedure

Prior to joining, the base materials are cleaned with acetone for removing impurities like dust or machining fluids. The polymeric base plate is fixed on the specimen holder, while the metallic rivet is clamped in the spindle adapter (chuck) of the welding head. The joining parameters (rotational speed, joining time, joining pressure) are set in the RSM 400 control panel and in the RQ-fuzzy software. Proceeding, the process is started manually from the control panel. Following that, the rotating spindle (containing the metallic rivet) is moved towards the polymeric plate on the clamping-table, when the set-up rotational speed is achieved. The actual joining process starts when the rivet touches down on the polymeric base plate. The process continues with the plunging of the rivet inside the base plate; when the pre-set friction time is accomplished, rotation is decelerated and the forging pressure is applied until the reaching of the end of the joining time. Finally, the forging pressure is released and the machine stops. Subsequently, the new formed joint is removed from the joining equipment, the samples are labeled and the monitoring data saved and exported, as necessary [35].

4.2.3. Microscopy

In order to measure the aspect ratio and to analyze the microstructure, and fracture surfaces from base materials and joints, stereo microscopy and light optical microscopy (LOM) were chosen. The microscopy samples consisted of cross sections from the centre of the rivet, across the whole joint thicknesses. The cross sections were cut using a Struers Axitom-5 cut-off machine [44]. Following that, cut offs were embedded in low cure-temperature thermoset epoxy-resin (Epoxicure, Buehler) to avoid structural thermal alteration of the polymer-metal interface [35]. The embedded samples were grinded and polished in an automatic metallographic sample preparation machine (Struers TegraPoll-15) according to standard metallographic procedures [43].

4.2.4. Tensile testing

For evaluating the tensile strength of the polymeric base materials, flat tensile testing specimens were machined in both warp and weft directions over the whole thickness of the 6,2 mm PEI-GF plates, according to EN ISO 527-4 [47]. For the tensile strength of the metallic rivet on the other hand, geometry was adapted from DIN EN ISO 898-1 [48]; round tensile specimens were machined to a nominal diameter 5 mm and a length of 60 mm, both plain and threaded (M5).

T-pull tensile specimens [35] (Figures 4.3 and 4.4) were selected to study the tensile strength of the joints, with the rivet having the geometries and dimensions of a half of a DIN EN 10002 [49] round-tensile bar and the PEI-GF base plate dimensions were 70x70x6,2mm. In the case of P-GF, the plate thickness was

10mm. The tests were undertaken at a strain rate of 1mm/min at room temperature (21°C) in a 100kN Zwick/Roell universal testing machine
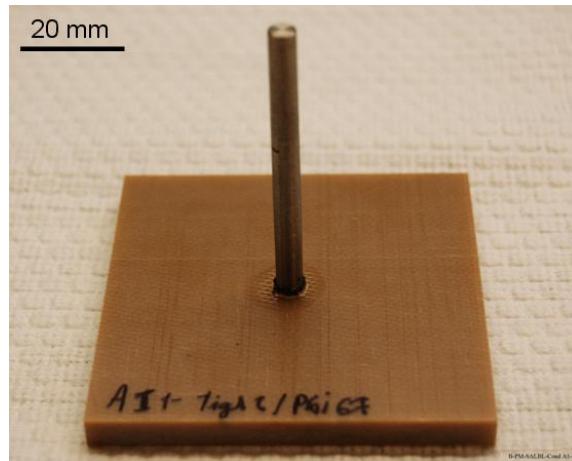

Figure 4.3 – T-pull PEI-GF/Ti gr.2 specimen
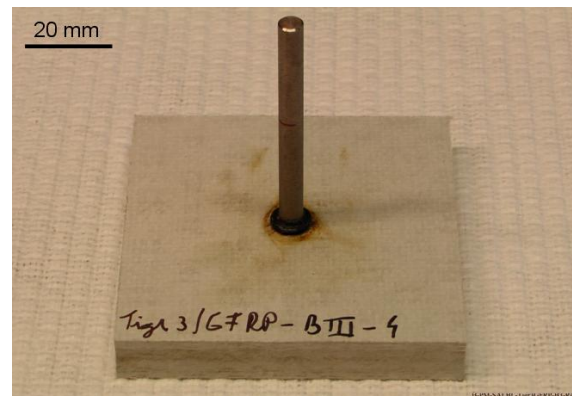
Figure 4.4 – T-pull P-GF/Ti gr.3 specimen

4.2.5. Lap shear testing

Lap shear tests were carried out using the same universal testing machine describe for tensile testing. Tests were performed at room temperature with a traverse speed of 2mm/min. Lap shear specimens were cut following the dimensions prescribed by ASTM D 5961 M – 08 [50]: 135 x 36 x 6,2 mm, overlap of 36 mm, free rivet length 12mm and Φ 5 mm rivet diameter. Each lap shear specimen was constituted of a PEI-GF specimen with Ti gr.2 rivet (M5-threaded) (Figure 4.5) and an aluminum plate (AA 2198 alloy) perforated with the through-hole diameter of 5 mm. Hole edges were chamfered at a 90° angle for reducing stress concentrations but also for providing space for the polymer flash on interface side between the two plates. Both composite and aluminum plates respected the described ASTM specifications. In the next step the two specimens were screwed together using stainless steel M5 nuts and washers, as shown in Figures 4.6 and 4.7. Stainless

steel nuts and washers were selected not only because of economical reasons, but also because of the better friction coefficient between titanium-stainless steel in comparison to titanium-titanium.
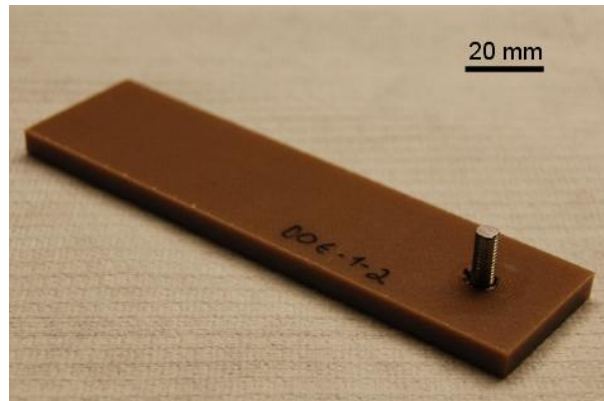

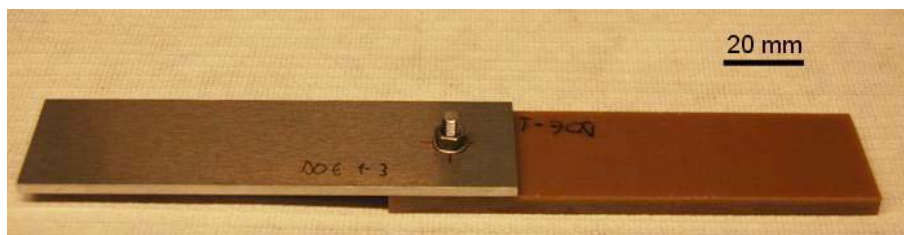Figure 4.5 – PEI-GF lap shear specimen with Ti gr.2 rivets.
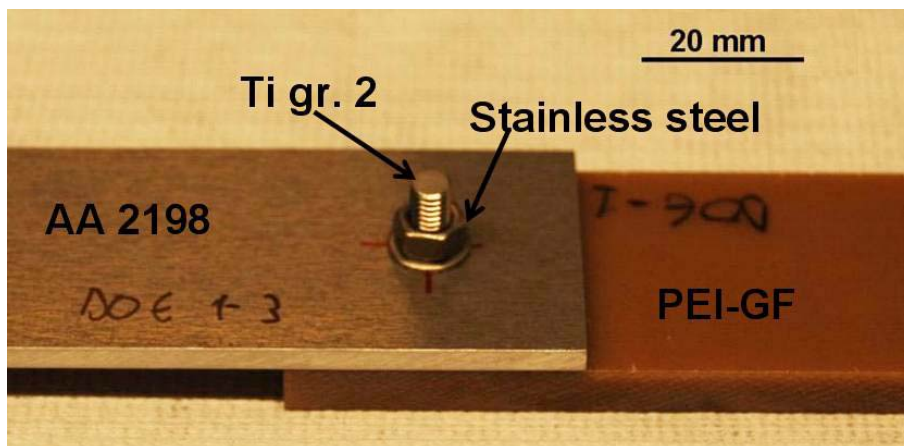

Figure 4.6 – PEI-GF/Ti gr.2/Al 2198 lap shear joint

Figure 4.7 – Close view on the PEI-GF/Ti gr.2/Al 2198 overlap joint used in the lap shear testing.

4.2.6. Design of experiments (DOE)

For the lap shear tests, a statistical DOE was conducted, in order to optimize the process for best mechanical performance. The aim of DOE is to find the relationship between various factors or variables and responses to them. This relationship can be expressed by Equation 4.1 [51]:

$$y = f(M, x1, x2, ..., xn) \qquad (4.1)$$

, where y is the output characteristic, M the input signal and $x1$, $x2$, … xn the noise factors.

There are several DOE approaches and models, but two designs commonly used in welding technology are:
- Design 1 - Full factorial design: in this case, all possible combinations of variables will be tested
- Design 2 – Taguchi method: pairs of combinations are tested

The main difference between these two designs will be discussed by the example of the DOE for lap shear testing of PEI-GF/Ti gr.2/Al 2198 overlap joints used in this thesis, as follows:

The whole process has five joining parameters:
1. rotational speed (RS)
2. friction time (FT)
3. forging time (FOT)
4. friction pressure (FP)
5. forging pressure (FOP)

Friction pressure, based on preliminary experiments and analysis (feasibility study), was set constant to 6 bar; while the levels of the other parameters were varied also according to the result of the preliminary investigation. Thus, only the influence of the four remaining parameters will be studied in the DOE, each at three different levels:
- RS: 8000, 10000, 12000 rpm
- FT: 700, 1200, 1500 ms
- FOT:1200, 1850, 2500 ms
- FOP: 6, 7, 8 bar

In the first scenario (factorial design), in order to test all possible combinations, a number of $3^4 = 81$ experiments are needed, without taking into account the number of replicates per each experiment!

In the second scenario, one can use the orthogonal array experimental design proposed by Taguchi [57], leading to a more condensed set of experiments. At first, we need to select the appropriate array, by using the array selector presented in Table 4.1. These arrays were created using an algorithm developed by Genichi Taguchi, allowing each parameter to be tested equally. The arrays are selected by the number of parameters (variables) and the number of levels. In our case, we have four parameters (RS, FT, FOT and FOP) and three levels (minimum, medium, maximum), so the proper array would be L9. The levels designated at 1, 2, 3 etc. should be replaced in the array with their actual values for each parameter (for example P1 will be "RS" and its level 1 will be "8000" and so on) and P1, P2, P3 and P4 should be replaced with RS, FT, FOT and FOP, respectively.

Table 4.1

Taguchi array selector

Number of parameters					
	32	L32			
	31	L32			
	30	L32			
	29	L32			
	28	L32			
	27	L32			
	26	L32			
	25	L32			
	24	L32			
	23	L32	L36		
	22	L32	L36		
	21	L32	L36		
	20	L32	L36		
	19	L32	L36		
	18	L32	L36		
	17	L32	L36		
	16	L32	L36		
	15	L16	L36		
	14	L16	L36		
	13	L16	L27		
	12	L16	L27		L50
	11	L12	L27		L50
	10	L12	L27	L32	L50
	9	L12	L27	L32	L50
	8	L12	L18	L32	L50
	7	L8	L18	L32	L50
	6	L8	L18	L32	L25
	5	L8	L18	L16	L25
	4	L8	L9	L16	L25
	3	L4	L9	L16	L25
	2	L4	L9	L16	L25
LEVELS		**2**	**3**	**4**	**5**

Generally, arrays can be found in literature. They also can be derived, drawn manually or derived from deterministic algorithms. Table 4.2 shows the general Taguchi-L9 array while Table 4.3 shows the filled L9 array with the parameters and values for the discussed DOE.

Table 4.2

Taguchi-L9 orthogonal array

Experiment	P1	P2	P3	P4
1	1	1	1	1
2	1	2	2	2
3	1	3	3	3
4	2	1	2	3
5	2	2	3	1
6	2	3	1	2
7	3	1	3	2
8	3	2	1	3
9	3	3	2	1

Table 4.3

Taguchi-L9 orthogonal array the lap shear testing performed on PEI-GF/Ti gr.2/Al 2198 FricRiveting overlap joints

Experiment	FS [rpm]	FT [ms]	FOT [ms]	FOP [bar]
1	8000	700	1200	6
2	8000	1200	1850	7
3	8000	1700	2500	8
4	10000	700	1850	8
5	10000	1200	2500	6
6	10000	1700	1200	7
7	12000	700	2500	7
8	12000	1200	1200	8
9	12000	1700	1850	6

Each experiment had a number of four replicates. In this work the ultimate lap shear strength (ULSS) was the response evaluated. For determination of the the effect of each variable (parameter) on the output, the signal-to-noise ratio (SN ratio) needs to be calculated for each experiment. The SN ratio is a measurement scale used in the communication industry (actual signal measurement and wave-to-sound conversion) and adopted in quality engineering. The quality of a measurement is expressed by the ratio of signal and noise [51]. For a measurement system, the input-to-output relationship is studied; the true value of the object is the input, while the result of the measurement is the output. SN ratios have three elements: sensitivity, slope variability. The SN ratio can be define with the following formula:

$$SN_i = 10\log\frac{\overline{y}_i^2}{s_i^2}$$
(4.2)

, where y is the value of the output and s is the variance.

Hereby:

$$\overline{y_i} = \frac{1}{N}\sum_{u=1}^{N} y_{i,u} \qquad (4.3)$$

$$s_i^2 = \frac{1}{N-1}\sum_{u=1}^{N}(y_{i,u} - \overline{y}_i) \qquad (4.4)$$

, with i – the experiment number, u – the trial number (replicate number) and N – the number of trials for each experiment.

For the case of maximizing the performance characteristic (output), the SN ratio should be defined as follows:

$$SN_i = -10\log\left[\frac{1}{N}\sum_{u_i}^{N}\frac{1}{y_u^2}\right] \qquad (4.5)$$

After calculating the SN ratio for each experiment, the average SN ratio for each factor and level is established. The range R for every parameter is calculated (max SN – min SN), meaning that, the larger R for a parameter, the higher its effect on the process. Using SN ratios enables the maximization of the robustness of a process simply by selecting the levels of control factors that have the largest SN ratio. Linearity, one of the components of the SN, is important for simplifying adjustment in process design as well as for calibration of measurement systems. When the input/output relationship is not linear, the deviations are evaluated as the error after decomposing the variations; therefore, the SN ratio becomes smaller [51].

All the experiment data were statistically analyzed with the MINITAB software for quality improvement. Analysis of Variance (ANOVA) was selected fo the statistical analysis. ANOVA compares the mean results of several groups of parameters and measures the variances of the recorded data. Variances are separated into systematic variances (due to experimental process effects) and unsystematic variances (due to errors and mal-functions). The ratio between these two variances is the so called "F ratio/value". There are one-way ANOVA (a single independent variable and more levels or groups) and factorial ANOVA (two-way, three-way etc., with two or more variables) [57].

4.2.7. Temperature measurement

The measurement of the temperature developed during FricRiveting of PEI-GF and Titanium grade 2 was carried out by infrared thermography. The temperature measurement system consisted of an infrared thermo camera (High-end Camera Series ImageIR, Infratech GmbH, Germany), connected to a computer with data collection and processing software (IRBIS 3 Professional).

The data was collected at 80Hz at a calibration range of 150ºC to 600 ºC. Titanium rivets and the PEI-GF plates were coated with mat black paint in order to minimize light reflections. The measuring working distance was 425 mm, from the

objective of the IR camera to the touch-down area of the rivet on the polymeric plate, at an incidence angle of 50°.

The temperature was recorded during joining, from the expelled polymeric matrix material, on the contact area between rivet and polymer. Because of the low thermal conductivity of the polymer, one can assume that the measured average temperature in the softened flash material is nearly the same as in the molten layer of polymer around the plasticized rivet tip [35]. Two replicates form each of the conditions used in the DOE were joined and measured with the IR camera, as shown in Figure 4.8 and 4.9.
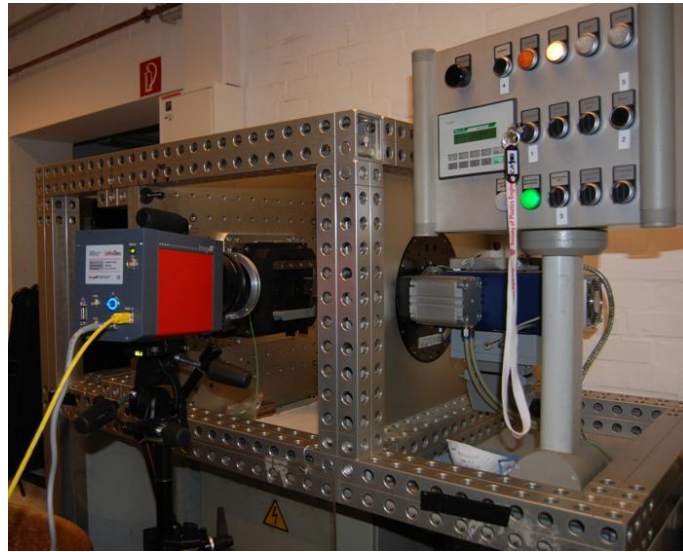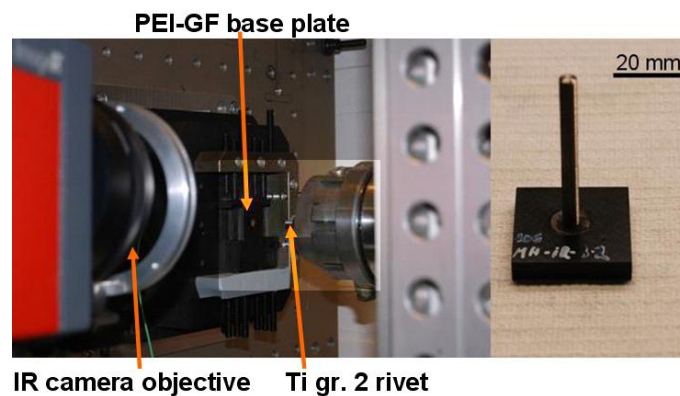

Figure 4.8 − Infrared temperature measurement assembly

Figure 4.9 − Specimen for temperature measurement
(left − clamped, prior to joining; right − after joining)

4.3. Materials

4.3.1. Aluminum AA 2024-T351 rods

Extruded rods of aluminum AA 2024 (Figure 4.10) were used to produce rivets for the point-on-plate friction riveted joints. Aluminum 2024 (AlCu4Mg) is a wrought heat treatable alloy of the 2000 aluminum series, with the main alloy elements Cu and Mg [52]. The nominal chemical composition of this alloy is presented in Table 4.4.
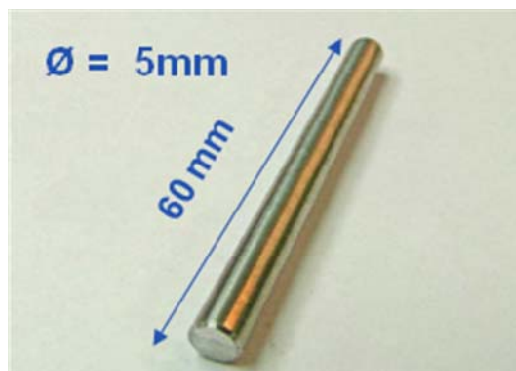

Figure 4.10 – Extruded AA 2025-T351 rod

Table 4.4

Chemical composition of aluminum AA 2024 [52]

Wt%	Cu	Mg	Si	Mn	Fe	Zn	Cr	Ti	Al
ASM (nominal)	3,8-4,9	1,2-1,8	<=0,5	0,3-0,9	<=0,5	<=0,25	<=0,1	<=0,15	bal.

The Al "2xxx" series have copper (Cu) as the main alloy component. The second digit in the designation indicates the alloy modification, ranging from 0 to 9, where 0 indicates the original alloy (no modification) and so on. The last two digits have no special significance, serving only to the identification purposes [52].

The designation system for aluminum alloys is based on the major alloying elements, as following [54]:
- 1xxx:aluminum of 99,0% purity or higher
- 2xxx: copper
- 3xxx: manganese
- 4xxx: silicon
- 5xxx: magnesium
- 6xxx: magnesium and silicon
- 7xxx: zinc
- 8xxx: other elements

The "T351" designation to the tempering: heat treatment, up to 495°C, cold worked by stretching and naturally aged to a stable condition. In the T351 tempering, the wrought alloy is heat-treated, stress-relieved by controlled

stretching and then naturally aged, as mentioned; there is no further straightening after stretching [54]. This alloy is characterized by good machinability and workability, having a fair corrosion resistance. It is widely used in the aeronautic industry, for fuse parts, fittings, bolts, nuts or fastening devices [52]. For improved corrosion performance, cladding is recommended. The main mechanical properties according to [52] are presented in table 4.5.

Table 4.5

Mechanical properties of AA 2024-T351

Property	Charactertistic value	units
Tensile strength, ultimate	441	MPa
Tensile strength, yield	290	MPa
Elasticity modulus	73	GPa
Shear strength	276	MPa

According to the same sources, AA 2024-T351 has a density of 2,78 g/cm³ and a thermal conductivity of 122W/m.K. For the joining plain-, hollow- and hollow-threaded rivets were used. The threads and hollows were produced by machining of the plain rivets with a Knuth Basic 180 Super lathe machine. Figure 4.11 shows the used Al 2024-T351 rivet geometries while their dimensions are displayed in table 4.6.
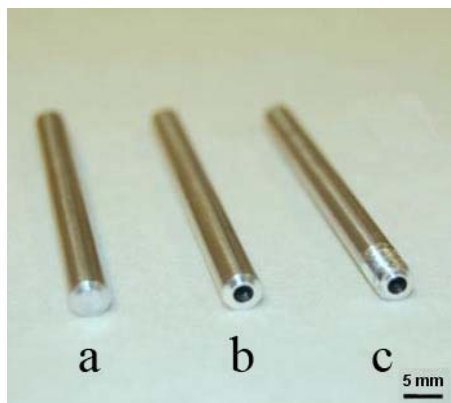

Figure 4.11 – rivet geometries (a – plain, b – hollow, c – hollow)

Table 4.6

Characteristics and dimensions of the rivets

Rivet type	Length [mm]	Diameter [mm]	Internal diameter [mm]	Depth [mm]
Plain	60	5	-	-
Hollow	60	5	2,5	20
Hollow / thread	60	5	2,5	20 / 8

4.3.2. Aluminum AA 2198 plates

AA 2198-T851 sheets of 3 mm thickness were used for the lap shear tests, as described in. The AA 2198 alloy has Al, Mg, Cu and Li as main alloy components. The lithium content offers the advantage of lower density compared to common Al alloys and an increase in elasticity modulus. Regarding the temper designation, "T8" means that the wrought alloy was heat-treated, and cold worked and then artificially aged [54].

The rolled sheets used in this work were previously characterized by Pieta and dos Santos [97], with the resulting chemical composition displayed in Table 4.7

Table 4.7

Chemical composition of Aluminum AA 2198-T851 [97]

Wt%	Fe	Cu	Li	Mg	Mn	Ag	Si	Ti	Zr	Al
nominal	0,04	3,40	0,80	0,27	0,04	0,18	0,03	0,03	0,10	bal.

4.3.3. Titanium rods

Extruded titanium grade 2 rivets with the length of 60 mm and a diameter of Φ 5 mm were used. Both plain surfaced rivets and M5-threaded rivets were tested. The chemical composition according to the literature [52] is presented in table 4.8

Table 4.8

Chemical composition of Titanium grade 2

Wt%	C	H	Fe	N	O	Ti
ASM (nominal)	<=0,10	<=0,015	<=0,30	<=0,030	<=0,25	bal.

Titanium grades 1, 2, 3, 4, 7, 11 and 12 are considered unalloyed (commercially pure grades) [52]. In order to understand the different behaviour of the titanium grades used in this approach, the main mechanical and thermal properties of the titanium grades affective the Fricriveting process are listed in Table 4.9

Table 4.9

Comparative mechanical and thermal properties of different titanium grades [52]

ASTM grade	Mechanical properties			Thermal properties
	Tensile strength, ultimate (MPa)	Tensile strength, yield (MPa)	Thermal conductivity (W/m-K)	Melting temperature (ºC)
Titanium grade 1	240	170	16,0	1670
Titanium grade 2	344	275	16,4	1665
Titanium grade 3	440	377	19,9	1600
Titanium grade 5	950	880	6,7	1660

Titanium grade 2 is a commercially pure titanium alloy with high strength, high specific strength and good corrosion resistance. It is usually applied in the automotive, aerospace or chemical plant industries. It has a density of 4,51 g/cm³ and a thermal conductivity of 16,4 W/m.K. Its melting point is at 1665 ºC.

In the course of the experimental program, other titanium grades were also investigated, mostly for the purpose of demonstrating the impact of joining parameters correlated with the different thermal and mechanical properties of the alloys. Subsequently, joint combinations of PEI-GF or P-GF with titanium grade 1, 3, and 5 were tested. According to the literature [52], titanium grade 5 (known also as Ti-6-4 or Ti6Al4V) has a tensile strength of 950 MPa (ultimate), Vickers hardness of 349 HV and a thermal conductivity of 6,7 W/m-K, therefore roughly over two times stronger than Ti gr. 2 at less than a half of its thermal conductivity.

4.3.4. Glass fiber reinforced polyetherimide (PEI-GF)

Glass-fiber-reinforced polyetherimide laminated sheets (Figure 4.15) were used for all conducted analysis, with a thickness of 6,2 mm. The PEI-GF composites were manufactured by TenCate Advanced Composites (Holland) by plying up 28 plies, at a ply thickness of 0,24 mm per ply. PEI-GF is a high strength, chemical and heat resistant composite, used mostly in the aerospace industry, for structural and interior applications, paneling and other industrial or recreational applications [7]. Due to its anisotropy, the mechanical properties (Table 4.10) of this composite will be referred to as in "warp" of "weft" directions. Basically, "warp" is along the length of the main fibers' direction and "weft" means along the width.

Table 4.10

Mechanical/physical properties of PEI-GF [53]

Property	Charactertistic value		units
	Warp	Weft	
Densidty	1,91		g/cm³
Tensile strength	484	445	MPa
Tensile modulus	26	24	GPa
Compression strength	727	676	MPa
Compression modulus	29	27	GPa
In plane shear strength	129		MPa

The stacking sequence of the plies was [0º, 90 º]. The resin content of the composite is situated at 50% in terms of volume and 33% by weight. PEI-GF has a glass transition temperature (Tg) of 210ºC and a thermal conductivity of 0,22 W/m-K. PEI is an amorphous polymer. In the solid state it is hard and rigid, whereby amorphous polymers are also transparent, thus being glass-like; due to this fact, the solid state of amorphous polymers is referred to as the "glassy state". Therefore, the glass transition temperature refers to the temperature above which the polymer translates into the rubbery state, in which molecular segment movements become possible. Semi-crystalline polymers have crystallites in addition to glassy regions; therefore they have an additional transition temperature, the melting temperature (Tm), above which the crystalline structure is destroyed. Tm is always higher then Tg [12].
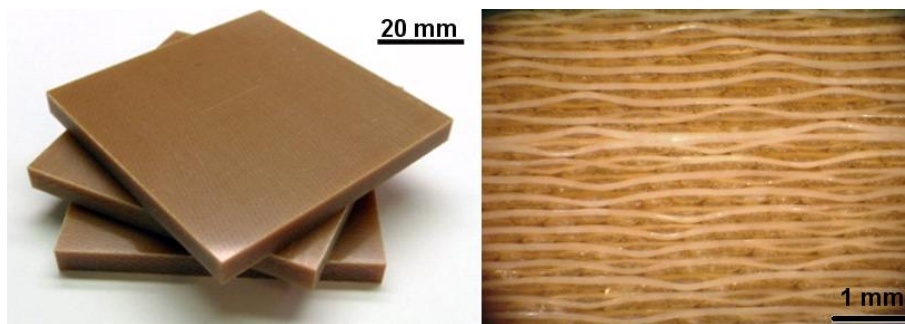

Figure 4.15 - PEI-GF T-pull specimens (left) and
cross sectional microscopy view (right)

4.3.5. Glass fiber reinforced polyester (P-GF)

Pultruded glass-fiber-reinforced polyester, commonly used in bridge construction [86] was selected to evaluate the feasibility of FricRiveting in thermoset composites. The pultruded composite sheets were produced by Fiberline Composites A/S, Denmark, designated as P-GF. The challenge was that, theoretically, thermoset polymers cannot be welded because they do not melt upon heating [6], while FricRiveting is a friction welding related process. The pultruded P-GF composite is used as structural profiles for bridges in various shapes and sizes, mostly cross sections common to steel constructions, as shown in Figure 4.16.
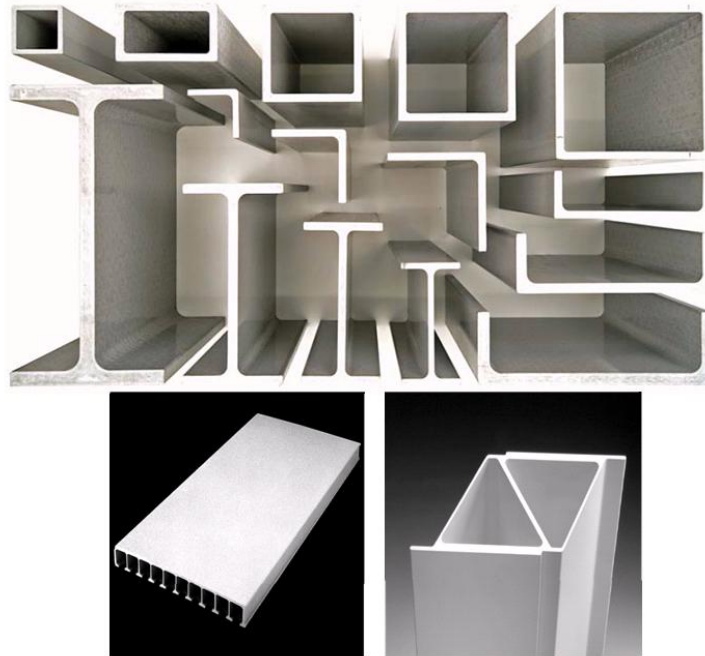
Figure 4.16 – Pultruded structural shapes used in bridge constructions
(Image courtesy of Fiberline Composites A/S) [4]

　　　For this anisotropic material, the mechanical properties are referred to as parallel (0º) or transversal (90 º) to the pultrusion direction. The parallel direction coincides to that of the main load carrying fibers. For the feasibility tests and the related T-pull tests, 10 mm thick GF-P sheets were used. The mechanical properties of this thermoset polyester based composite, as provided by the manufacturer, are shown in Table 4.12. The thermal conductivity of P-GF ranges from 0,25 to 0,35 W/m-K.

Table 4.12

Mechanical properties of GF-P [4]

Property	Charactertistic value		units
	0º	90º	
Densidty	1,89		g/cm³
Tensile strength	240	50	MPa
Elasticity modulus	28	8,5	GPa
Compression strength	240	70	MPa
Shear strength	25		MPa

5. RESULTS AND DISCUSSION

5.1. Overview

Results will be presented in accordance to the experimental approach described in chapter 4.1 in order to provide the experimental part of the thesis a logical structure. Therefore, each subchapter discussing results will be divided into parts related to the different materials combinations tested. The feasibility studies in chapter 5.2 have an eliminatory character in the experimental approach, meaning that further mechanical testing (chapter 5.3) was carried out only for selected material combinations were the full and direct feasibility has been proved. For the other materials combinations, further research is needed, as it will be addressed in chapter 8. Finally the most adequate combination of GFR/metal was optimized and evaluated by design of experiments (chapter 5.4 to 5.6). From this analysis the optimal joining condition was selected for further structural analysis (chapter 5.7) where a bridge structure and a connector element were presented and discussed.

5.2 Feasibility study

5.2.1. Fricriveting of PEI-GF / Aluminium AA 2024-T351

The initial Fricriveting parameters for this material combination were selected on the basis of previous work with unreinforced PEI joined with AA 2024-T351 [35]. The mechanical and thermal material properties are important factors influencing the heat generation and deformation of the rivet tip [35]; therefore they must be considered when selecting the joining parameters necessary to allow friction riveted joints to form. Nevertheless, FricRiveting of GFRP bring up new several challenges in comparison to the unreinforced Plastics. For the specific case of the PEI-GF laminates the challenges identified were:
- increased toughness of the base plate
- elevated number of woven plies (28 stacked up plies) across the thickness of the composite, each providing additional resistance to the penetration of the metallic rivet into the composite
- glass fiber reinforcement can be severely damaged by the insertion of the rivet.
- the reduced amount of polymeric matrix and the high amount glass fiber reinforcement will also change the generation and conduction of frictional heat to the polymeric matrix, the later due to its high thermal isolation effect
- in case of excessive heat generation, glass fibers are prone to ignite

5.2.1. a Parameter study

The influence of the parameters on the formation of the joints has been studied through the one-fact-at-a-time (OFAT) design of experiments. For the first

trials, similar parameters were chosen as in the case of the unreinforced PEI (Joining Time of 3s, Friction Pressure of 4 bar and Forging Pressure of 6 bar [35 rotational speed was decreased to 12000 rpm, having in mind the above mentioned issues related to influence of the glass fiber reinforcement on heat generation. In first instance, the joints were evaluated through qualitative observations: rivet anchoring in the composite (by manually moving the rivet forwards and backwards perpendicular to the rivet length axis) and the generation of smoke, ashes, sparks or even fire. Plain rivets have been used initially, with a length of 60 mm and an Φ 5 mm diameter. The reference free rivet length was 36,5 mm, the rest of the length being clamped in the spindle of the described Fricriveting joining equipment.

The parameters used in the first Fricriveting trials for PEI-GF and AA 2024-T351 are shown in Table 5.1. Specimen designations for all the conducted tests have been made using the name of the composite first, separated by a dash line followed by the material of the metallic rivet and an assigned number of the trial.

Table 5.1

Fricriveting joining table – initial tests for PEI-GF/AA 2024-T351.

Sample	RS (rpm)	FT (ms)	FOT (ms)	FP (bar)	FOP (bar)
PEI-GF/Al2024-1	12000	1500	1200	4	6
PEI-GF/Al2024-2	12000	1500	1200	4	6,5
PEI-GF/Al2024-3	12000	1500	1200	4	7
PEI-GF/Al2024-4	15000	1500	1200	4	6,5
PEI-GF/Al2024-5	12000	1200	1200	4	6,5
PEI-GF/Al2024-6	12000	1200	1200	4	6

The observations on the initial tests revealed, in accordance to the issued challenges stated above, the generation of smoke, a high amount of ashes and even spark. Therefore, rivet anchoring was not achieved and the two materials could not be joined in this stage. In order to continue the pursuit for the joint formation, the failed joints had to be analysed and compared in terms of geometrical and microstructural aspects (from the optical micrograph of the rivet mid cross section), meaning deformation of the rivet tip, insertion depth and level of dark material at the rivet vicinity and ashes on the surface of the joint (an indication of thermal degradation of the material in the joint area).

Figure 5.1 present an example for the analysis of the influence of the forging pressure (FOP) on joint geometry and microstructure of PEI-GF /AA 2024-T351. The influence of other joining parameters on the features of the PEI-GF/Al2024 joints is presented in Appendix 2. It can be observed from Figure 5.1, that the deformation of the rivet tip has been achieved for all specimens on one hand, while on the other hand, the level of thermally degraded material (ashes), mostly on the surface of the composite, led to the lack composite volume around the deformed rivet. The insertion depth was also insufficient; parts of the deformed rivet could be seen outside of the joint area, over the surface of the composite. Therefore rivets were not fixed in the composite.
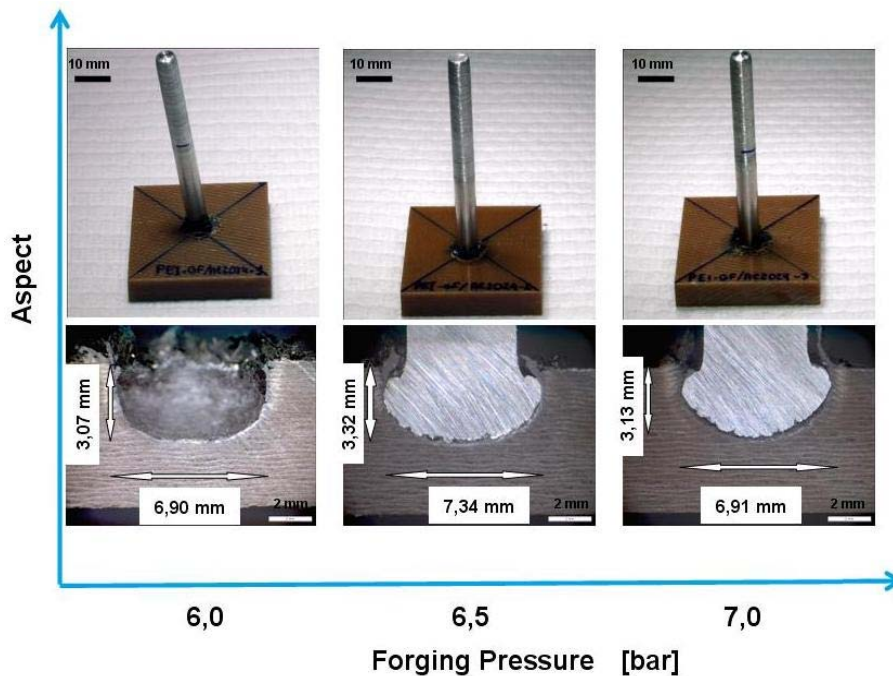
Figure 5.1 – Influence of the forging pressure on the defective PEI-GF/Al 2024 joints (conditions PEI-GF/Al2024 1, 2, 3 with constant RS= 1200 rpm, FT= 1500 ms, FOT= 1200 ms, FP= 4 bar)

One of the preliminary observations during the first parameter study was that the free rivet length used could be too short, a possible reason for the generally low rivet insertion in comparison to the results for unreinforced PEI / AA 2024-T351 [REF].

Therefore, in order to try to increase insertion depths, the rivet length was increased to 38,5 mm. Considering that the FricRiveting machine in use is time-controlled, longer rivet lengths would possibly allow the frictional heat generation to start earlier, by the occurrence of a faster touchdown of the rotating rivet on the composite surface. Therefore rivet would theoretically penetrate more in the composite. The new parameters combinations tested with the longer rivet are presented in Table 5.2.

Table 5.2

Fricriveting joining table – free rivet length of 38,5 mm for PEI-GF/AA 2024-T351

Sample	RS (rpm)	FT (ms)	FOT (ms)	FP (bar)	FOP (bar)
PEI-GF/Al2024-8	12000	1500	2000	3,5	6
PEI-GF/Al2024-9	10000	1500	2000	3,5	6
PEI-GF/Al2024-10	8000	1500	2000	3,5	6
PEI-GF/Al2024-11	8000	2000	2000	3,5	6
PEI-GF/Al2024-12	10000	1500	2000	3,5	5
PEI-GF/Al2024-13	10000	2000	2000	3,5	6

The joints produced with the conditions from table 5.2 were valid, meaning that, at observational level, the rivet was fixed, as a sign of anchoring in the composite and joint formation. In figure 5.2, the influence of the rotational speed on the valid joints was selected to exemplify the second parameter study. As it can be observed in the figure, in the case of the valid joints, the thin layer of degraded material around the tip of the rivet (revealed as dark material) seems to be slightly reduced. Although the two parts have been joined, results are still unsatisfactory in respect to the rivet insertion depth, which appears not be strongly changed by the increase in the free length of the rivet (compare Figures 5.1 and 5.2). The ratio of width (deformation) to depth of the deformed rivet tip, is witness of a low anchoring level and thus a probable low strength of the joints is expected. More on aspect ratio of the deformed rivet will be discussed in chapter 5.3 (tensile testing).

As a preliminary conclusion, Fricriveting for PEI-GF and aluminium AA 2024-T351 plain rivets was evaluated as unfeasible. It was possible to insert the rivet into the composite plate; the whole process of Fricriveting took place, with the tip of the rivet being deformed. Nevertheless, due to the high thermal conductivity of the aluminium alloy- which helps to accelerate the taking up of the heat being generated - and the several successive plies of PEI-GF having to be penetrated, the plasticizing of the rivet took place to close to the surface of the composite. Extensive thermal degradation (burning) of polymer and fibres associated with excessive heating was present around the tip of the rivet and on the surface of surface of the composite for all investigated specimens. Therefore only deficitary anchoring zones were formed, leading to weak joints.

The generated heat during the process was considerably high and barely controllable. This led to the generation of a high amount of smoke, sparks and even fire, a witness thereby being the degraded burned up material. An important general aspect, observed from the microstructural analysis the, is that the thermal degradation did not appear to be strongly spread inside the composite, but mainly on the surface, around the rivet insertion area. Further thermal analysis (a subject out of the scope of this work) is required to better understand the influence of heat on the thermal degradation of the PEI-GF composite.
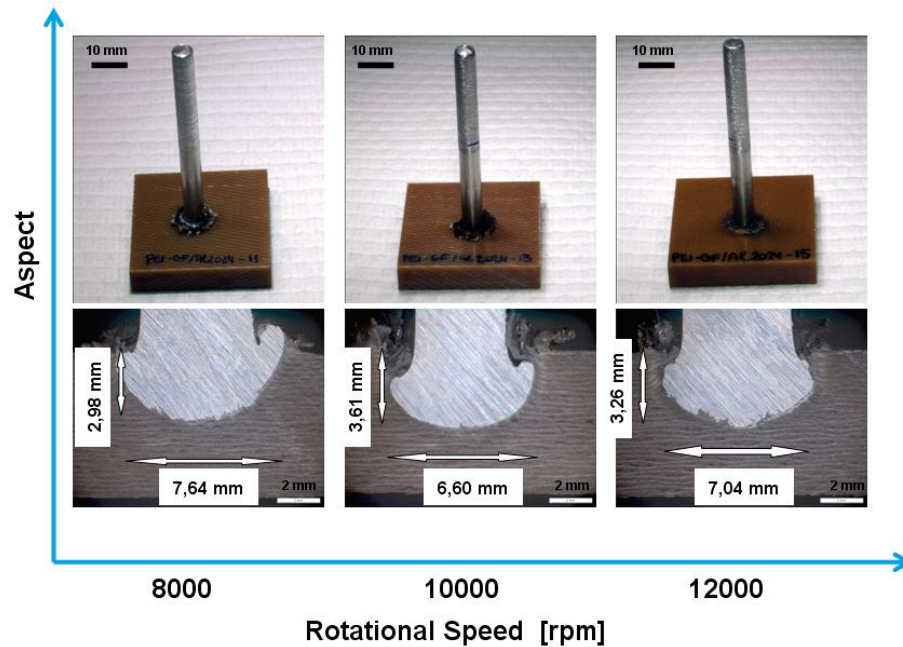
Figure 5.2 – Influence of the RS on the valid PEI-GF/Al 2024 joints
(conditions PEI-GF/AA204- RS 8000-10000-12000 rpm with constant FT 2000 ms,
FOT 2000 ms, FP 3,5 bar, FOP 6 bar)

5.2.1. b Influence of the rivet tip geometry

The feasibility study for PEI-GF and AA 2024-T351 was not abandoned after the preliminary conclusion. Another approach was to try to decrease the heat input, by decreasing the frictional surface between the rivet and the composite plate. This was attempted by and using hollow rivets. Therefore, as mentioned in chapter 4.3, the plain rivet tips were machined, producing Φ 2,5 mm diameter holes, 20 mm deep through the length of the rivet (see Table 4.6, Chapter 4.3.1). Additionally to the holes, some rivets have M5 threads cut over a length of 10 mm. They were applied in order to evaluate the additional drilling effect (similar to effect found in self-thread cutting screws), which would allow a better puncture of the stacked plies. In this way hollow-threaded rivets would assumedly lead to a deeper insertion in the composite plate. The appearance of the different types of rivet geometries used in this work can be seen in Figure 5.3.
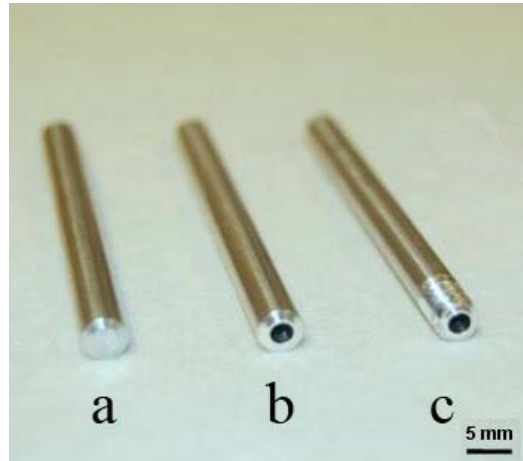
Figure 5.3 – rivet tip geometries used for PEI-GF/AA 2024-T351
(a – plain, b – hollow, c – hollow–threaded)

In order to conduct the study of the influence of the different rivet geometries, a condition was selected from the initial feasibility study, where the resulted joint had relatively good values for deformation and insertion depth and with a reduced degree of thermal degradation at the same time: Rotational Speed of 10000 rpm, Friction Time of 1500 ms, Forging Time of 2000 ms, Friction Pressure of 3,5 bar and Forging Pressure of 6,0 bar. The cross sectional view of the investigated joints is shown in Figure 5.4, for the comparison of the three cases (plain rivet, hollow rivet and hollow-threaded rivets).
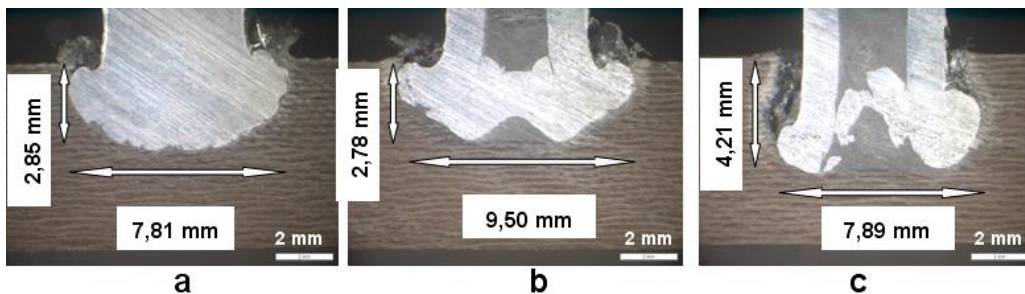
Figure 5.4 – Cross sectional views of PEI-GF/AA 2024 joints for the rivet geometry comparison : a – plain rivet, b – hollow rivet, c – hollow threaded rivet (condition PEI-GF/Al2024- with RS= 10000 rpm, FT= 2000 ms, FOT= 2000 ms, FP = 3,5 bar FOP= 6 bar)

Figure 5.5 shows the graph of the variation of the rivet width (representing the deformation) and depth (representing the insertion) of the specimens analysed. In both cases of modified rivet geometries - hollow and hollow-threaded- an large variation in the level of rivet deformation (width) was not observed in comparison to the plain rivet (compare Figures 5.5 a, b and c). But, as previously mentioned, this approach had the purpose of achieving higher insertion depths, while it was already proved that the rivet could be deformed. The threads had the initial presumed role of providing a drilling effect, thus achieving a better insertion. Although a slight

increase in the insertion for the hollow-threaded riveted specimen was observed on one hand, on the other hand the amount of volumetric flaws and thermally degraded material seems to be higher than for the plain rivet specimens. Therefore, such a joint, event tough valid in terms of deformation and insertion depth, would most certainly be unstable from the mechanical strength point of view.
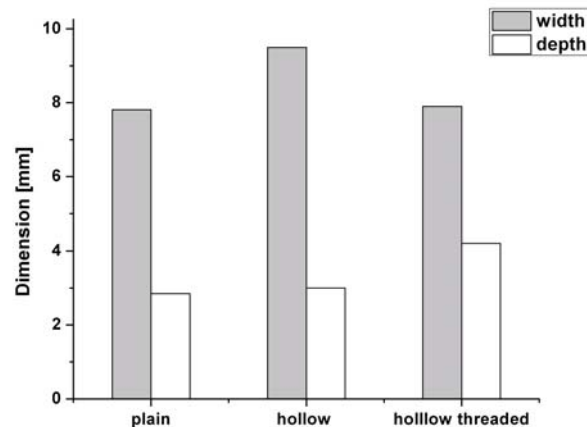

Figure 5.5 – Variation of the width (deformation) and depth (insertion) of the deformed rivet related to the rivet tip geometry characteristics in Figure 5.4.

Another important aspect that can be observed in the hollow-threaded rivet specimen is the fracture of a part of the metallic material inside the hole. This might have been caused by the different temperatures of the inner (colder) and outer (hotter) surfaces of the rivet, which may induce an inhomogeneous plasticizing of the rivet's tip. This difference in the temperature of the inner and outer regions of the rivet in the frictional area, was reported to be related to the influence of the rivet radius on the rivet's tangential speed [35]. Amancio-Filho reported that tangential speed plays an important hole in heat generation and therefore in the temperature distribution [36]. A magnified view of the thermal degraded material around the deformed hollow threaded rivet can be seen in Figure 5.6.

Regardless the presence of flaws and thermally degraded materials in their microstructure, the three rivet geometry conditions were separated to be part of the selection of the best GFRP/Rivet combination to be discussed in chapter 5.3.
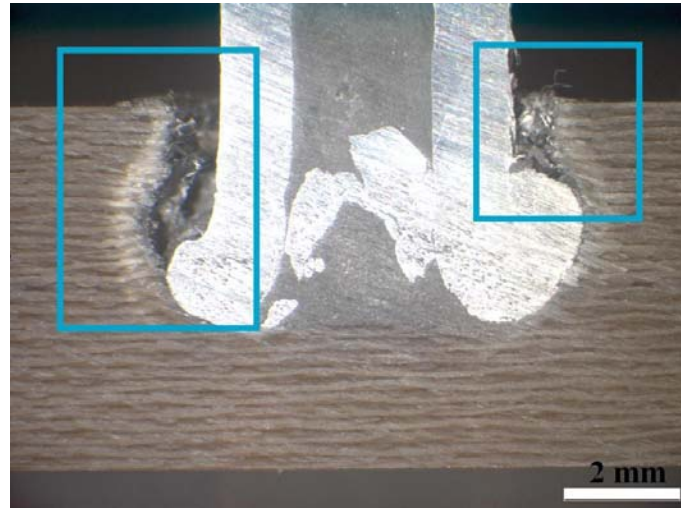
Figure 5.6 – Magnified view of the of the hollow-threaded rivet specimen presented in Figure 5.4 b: the rectangles indicate the thermally degraded composite material.

5.2.2. Fricriveting of PEI-GF / Titanium grade 2

The initial parameters for the feasibility study on PEI-GF / Ti Gr. 2 alloy were chosen, by taking into account the preceding experience with the combination PEI-GF / AA 204 aluminium alloy. Both alloys have similar tensile strengths, however Ti Gr.2 has about seven times smaller thermal conductivity of than the aluminium alloy (see Chapter 4.3.3). Therefore the heat dissipation and deformation of the plasticized titanium rivet will follow a different pattern than of the aluminium rivets. Plain titanium grade 2 rivets was used in this feasibility study. Table 5.3 shows the parameters used in the initial tests:

Table 5.3
Fricriveting joining table – initial tests for PEI-GF/Tigr2 materials combination.

Sample	RS (rpm)	FT (ms)	FOT (ms)	FP (bar)	FOP (bar)
PEI-GF/Tigr2-1	20000	700	1200	6	10
PEI-GF/Tigr2-2	15000	700	1200	6	10
PEI-GF/Tigr2-3	10000	700	1200	6	10
PEI-GF/Tigr2-4	8000	700	1200	6	10
PEI-GF/Tigr2-5	7000	700	1200	6	10
PEI-GF/Tigr2-6	6000	700	1200	6	10
PEI-GF/Tigr2-7	4500	700	1200	6	10
PEI-GF/Tigr2-8	6000	800	1200	6	10
PEI-GF/Tigr2-9	6000	900	1200	6	10
PEI-GF/Tigr2-10	6000	1000	1200	6	10
PEI-GF/Tigr2-11	6000	1100	1200	6	10
PEI-GF/Tigr2-12	6000	1200	1200	6	10
PEI-GF/Tigr2-13	12000	700	1200	6	10
PEI-GF/Tigr2-14	12000	500	1200	6	10

PEI-GF/Tigr2-15	10000	700	1300	6	10
PEI-GF/Tigr2-16	9000	700	1200	6	10
PEI-GF/Tigr2-17	8000	500	1200	6	10
PEI-GF/Tigr2-18	8000	400	1200	6	10
PEI-GF/Tigr2-19	8000	600	1200	6	10
PEI-GF/Tigr2-20	8000	700	1300	6	10
PEI-GF/Tigr2-21	8000	700	1500	6	10
PEI-GF/Tigr2-22	8000	700	2000	6	10
PEI-GF/Tigr2-23	8000	700	2500	6	10
PEI-GF/Tigr2-24	8000	700	3000	6	10
PEI-GF/Tigr2-25	8000	700	3500	6	10
PEI-GF/Tigr2-26	6000	700	1500	6	10
PEI-GF/Tigr2-27	6000	700	2000	6	10
PEI-GF/Tigr2-28	6000	700	2500	6	10
PEI-GF/Tigr2-29	6000	700	3000	6	10
PEI-GF/Tigr2-30	6000	700	3500	6	10
PEI-GF/Tigr2-31	8000	700	2500	6	10
PEI-GF/Tigr2-32	9000	700	2500	6	10
PEI-GF/Tigr2-33	10000	700	2500	6	10

. The qualitative observations (the same as in the case of PEI-GF/AA2024) revealed the anchoring of the rivet inside the composite plate, in all cases. (see Appendix 3 for cross sectional views of the joining conditions presented in Table 5.3). On the other hand, the amount of smoke generated was relatively high, stating a high heat input of the process and thereby possible thermal degradations of the composite material. Therefore, the heat input was gradually reduced, by decreasing of the rotational speed [40], from the initial 20000 rpm until 4500 rpm.

Figure 5.7 shows the first actual valid PEI-GF/Tigr2 friction riveted joint. The thermal degraded material (darkened flash) can be seen around the inserted rivet, consisting partly of molten composite material and mainly from burned molten glass fibers.
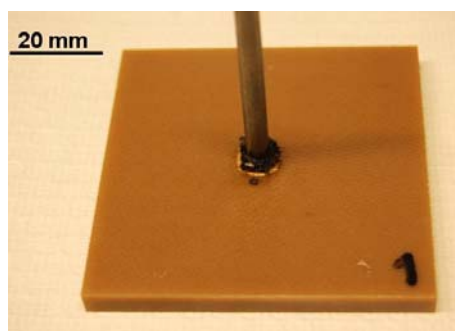

Figure 5.7 – Surface view of first successfully obtained PEI-GF/Tigr2 point-on-plate joint through FricRiveting (RS= 20000 rpm, FT= 700 ms, FOT= 1200 ms, FP= 6 bar, FOP= 10 bar)

The geometry of the deformed tip of the rivet and microstructure of the joint presented in Figure 5.7 can be observed in Figure 5.8. As previously mentioned, the

heat input of the process was reduced. This led not only to less smoke being generated, but also to lower levels of rivet deformation. In other words, the lower thermal degradation of the composite came at the expense of reduced widths and depths of the deformed rivet, causing a presumptive less strong rivet anchoring. Nonetheless, the smoke generation has to be taken into consideration, for Fricriveting being a potential environment friendly joining process. Therefore lower rotational speeds are preferred.
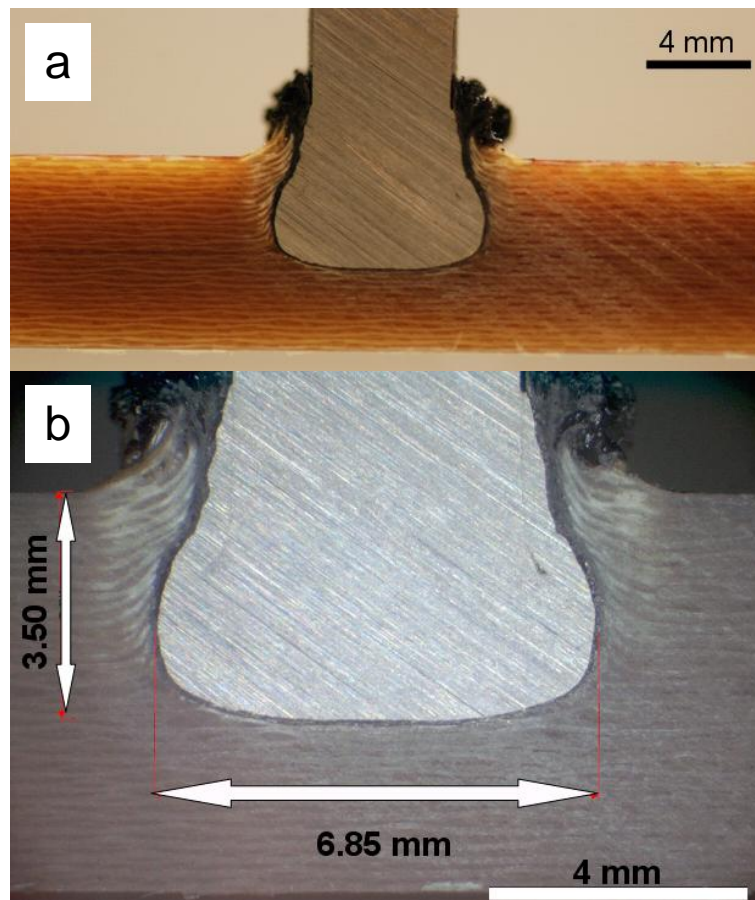
Figure 5.8 – Cross sectional view through the centre of PEI-GF/Tigr2 Friction riveted joint from Figure 5.7

Before reaching forward to mechanical testing of the joints, the optimal conditions (with reduced volumetric flaw, thermally degraded material and good rivet anchoring) were evaluated through an OFAT parameter study. For instance, the valid joints with the lowest rotational speed were the ones with 6000 rpm. The 6000 was established as the lower limit of rotational speed. Valid joints are considered the ones where rivet anchoring was achieved.

Thereafter, while the joining pressure remained constant (FP= 6 bar, FOP= 10 bar), the influence of varying the forging time was analyzed. As expressed in the state of the art in Fricriveting [35, 36, 40], the parameters influencing rivet

deformation are Forging Time and Forging Pressure. With the forging pressure limited to 10 bar on the RSM 400 welding system (see Appendix 1), the only approach remaining in terms of forging was the variation of forging time. With the constant parameters at RS= 6000 rpm, FT= 700ms, FP= 6 bar, FOP 10 bar, the FOT was progressively increased from 1200 ms to 3500 ms. All the conditions having more than 2000ms had the rivet loosened and not anchored and therefore were considered not valid. Rivet deformation in both cases was small, as shown in the PEI-GF / Ti Gr.2 joint in Figure 5.9:
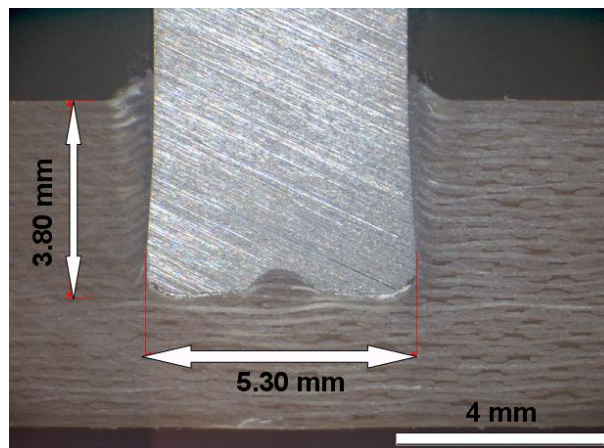
Figure 5.9 – Example of a PEI-GF/Tigr2 specimen showing the limited level of deformation of the rivet. (Condition: PEI-GF/Tigr2-26: RS= 6000 rpm, FT= 700 ms, FOT= 1500 ms, FP= 6 bar, FOP= 10 bar)

A similar analysis has been conducted for the rotational speed of 8000 rpm, friction time of 700 ms and the same constant joining pressure described above. As it cat be seen in Figure 5.10, the analysis revealed that the widths, after initially progressively increased with the FOT, had a descendent trend beyond 2500 ms. In the case of the depths (insertion of the rivet) FOT did not seem to cause any clear changes for this selected joining parameters range. This is in agreement with the observations of Amancio-Filho [35]; he reported that for unreinforced PEI / AA 2024 joints the increases in FOT and FOP did not bring any relevant increase in the rivet insertion. The graph in Figure 5.11 shows the variation of the width and depth related to the forging time.

Consequently the forging time of 2500 ms was set constant as the upper limit for FT in the next step of the parameter studies.
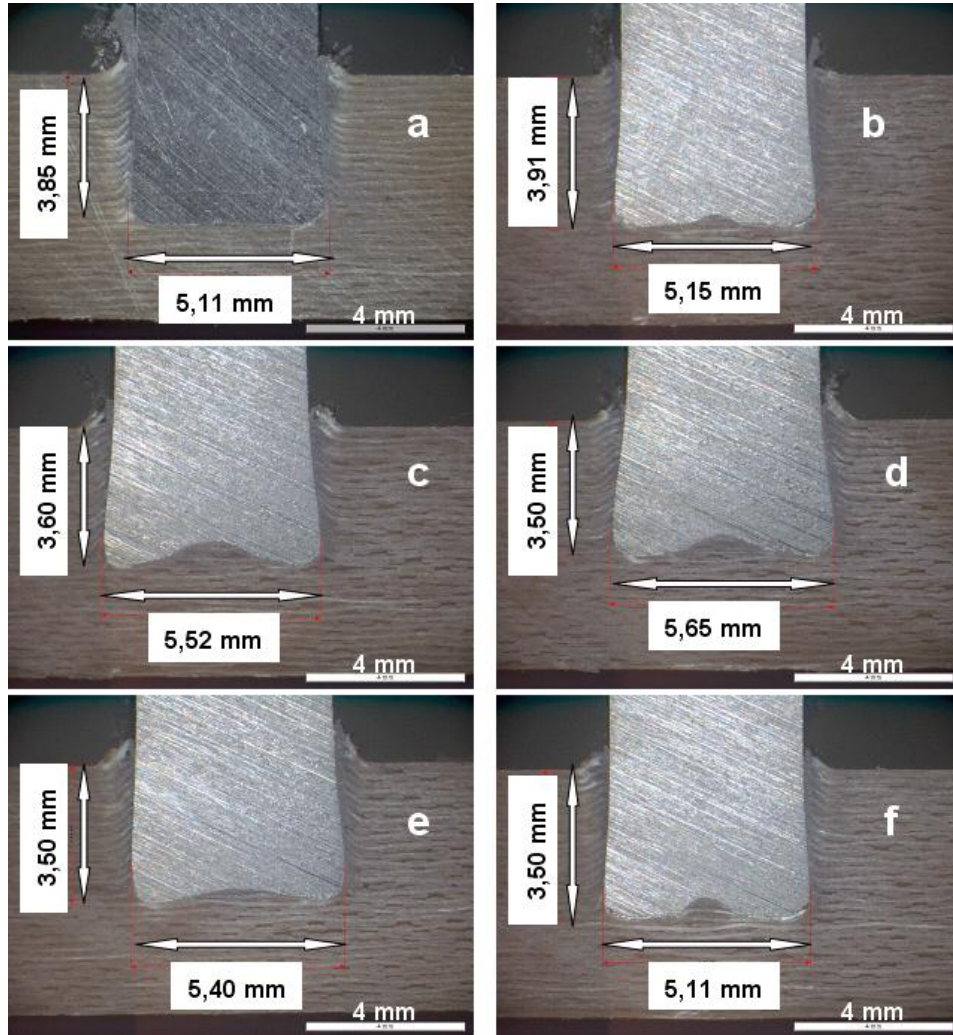
Figure 5.10 – Influence of the forging time on the microstructure of PEI-GF/Ti Gr.2 joints and varying FOT: a – 1200 ms, b- 1500 ms, c – 2000ms, d – 2500 ms, e – 3000 ms, f – 3500 ms (with constant RS= 8000 rpm, FT= 700 ms, FP= 6 bar, FOP= 10 bar).
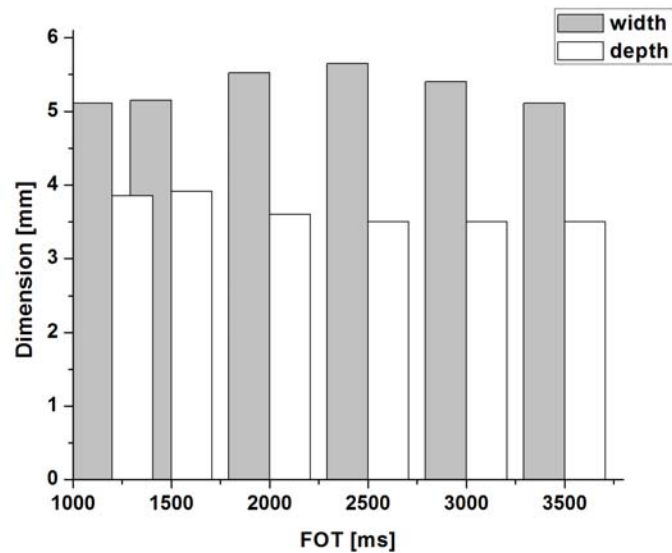
Figure 5.11 – Influence of forging time on the deformed tip of the rivet (width and depth) of specimens shown in Figure 5.10

With the objective to close the feasibility study of the PEI-GF /Ti Gr.2 joints, an evaluation of the influence of the rotational speed on the joint formation was carried out for the improved specimen with FT= 700 ms, FOT= 2500 ms FP= 6bar and FOP= 10 bar. The cross section views corresponding to the three conditions can be further seen in Figure 5.12. The changes in the geometry of the theses specimen are given in the graph of Figure 5.13.
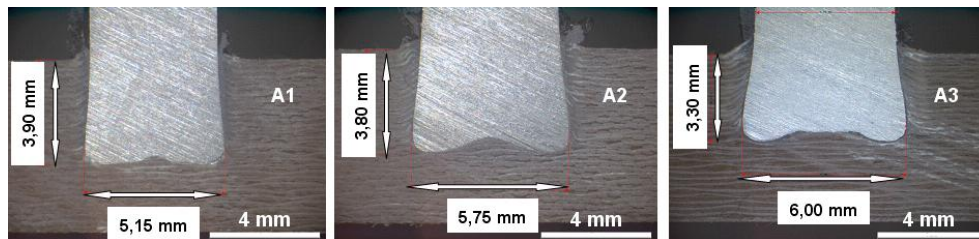
Figure 5.12 – Cross Sectional view of PEI-GF/RI Gr.2 specimens with varying rotational speeds: A1) 8000 rpm, A2) 9000 rpm and A3) 10000 rpm (conditions PEI-GF/Tigr2- 31, 32 and 33 at constant FT= 700 ms, FOT= 2500 ms, FP= 6 bar, FOP= 10 bar).
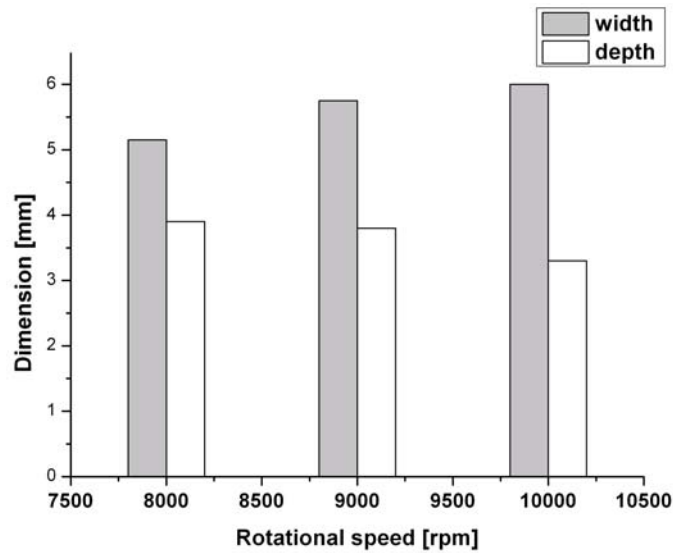
Figure 5.13- Influence of the rotational speed on the deformed tip of the rivet (width and depth) of specimens shown in Figure 5.12.

It is possible to observe from both figures that increasingly rotational speeds resulted in higher deformation (widths) on one hand, an on the other hand there was a slight reduction in the rivet insertion (depths). Moreover it appears, that the level of dark material around the deformed rivet was visually small and did not follow any precise variation pattern.

Amancio and dos Santos [39] have studied the influence of the rotational speed on the process temperature and the number of flaws in the consolidated polymer layer of PEI/AA 2024 friction riveted joints. They observed that the higher the rotational speed, the higher the process temperature was. It may explain the larger deformations and lower insertion depths observed at higher RS. At higher temperatures more heat is generated inducing a greater level of material plasticizing at the tip of the rivet. In the case of the PEI-GF laminate and its lay-up structure of plies, rivets with high plasticizing levels – in other words with lower mechanical resistance – will not be able to perforate the woven reinforcement deforming at smaller insertion depths, as seen in Figure 5.12.

Furthermore, the authors realized that, although process temperature appears to be directly proportional to rotational speed, the amount of thermo mechanically degraded polymer did not follow any clear pattern, as it was observed for the PEI-GF/Ti Gr.2 joints. This is probably associated to the high thermal resistance of the PEI matrix, which did not present high level of degraded material in the investigated range of joining parameters [40].

Considering that these three specimens qualitatively presented good rivet anchoring and reduced evolution of smoke and ashes, as well as absence of spark and fire these three conditions were selected for the tensile testing in chapter 5.3.

5.2.3 Fricriveting of thermosetting P-GF with titanium alloys

As a result of the observations from the other material combinations used in the previous tests, it was decided to undergo further basic feasibility studies for the thermosetting glass fiber reinforced polyester (P-GF). The parameter study for the thermoset was based on the heat generation (at qualitative level – smoke generation) and the level of deformation achieved when joining thermoplastic PEI-GF and titanium grade 2. As mentioned in chapter 4.3.3, the material of choice was a 10 mm thick pultruded plate and the composite and different grades of titanium (grades 1, 2, 3 and 5).

Using titanium grade 1 and grade 2 rivets, with similar joining parameters to the PEI-GF combinations, no valid joints could be produced. There was a high amount of dust generated and the rivets could not be anchored. Further tests using this material combination were abandoned for the research in this thesis. Table 5.4 presents the parameters used to produce the first valid joints of thermosetting P-GF with titanium grade 3 and titanium grade 5.

Table 5.4

Fricriveting joining table for P-GF and titanium grade 3 and 5

Sample	RS (rpm)	FT (ms)	FOT (ms)	FP (bar)	FOP (bar)
P-GF/Tigr3-1	8000	700	1200	6	10
P-GF/Tigr3-2	9000	700	1200	6	10
P-GF/Tigr3-3	10000	700	1200	6	10
P-GF/Tigr5-1	8000	700	1200	6	10
P-GF/Tigr5-2	10000	700	1200	6	10
P-GF/Tigr5-3	12000	700	1200	6	10

As a major breakthrough, it is worth mentioning that from the current knowledge of the author, the first joining of a thermoset with a metal was achieved (glass fibre reinforced thermosetting polyester with titanium grade 3 and titanium 5), through Fricriveting, as it is shown in Figure 5.13.
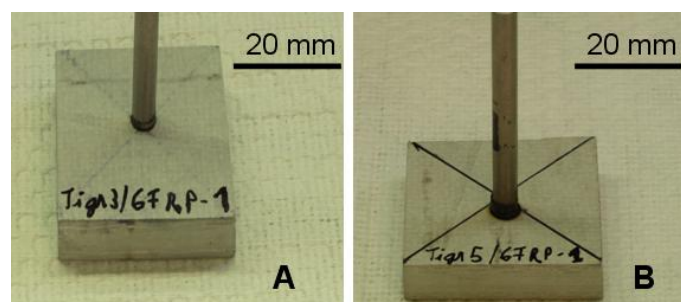

Figure 5.13 – Surface view of the first ever joints between a thermoset and titanium alloys: A) P-GF/Titanium grade 2 (condition P-GF/Tigr3-1) and B) P-GF/Titanium grade 5 (condition P-GF/Tigr5 -1)

It has to be also mentioned, that the heat generation at observational level was very high, producing a relatively large amount of dust and for some conditions

(e.g. with the highest rotational speeds) even glowing sparks. For both combinations (P-GF/Tigr3, respectively P-GF/Tigr5) the parameter study focused on the influence of the rotational speed. The macrographs of the P-GF/Tigr3 can be seen in Figure 5.14, with a detailed graph of the rivet deformations in Figure 5.15.
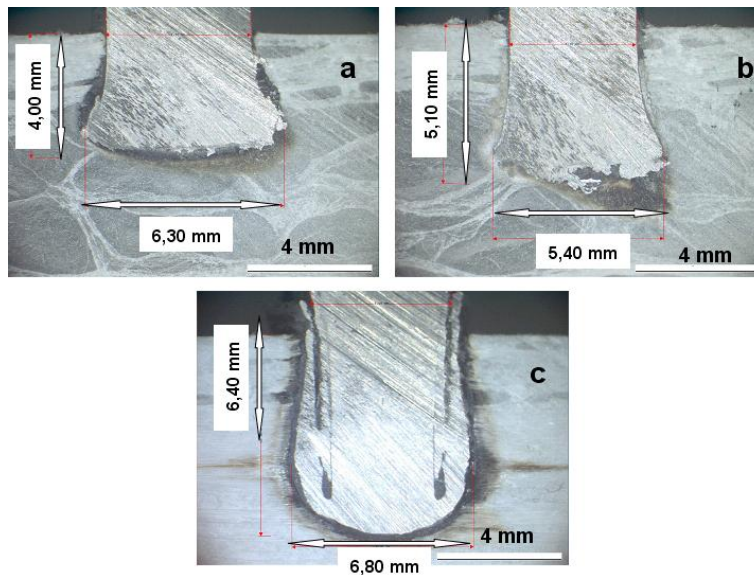

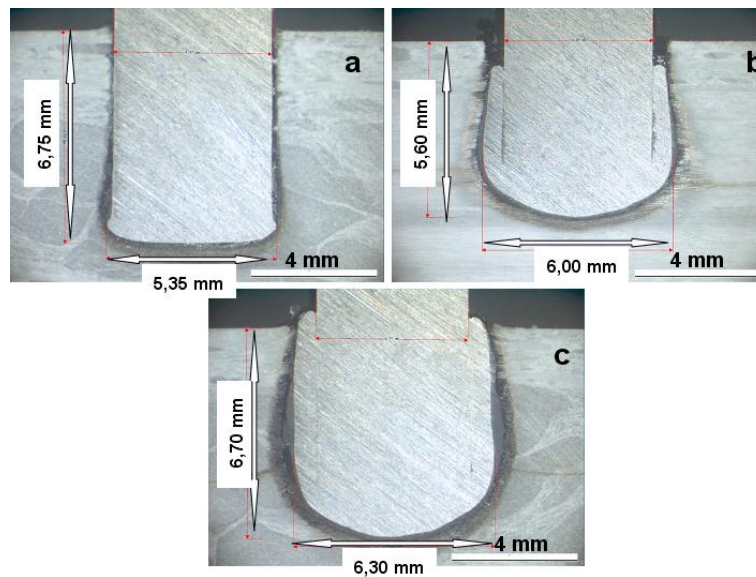Figure 5.14 – Cross sectional views of the P-GF/Tigr3 specimens: a) RS= 8000 rpm, b) RS= 9000 rpm and c) RS= 10000 rpm (conditions P-GF/Tigr3-1, 2, 3 at constant FT= 700 ms, FOT= 1200 ms, FP 6= bar, FOP= 10 bar).
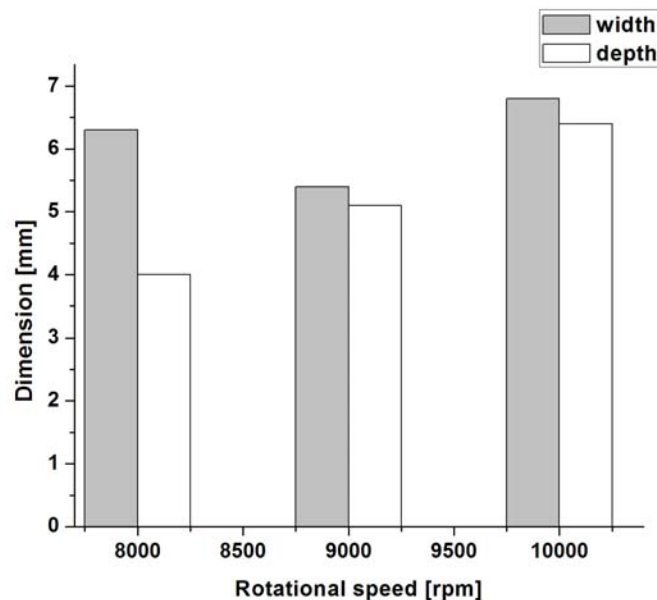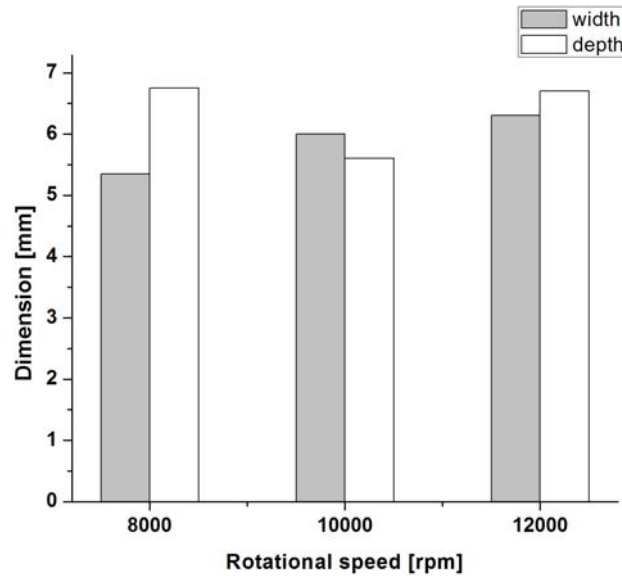

Figure 5.15 – Influence of rotational speed on the deformed tip of the rivet (width and depth) of specimens shown in Figure 5.14

The utilized approach in the case of the titanium grade 5 rivets was similar (variation of RS), , as it can be deduced from Table 5.4. One can observe that the level of rotational speed was selected higher than for P-GF/Ti Gr.3 specimens. This was intended to increase heat input and generate enough level of plasticizing at this high strength and low thermal conductive titanium alloy, Figure 5.16 presents the microstructure of the P-GF/Ti Gr. 5 specimens. The analysis of rivet anchoring (width and depth) is shown in Figure 5.17.

Figure 5.16 – Cross sectional views of the P-GF/Tigr5 specimens: a) RS= 8000 rpm, b) RS= 10000 rpm, and c) RS= 12000 rpm (conditions P-GF/Tigr5-1, 2, 3 at constant FT= 700 ms, FOT= 1200 ms, FP 6= bar, FOP= 10 bar).

Figure 5.17 – – Influence of rotational speed on the deformed tip of the rivet (width and depth) of specimens shown in Figure 5.16

Although anchoring zone (the deformed tip of the rivet) was observed in both cases, Ti Gr. 3 alloys displayed higher level of deformation (larger widths) in comparison to Ti Gr. 5 alloys. This is assumed to be associated with the higher strengths of the Ti Gr. 5 in comparison to Gr. 3 on one hand, and on the other hand the lower thermal conductive of the Ti Gr. 5. This titanium alloy presents a ultimate tensile strength about 54% higher and a thermal conductivity about 66 % lower than Ti Gr. 3 (see Table 4.9, chapter 4.3.3). These two characteristics combined means that Ti Gr. 5 requires either more heat energy to allow the formation of the rivet anchoring zone, or more forging pressure to induce more deformation.

The conditions tested in the preliminary study of P-GF/Ti Gr.5 were evaluated as unstable and further optimization is needed. Considering that the evaluation of P-GF/Titanium joints is not the main focus of this work, only the combination of P-GF/Tigr3 was selected to take part in the selection of best material combinations (tensile testing).

5.3. Selection of GFRP/rivet combinations

5.3.1. Overview

In the following sections the conditions for PEI-GF/AA 2024-T351, PEI-GF / Ti Gr.2 and P-GF/Ti Gr.3 defined in the previous chapters will be evaluated in terms of mechanical performance (tensile testing and aspect ratio). From this study a GFRP/rivet material combination displaying the highest mechanical performance will be selected for further optimization and statistical analysis. Furthermore Chapter 5.3 will present a new concept to estimate the anchoring performance of the rivet.

5.3.2. Tensile testing of PEI-GF/AA 2024 joints

As mentioned in the previous sections, after the feasibility tests, only 3 conditions were selected for tensile testing (T-Pull test) of PEI-GF/AA 2024, all with the same joining parameters but with different rivet tip geometries: plain rivet, hollow rivet and hollow-threaded rivet. The joining parameters were: Rotational Speed 10000 rpm, Friction Time of 1500 ms, Forging of Time 2000 ms, Friction Pressure of 3,5 bar and Forging Pressure of 6,0 bar.

Three replicates have been tested for each rivet geometry. Figure 5.18 shows the surface view of the T-pull test samples prior to testing. The whole T-pull test procedure was described previously in chapter 4.2.4. The values of the average ultimate tensile forces for the three conditions are detailed in Table 5.6. The graph with the complete set of tested tensile specimens can be found in Appendix 7.

All tested specimens failed by the failure mode "full rivet pullout" (Type III, Chapter 3.4.5) where the rivet is fully pulled out of the composite plate. Figure 5.18 presents the surface views of the tested specimens of the tested specimens and their level of rivet deformation (width) and insertion (depth) is shown in Figure 19.
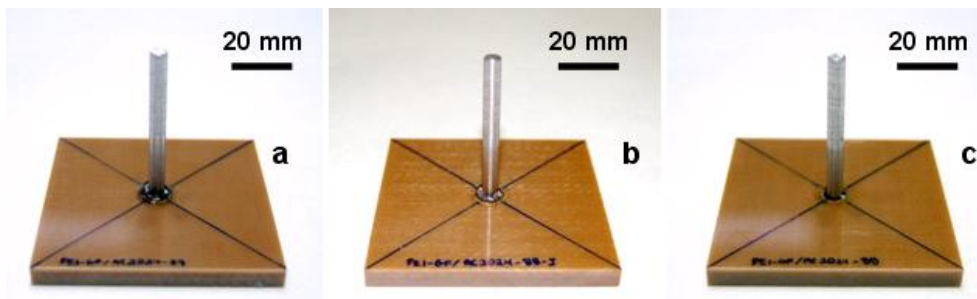

Figure 5.18 – Surface views of the T-pull test specimens for PEI-GF/AA 2024-T351 joints prior to testing (a – plain rivet, b – hollow rivet, c – hollow-threaded rivet)

Table 5.6

T-pull test: average ultimate tensile forces for PEI-GF/AA 2024-T351 joints

Type of rivet	Average ultimate tensile force [N]	Standard deviation [N]
Plain	294	80
Hollow	400	90
Hollow-threaded	1481	230

From this table, it is possible to make two straight forward observations. Firstly specimens have a rather large standard deviation (Plain: ± 27%; Hollow= ± 22,5%; Hollow-threaded= ± 15,5%). Secondly, the Hollow-threaded friction riveted specimens presented an increase of about 4 to 6 times the average ultimate tensile force from Hollow and Plain riveted specimens, respectively.

The rather large standard deviations in tensile strength (in polymer welding standard deviations lay usually within ± 10%) can be associated with the microstructural aspects of the joints, as discussed in Chapter 5.2. It was possible to see that specimens presented volumetric flaws associated with high heat generation and differential deformation (for the hollow and hollow-threaded rivets), as show in Figure 5.4.

The larger increase of strength in the case of the hollow-threaded specimens can be explained on the basis of geometry of the deformed tip of the rivet. This fact can be related to deeper rivet insertions, while deformation stay virtually unchanged (see Figure 5.19). Therefore the rivet anchoring performance will increase, resulting in higher tensile strengths.

The relationship between rivet deformation (width) and its insertion depth and its influence onto the tensile strengths will be further referred to as "Aspect Ratio" and discussed in chapter 5.3.4
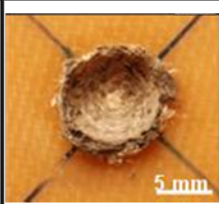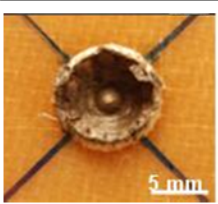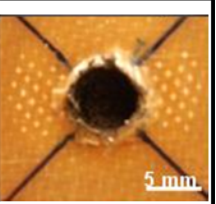
Fracture Surface	Plain	Hollow	Hollow-Threaded
Width [mm]	7,8	9,5	7,9
Depth [mm]	2,8	2,9	4,2

Figure 5.19 – Overview of the fracture appearance of the PEI-GF composite plates after T-pull tensile testing and the values of AA 2024-T351's rivet deformed geometry from the cross sectional views of the samples in Figure 5.18.

5.3.3. Tensile testing of PEI-GF/Ti Gr.2 joints

The three different conditions selected in Chapter 5.2.2 for PEI-GF/Ti Gr. 2 material combination were tested by T-Pull tensile testing. The joining parameters for these conditions can be summarized as follow:
- condition A1 with RS= 8000 rpm, FT= 700 ms, FOT= 2500 ms, FP= 6 bar, FOP= 10 bar;
- condition A2 with RS= 9000 rpm, FT= 700 ms, FOT= 2500 ms, FP= 6 bar, FOP= 10 bar
- condition A3 with RS= 10000 rpm, FT= 700 ms, FOT= 2500 ms, FP= 6 bar, FOP= 10 bar

Figure 5.20 shows the surface view of the T-pull test samples prior to testing. Table 5.7 summarizes the values of the average ultimate tensile forces for three replicates on PEI-GF/Ti Gr.2 T-pull tensile specimens. Testing curves for this material combination are presented in Appendix 7.
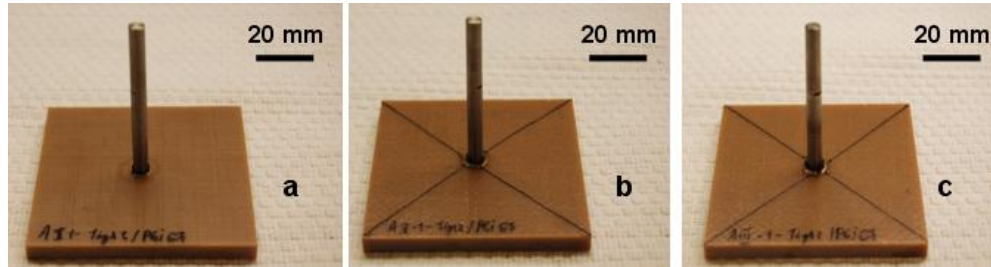
Figure 5.20 – Surface views of the T-pull test specimens for PEI-GF/Ti Gr.2 joints prior to testing. a) condition A1. b) condition A2, c) condition A3.

Table 5.7

T-pull tests: average ultimate tensile forces and standard deviations for PEI-GF/Ti Gr.2 joints

Sample	Average ultimate tensile force [N]	Standard deviation [N]
A1	1880	225
A2	3300	200
A3	4000	100

From this table, it is possible to observe that, an decrease in standard deviation (A1: ± 12,0 ; A2= ± 6,7%; A3= 2,5%) took place from A1 to A3 specimens. Additionally there was an increase in ultimate tensile force of about 2,1 times for the condition A3 in comparison with A1. All specimens have failed by the Type III "full rivet pullout" mode (Chapter 3.4.5)

The reduction in standard deviation can be generally regarded as a result of the decrease in volumetric flaws and geometrical consistence of the deformed tip of the rivet (see cross sectional views for these joints in Figure 5.12) due to more homogenous deformation of the rivet tip.

Figure 5.21 summarizes the characteristics of fractured PEI-GF/Ti Gr.2 T-pull samples and their rivet deformation and insertion. The increase in ultimate tensile force can be associated with the enlargement of the rivet anchoring performance, as discussed in Chapter 5.2.2.
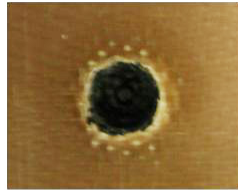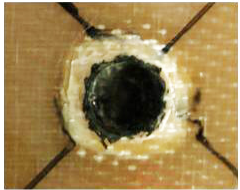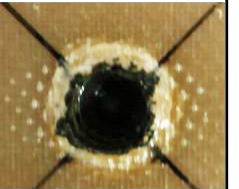
	A1	A2	A3
Fracture surface			
Width [mm]	5,15	5,75	6,0
Depth [mm]	3,90	3,80	3,30

Figure 5.21 - Overview of the fracture appearance of the PEI-GF composite plates after T-pull tensile testing and the values of Ti Gr. 2's rivet deformed geometry from the cross sectional views of specimens presented in Figure 5.20.

As it can be seen in Figure 5,21 the growth of average ultimate tensile force appears to be more likely related to the increase of the deformation (an increase of about 16,5% for A3 in comparison to A1), considering that the rivet insertion (depth) slightly decreased (about 15,4% for A3 comparing to A1). It is clear from these observations that most of the times, both width and depth of the rivet have to be considered concomitantly. It means that the Aspect Ratio of the deformed tip of the rivet seems to be more adequate to discuss this influence. The evaluation of the Aspect Ratio of PEI-GF/Ti Gr.2 will be addressed in Chapter 5.3.5)

A way to explain the influence of the rotational speed on the increase of rivet deformation (rivet plasticizing) is by analysing their influence on the theoretical heat input.. Heat estimation in FricRiveting can be estimated from equation 5.1, of the total heat input, as proposed by Amancio-Filho [35]:

$$Q_{total} = \left[\left(\frac{2}{3} \cdot \mu \cdot P(r) \right) + \frac{\eta \cdot V_{max}}{H} \right] \cdot V_{max} \quad (5.1)$$

, where:

μ is the kinematic friction coefficient

$P(r)$ is the normal pressure distribution on the frictional area

η is the polymer viscosity in the molten state

V_{max} is the maximal tangential speed of the rivet

H is the average width of the consolidated polymeric layer

From this equation we can observe that A3 will lead to higher theoretical heat input than A1 and A2 due to the higher rotational speeds represented in the model by Vmax, a variable directly proportional to the heat generation with quadratic influence on the average total heat input. In this way the larger values of deformation in A3 can be related to the larger rotational speeds.

5.3.4. Tensile Testing of P-GF/Ti gr. 3 joints

T-pull specimens were produced and tested from the conditions described in Chapter 5.3. The values of the joining parameters are:
- P-GF/Tigr3-1 with RS= 8000 rpm, FT= 700 ms, FOT= 1200 ms, FP= 6 bar, FOP= 10 bar;
- P-GF/Tigr3-2 with RS= 9000 rpm, FT= 700 ms, FOT= 1200 ms, FP= 6 bar, FOP= 10 bar
- P-GF/Tigr3-3 with RS= 10000 rpm, FT= 700 ms, FOT= 1200 ms, FP= 6 bar, FOP= 10 bar

Three specimens from each condition have been tested.

Figure 5.22 shows the surface view of the P-GF/Ti Gr.3 T-pull test samples prior to testing. Table 5.8 summarizes the average values of the ultimate tensile forces of PEI-GF/Ti Gr.3 T-pull samples obtained from three replicates.
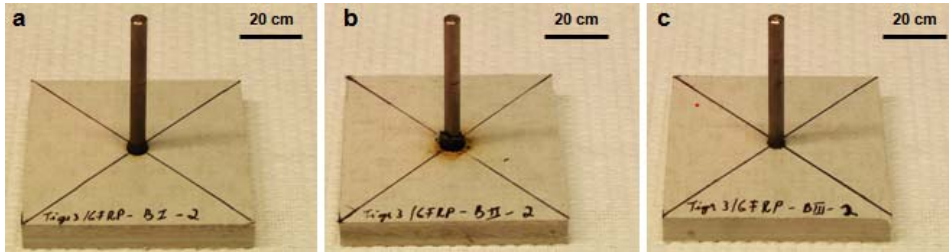

Figure 5.22 – Surface views of the T-pull test specimens for P-GF/Ti Gr. 3 joints prior to testing. a) condition P-GF/Tigr3-1. b) P-GF/Tigr3-2. c) P-GF/Tigr3-3.

As it will be shown in Table 5.8, the values of the ultimate tensile forces were not satisfactory and the standard deviations were too high (over the acceptable 15%).

Table 5.8

T-pull test: average ultimate tensile forces for P-GF/Ti Gr. 3 joints

Specimen	Average ultimate tensile force [N]	Standard deviation [N]
P-GF/Tigr3-1	2130	1200
P-GF/Tigr3-2	730	375
P-GF/Tigr3-3	1460	1155

An important first observation from this table is the extremely large standard deviation for the P-GF (P-GF/Tigr3-1= 56,3%, P-GF/Tigr3-2= 51,4% and P-GF/Tigr3-3= 79,0%). This is probably related to the relative high level of thermal degraded composite material around the tip of the rivet (see Figure 5.14) , which in turn could be associated with the high and uncontrollable heat input, as discussed in Chapter 5.2.3.

Hence further investigation of the relationship between rivet deformation and insertion and tensile strength were not carried out. Further research is required in order to optimize the FricRiveting process for this material combination.

5.3.5. Aspect ratio and anchoring efficiency of GFRP/metal point-on-plate joints

According to previous studies [55], the anchoring performance of the rivet can be estimated through the Aspect Ratio (AR), a relation between width of the deformed rivet (W) and its insertion depth (H) calculated as follows:

$$AR = \frac{H}{W}$$

(5.2)

, for W>H or:

$$AR = \frac{W}{H}$$

(5.3)

, for W<H.

The AR was calculated according to Equations 5.2 and 5.3 for the conducted T-pull tests on PEI-GF/AA 2024-T351 and PEI-GF/Ti Gr.2 combinations. For the P-GF/Ti Gr.3, analysis were skipped because of its large standard deviations (Chapter 5.3.4). The calculated values for ARs are shown in Appendix 8.

An attempt to evaluate the influence of AR on the ultimate tensile force (UTF) of the joints evaluated in Chapters 5.3.2 and 5.3.3 was carried out. Figure 5.23 shows the influence of the aspect ratio on the ultimate tensile force of the PEI-GF/AA 2024-T351 T-pull specimens, with the values of the ultimate tensile forces listed previously in Table 5.6.
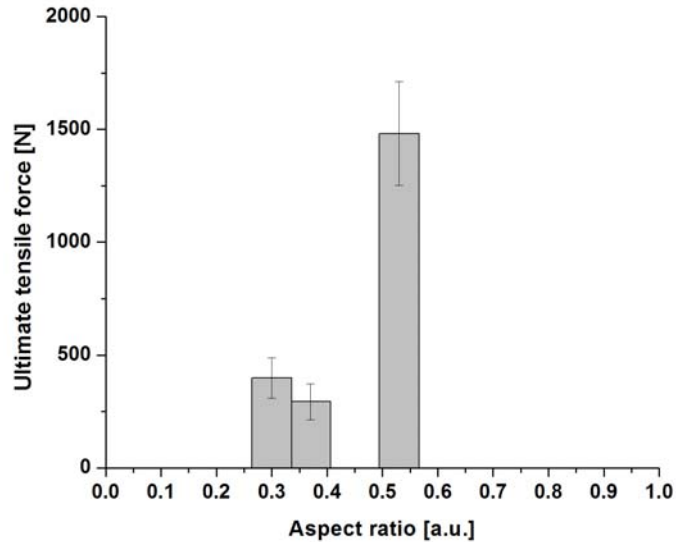
Figure 5.23 – Interaction of the aspect ratio and the ultimate tensile force for PEI-GF/AA 2024-T351 specimens (Chapter 5.3.2, Table 5.6)

The influence of the AR on the UTF for the friction riveted PEI-GF/Ti gr.2 T-pull specimens is shown in Figure 5.24, based on the average values from Table 5.7.
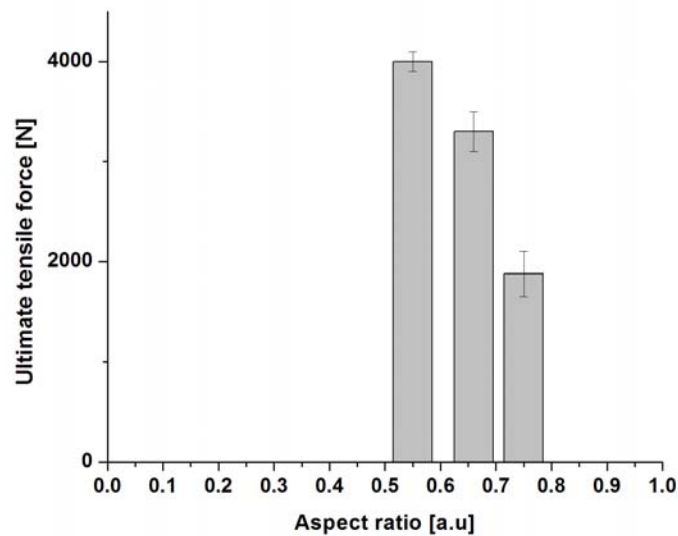

Figure 5.24 – Interaction of the aspect ratio and the ultimate tensile force for PEI-GF/Ti Gr.2 specimens (Chapter 5.3.3, Table 5.7))

As it can be seen in the two graphs, the influence of the AR on the UTF is follows different trends for different materials. On one hand, the trend is ascending, the higher the AR, the higher UTF for the PEI-GF/AA 2024-T351 combination (Figure 5.23). On the other hand, like for the PEI-GF/Ti Gr.2 specimens in the graph from

Figure 5.24, an opposite descending trend, where the higher the AR, the smaller the UTF will be.

In both materials combinations the W-values are larger then the H-values; As a consequence AR was calculated by Equation 5.2. However two observations can be made by studying the W- and H-values from Tables 5.6 and 5.7. Firstly, PEI-GF/AA 2024-T351 specimens displayed similar W-values, while there was a considerable increase in H-values for the specimen with higher UTF. Secondly PEI-GF/Ti Gr. 2 presented similar H-values, while W-values are larger for specimens displaying higher UTF.

Amancio and dos Santos [39], have studied the influence of the AR on the tensile strength of unreinforced PEI/AA 2024-T351 specimens. The interval of joining parameters studied resulted in similar rivet anchoring geometries in comparison to the results for the PEI-GF/AA 2024-T351 specimens, where their specimens presented W>H and similar W-values. They also found a similar ascending trend for the AR-UTF. However they did not addressed the case, where the H-values are similar while the W-values increase, as for the current PEI-GF/Ti Gr.2 specimens.

As a preliminary conclusion, the AR-UTF is a practical way to evaluate the ultimate tensile forces of friction riveted joints but seems not to be applicable for all geometrical variations of the anchoring zone. The simple formulations proposed for AR [55] has dimensional limitations, which were initially not considered. Therefore, a new way of estimating the effect of the geometry of the rivet anchoring zone should be introduced, aiming at to take into account all possible variations of width and depth.

Having an Aspect Ratio based only on two dimensions (width and depth) can be misleading in the evaluation as discussed. A volumetric approach might be therefore more appropriate. In this way a more reasonable mathematical formulation of the anchoring performance could be achieved by introducing in the calculations:

- The volume of the deformed metallic rivet (Vriv)
- The volume of the dislocated polymeric material (Vdp), which can be considered a virtual "drilling" hole created by the rivet (with an annular area)
- The volume of the "loaded" polymeric material (Vlp) beyond the anchoring zone of the deformed rivet

Figure 5.25 schematically shows the interactions of the different volumes of the analytical model.
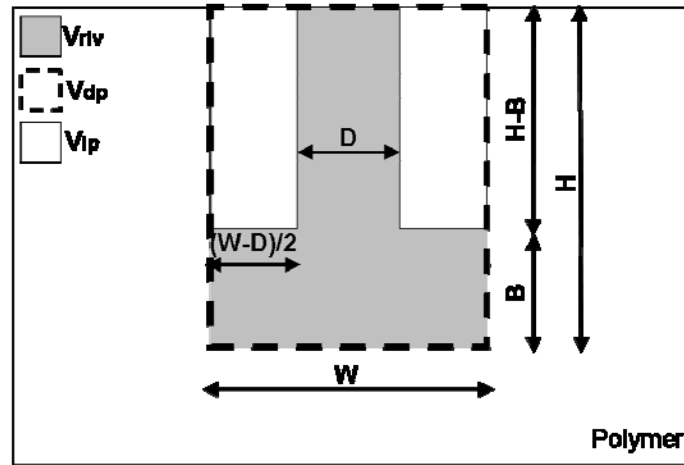
Figure 5.25 – Geometry of a simplified FricRiveting joint used to calculate the volume ratio.

At first, some dimensional simplifications will be made, in respect to the shape of the inserted and deformed rivet, the simple geometry of the rivet will be considered as shown in Figure 5.25; this shape will be kept constant and used for all calculations.

The new approach, hereby called Volumetric Ratio (VR) can be calculated according to the volumes schematically shown in Figure 5.25. Vriv will be considered the cylinder having the diameter of the deformed rivet tip (W) and the height of its insertion depth (H). VR is then the ratio of Vlp (with an annular cross sectional area forming a tube cylinder) and the Vdp. After the calculus and simplifications, the volumetric ratio can be expressed in the following equation:

$$VR = \frac{(H - B) \cdot (W^2 - D^2)}{W^2 \cdot H}$$

(5.4)

, with H – Insertion depth

W - Width of the deformed rivet

D – Initial diameter of the rivet

B – Height of the deformed tip of the rivet

The proposed analytical model for the rivet anchoring performance includes in a very simple way, both the adhesion forces (an additional bonding mechanism reported to be present in FricRiveting [35]), related to the contact surfaces between the two dissimilar materials, as well as the reactive forces associated with the reactions in the polymeric material (in resistance to the movement of the axially loaded rivet).

VR was calculated for the previous two cases for which the AR was evaluated. Figure 5.26 shows the interaction between VR and UTF for the PEI-GF/AA 2024-T351 T-pull specimens. The calculated values of the VRs are show in Appendix 8.
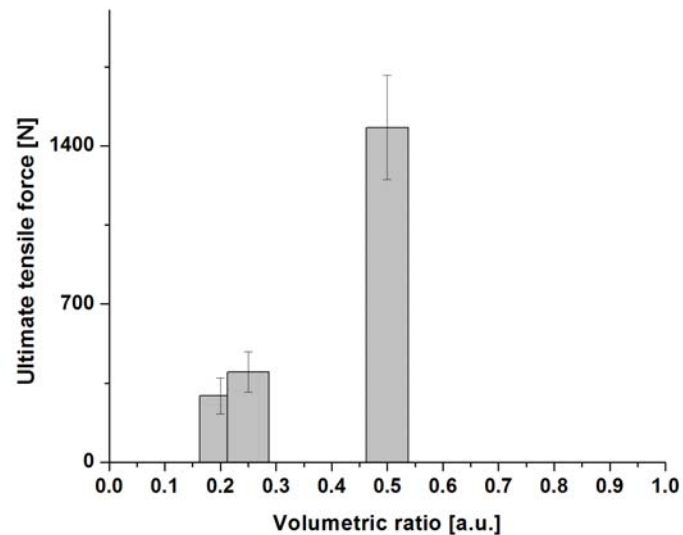
Figure 5.26 - Interaction of the volumetric ratio and the ultimate tensile force for
PEI-GF/AA 2024-T351 samples.

The same was evaluated for the case of PEI-GF/Ti gr. 2, presented in Figure
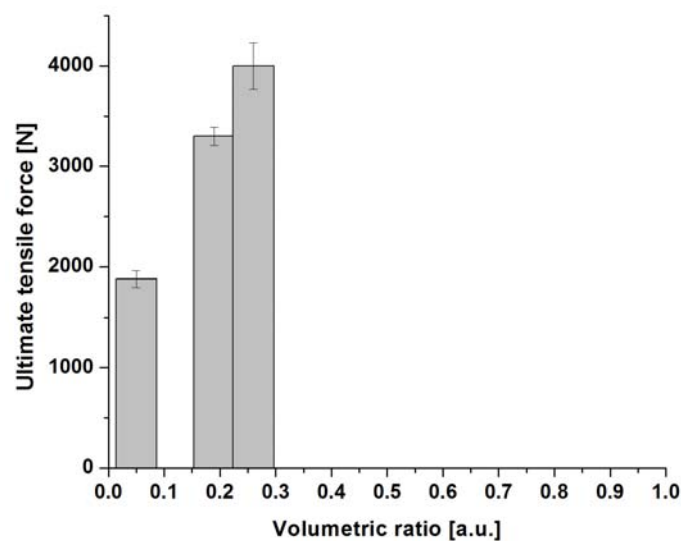5.27.

Figure 5.27 - Interaction of the volumetric ratio and the ultimate tensile force for
PEI-GF/Ti Gr.2 specimens

For additional validation of the newly introduced VR model, an evaluation
was conducted, with the results of tensile testing and geometrical analysis of the
unreinforced PEI/AA 2024-T351 specimens, by S. Amancio [35]. The VR calculated
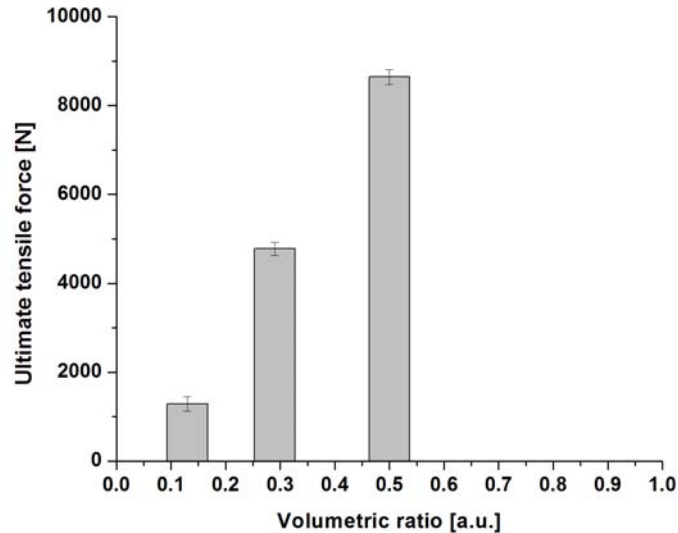results are shown in Figure 5.28.

Figure 5.31 - Interaction of the volumetric ratio and the ultimate tensile force for reinforced PEI/AA 2024 studied by Amancio [35]

Consequently, the anchoring performance of the rivet (in this case represented by the ultimate tensile force) can be estimated through the proposed approach to calculate the volumetric ratio, providing information on the anchoring efficiency of the deformed rivet is available. Therefore the higher the VR, the higher the rivet anchoring will be.

5.3.6. Selection of adequate GFRP/rivet material combination

With the results analysed in Chapters 5.2 and 5.3 the selection of the best combination of materials for the process optimization and determination of the parameters for structural analysis can be carried out in a simple manner.

The three combinations of GFRP/rivet materials can be compared in terms of tensile strength (anchoring performance). For that the maximal values of ultimate tensile strength and their standard deviations were selected and directly compared.. These results are summarized in Table 5.9.

Table 5.9

Comparison of the GFRP/rivet material combinations for further evaluation.

Materials Combination	Max. Average UTF [N]	Std of Max. Average UTF [N]	Ranking for Materials Selection
PEI-GF/AA 2024	1481	230	2
PEI-GF/Ti Gr.2	4000	100	1
P-GF/Ti Gr. 3	2130	1200	3

A simple classification ranking was established where the material combinations with higher maximum average strength and lowest standard deviation

occupies higher positions. From the Table 5.9, it is possible to see that the material combination with best strength/standard deviation ratio is the PEI-GF/Ti Gr.2 combination. This will be the materials combination to be used in the structural analysis.

5.4. Process optimization and analysis

5.4.1. Lap-shear testing of friction riveted PEI-GF/Ti gr. 2 point-on-plate joints with threaded rivets

Lap shear specimens were produced with threaded rivets in this work. Up to this point only plain rivets were evaluated for the selected PEI-GF/Ti Gr.2 materials combination. Considering this it is necessary to evaluate the joinability of threaded Ti Gr.2 rivets in the investigated composite.

When welding threaded rivets, buckling can take place during FricRiveting due to the axial force induced by the spindle of the welding system and the effect of the thread pitch in the unclamped free length of the rivet shaft. In order to prevent rivet buckling during the process, lower forging pressures have to be used. Additionally a cylindrical adaptor was used to strengthen the threaded rivets shaft over the free length. Therefore a reduction in the forging pressure from 10 bar to 6 bar was utilized to establish the parameter study of threaded specimens. The other parameters were maintained constant at RS of 10000 rpm, FT of 700 ms, FOT of 1200 ms and FP of 6 bar. Conditions with 10 bar FOP revealed buckling of the rivet, while conditions with less than 6 bar failed to achieve rivet anchoring. Concluding, for threaded rivets, the minimum FOP was established to 7 bar and the maximum was limited to 8 bar, due to higher visual amount of thermal degraded material present in the conditions with 9 bar.

Within the conditions described above all tested joining conditions, anchoring zones with large deformation were obtained so the tested conditions were valid for further analysis. The results on the microstructure and geometry of the PEI-GF/Ti Gr.2 M5-threaded rivet specimens for this parameter study can be found in Appendix 9. Figure 5.29 shows an example of the microstructure and anchoring zone of a non-defective joint produced with Ti Gr.2 threaded rivets
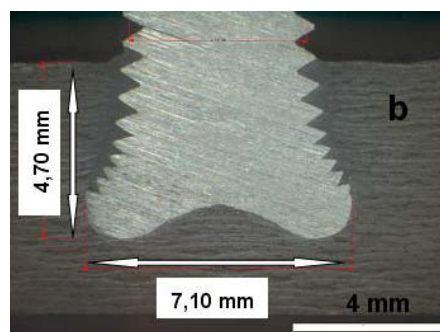

Figure 5.29 – Example of a sound friction riveted joint on PEI-GF/Ti Gr.2-M5 threaded rivets
(RS= 10000 rpm, FT= 700 ms, FOT= 1200 ms and FP= 6 bar FOP= 7 bar)

5.4.2. Design of experiments.

As previously mentioned in chapter 4, the Taguchi method was used in the design of experiments to optimize process performances in terms of ultimate lap shear strength (ULSS). This powerful statistical tool allows the reduction of material consumption and experimental time [56]. This method combines the experimental design theory and the concept of loss function and determines thereby the most influential parameters in the overall performance of the process. The optimum process parameters obtained through the Taguchi method are insensitive to noise factors [57].

In order to identify the most influencing parameters and the contribution of each parameter on the shear strength of the friction riveted PEI-GF/Ti gr.2 joints, a L9 Taguchi orthogonal array was selected, conducting a minimum number of experiments. A number of 9 experiments were conducted with 4 replicates per experiment

5.4.2. a. Lap shear testing results for PEI-GF/AA 2198/Ti Gr.2 hybrid joints

The conditions (parameters and levels) for each experiment on PEI-GF/AA 2198/Ti Gr.2-threaded hybrid joints have been previously described in Chapter 4.2.6, Table 4.3 (Taguchi L9- array for the lap shear DOE). The lap shear experiments were performed in a random order, generated with the MINITAB software. Table 5.10 presents the results of the Taguchi-L9 experiments. The response chosen for statistical evaluation was the ultimate lap shear force (ULSF).

Table 5.10

Experimental results for Taguchi-L9 – Ultimate lap shear forces of PEI-GF/AA 2198/Ti gr.2 joints for four replicates per experimental condition

Experiment	ULSF 1 [N]	ULSF 2 [N]	ULSF 3 [N]	ULSF 4 [N]	Average ULSF [N]	ULSF Standard Deviation [N]
1	4000	3930	2300	4980	3800	1110
2	5050	3800	5500	3700	4500	900
3	4250	3140	2910	3850	3500	621
4	4990	4915	4600	5800	5000	511
5	5370	5070	3700	3500	4400	947
6	3320	3850	3100	3830	3500	375
7	4800	4050	5430	5900	5000	802
8	3950	4090	4680	4060	4200	329
9	3810	4870	4400	4400	4400	434

From the 36 tested specimens, only two failed through the bearing failure type in the polymeric plate. The bearing failure aspects of the two joints can be observed in Figure 5.30. As it was addressed in the Chapter 3.3.3 the bearing failure type can be explained related to the compressive forces acting on the edge of the hole in contact with the rivet; these cause the crushing (plastic deformation) of the composite material [40].

Due to the stress concentration introduced in the section by the hole, the fracture took place in the polymeric material instead of the metallic rivet, leading to a lower strength of the joint [60]. Borges et al. [97] evaluated the deformation of FricRiveting lap shear specimens presenting bearing failure. They observed that, the plastic deformation initial takes place around the rivet; by the moment when the secondary bending moment becomes too large, the overlapped area of the specimen starts rotating shifting itself from the loading direction. This excessive rotation of the overlapped area can cause net-tension failure in the specimens or can lead to the pulling out of the rivet as reported by Amancio [35]. The later was observed in the current bearing failed specimens.

A valid explanation for the different behaviour of the two mentioned specimens can be the insufficient bolt torque applied to clamping nuts. A bolt torque of 0,5 Nm was applied by using a dynamometric key to assemble the aluminum AA 2198 onto the friction riveted PEI-GF coupon. The excessive presence of thermo-mechanically degraded material around the rivet in Figure 5.30.B can also serve as an explanation of the lower mechanical performance in this case. Further investigations of the level of thermally degraded material should be performed in order to achieve better understanding of this behaviour.
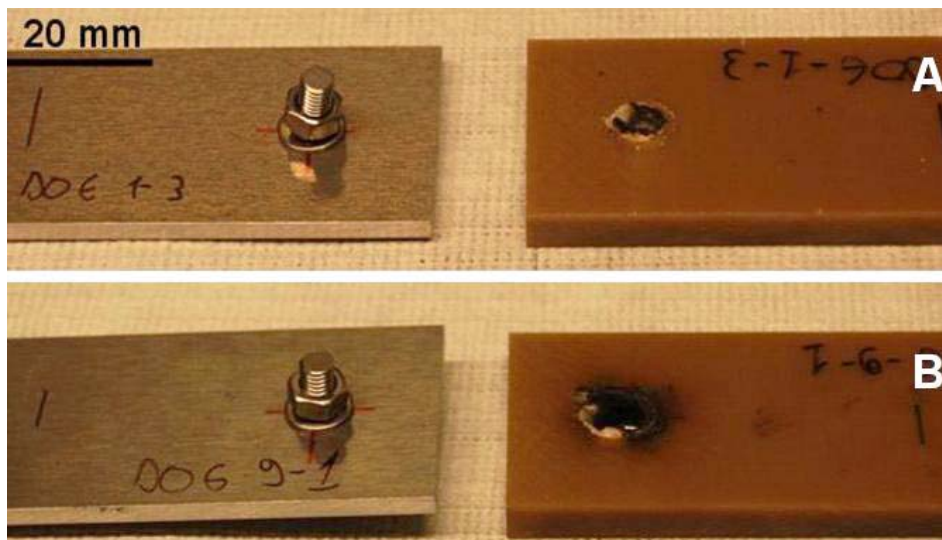

Figure 5.30 – Bearing failure in lap-shear specimens. A) Condition 1, replicate 3 (RS= 8000 rpm, FT= 700 ms, FOT= 1200 ms, FP=6bar, FOP 6 bar) and B) Condition 9, replicate 1 (RS= 12000, FT= 1700 ms, FOT= 1850 ms, FP= 6 bar, FOP= 6 bar)

The majority of 34 tested lap-shear specimens failed through shear in the metallic rivet material, as it can be observed in Figure 5.31.
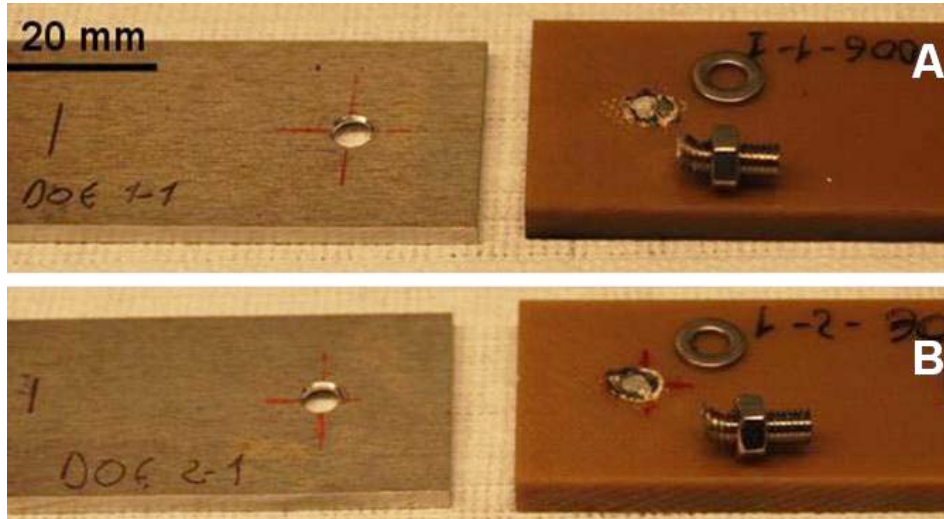
Figure 5.31– Rivet shear failure in lap-shear specimens. A) Condition 1, replicate 1 (RS= 8000 rpm, FT= 700 ms, FOT= 1200 ms, FP=6bar, FOP 6 bar) and B) Condition 2, replicate 1 (RS= 8000, FT= 1200 ms, FOT= 1850 ms, FP= 6 bar, FOP= 7 bar)

Figure 5.32 shows typical force-displacement curves during the lap-shear tests for the experiments of condition 4. These resulted in the highest mean ultimate forces under the nine Taguchi-L9 conditions. All tests were carried out upon rupture for a complete understanding of the behaviour of the friction riveted overlap joints. The remaining force-displacement curves for all the DOE experiments are presented in Appendix 4 together with a examples of a fractured specimens.
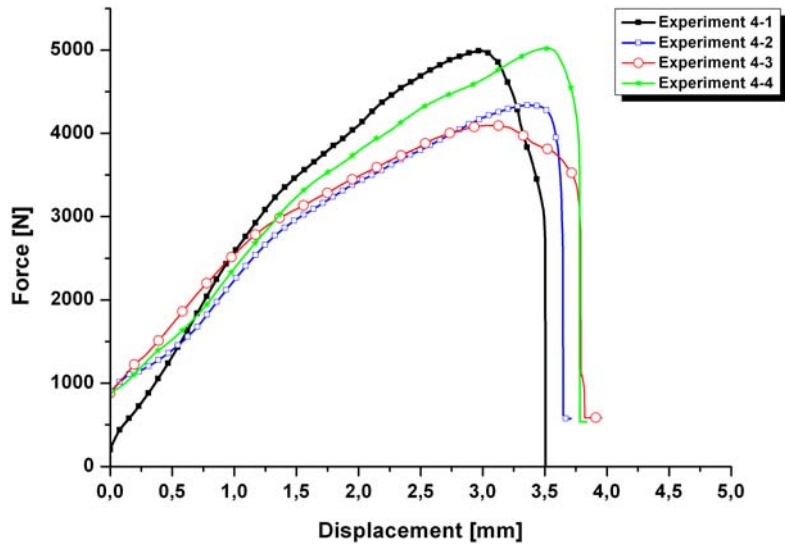
Figure 5.32 – Force-displacement curves for the DOE Taguchi-L9 Condition 4
(RS=10000 rpm, FT= 700 ms, FOT= 1850 ms, FP= 6 bar, FOP= 8 bar

The lap shear strength of the joints will be expressed as the ratio between the ultimate lap shear force and the nominal area of the hole for each friction riveted joint. The nominal area of the hole can be simplified calculated as the coupon's thickness times the nominal diameter of the hole, as addressed by ASTM D 5961 M-08 [50] and indicated in Equation 5.5. In reality, this area should be the actual area of the deformed inserted rivet in the polymeric base plate, with the depth measured from the joint's anchoring zone. This area (see Equation 5.6) can be graphically measured from the cross-section view of the joints.

$$R = \frac{F}{t \cdot d}$$ (5.5)

, where R – simplified lap-shear strength
F – the ultimate lap shear force
t – coupon thickness
d- nominal diameter of the hole
and the actual lap-shear strength:

$$R_{real} = \frac{F}{A_d}$$ (5.6)

, with A_d - the real measured area of the inserted deformed rivet

The calculated values of the nominal and the real lap-shear strengths achieved in the experiments are listed in Table 5.11.

Table 5.11

Experimental results – lap shear strengths of PEI-GF/AA2198/Ti gr.2 joints

Experiment	Average ULSF [N]	Nominal ULSS [MPa]	Real ULSS [MPa]	Difference Real/ Nominal [Mpa]
1	3800	132,00	178,40	46,4
2	4500	156,25	168,00	11,7
3	3500	121,50	100,00	21,5
4	5000	173,60	178,60	5,0
5	4400	152,80	145,00	7,8
6	3500	121,50	100,00	21,5
7	5000	173,60	199,20	25,6
8	4200	145,80	126,50	19,3
9	4400	152,80	122,20	30,6
Avg.	**4275**	**147,80**	**146,40**	**21,0**
StD.	**576**	**19,7**	**38,95**	**13,9**

From the table it is possible to see that both nominal and real ULSS specimens have comparable average ULSS values (an average difference of 21,0 MPa). However the real ULSS specimens have presented a larger standard deviation than the nominal ULSS specimens. This is probably related to imprecision of the graphical measurement of the real area, carried out on cross sectional views. In this way one can conclude that the nominal ULSS is an acceptable way to estimate the Lap Shear Strength of PEI-GF/AA 2198/Ti gr.2 hybrid joints.

The PEI-GF/AA 2198/Ti gr.2 hybrid joints could achieve the shear up to 0,7 of the tensile resistance of the metallic rivet (see results for tensile strength of Ti Gr.2 rivets in Appendix 10) and about the same the in-plane shear strength of the composite PEI-GF base plate (see Table 4.10).

5.4.2. b. Statistical evaluation of the results

The results of the lap shear test have been statistically evaluated toward process optimization, using the MINITAB 15 software. The main effects plots for the means and signal-to-noise ratios for ultimate shear force of the conducted lap shear experiments can be seen in Figure 5.33 and Figure 5.34. The statistical analysis of variation (ANOVA) is presented in Appendix 5.

From the graphs in Figures 5.33 and 5.34, the forging time (FOT) resulted as the main parameter influencing the results, followed nearly by the friction time (FT) and Rotational Speed. This can be concluded from the slopes of the curves for the means and S/N ratio curves. The steeper the slope the higher will be the influence of one parameter in the respective response. One can affirm thereby that the joining time (JT) and the Rotational are the parameters that will influence the lap-shear strength of the joints the most, contributing to the rivet's deformation and insertion depth.

The means and S/N ratio plots also provide the indication of the optimal response (the so called "the larger, the better approach) [51]. The optimal condition can be identified from the peaks of the curves in Figures 5.33 and 5.34.

In this way, the optimal parameters for lap-shear strength determined from the data means curves were:
- Rotational speed: 12000 rpm
- Friction time: 1200 ms
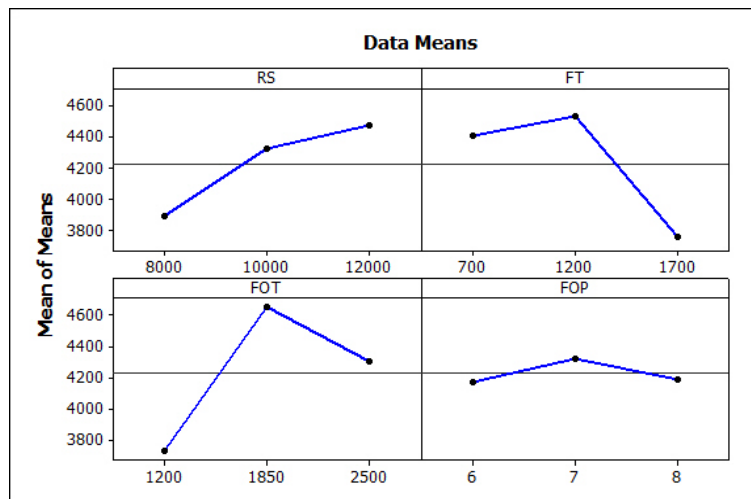- Forging time: 1850 ms
- Forging pressure: 7 bar

Figure 5.33 – Main effects plot for the means of ultimate lap shear forces (ULSF)
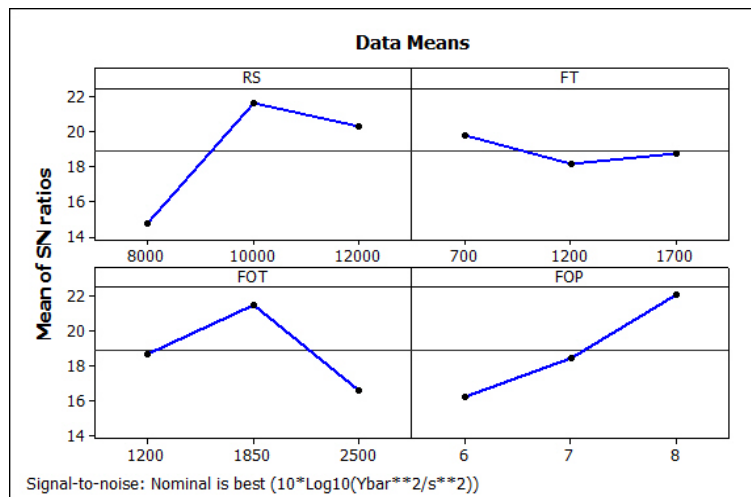

Figure 5.34 – Main effects plot for SN ratios for the ultimate lap shear forces (ULSF

In order to validate the model of the selected design of experiments, the ultimate shear forces was predicted (with the aid of MINITAB software) for complimentary conditions, these validation condition were intentionally selected within the parameters range of the Taguchi-L9 array as recommended in the literature [51]. Table 5.12 presents the validation conditions and their parameter,

with their predicted and experimental ultimate average shear forces. Four conditions were tested: V1 with all maximum levels, V2 with all minimum levels, and V3 and V4 with intermediate joining parameters values.

Table 5.12

Validation parameters, predicted and experimental average ultimate shear force values for the Taguchi-L9 model

Validation conditions	RS [rpm]	FT [ms]	FOT [ms]	FOP [bar]	Experimental ULSF [N]	Predicted ULSF [N]	Error %
V1	12000	1700	2500	8	4400	4100	6,8
V2	8000	700	1200	6	4170	3800	8,9
V3	12000	700	1200	6	4000	4400	9,1
V4	8000	700	1850	8	3600	3830	6,0

As generally accepted by the polymer welding community, a deviation of 10% is considered normal, usually due to the variations in the base material properties. Considering that the model error varied from 6,0% to 9,1 % the model can be considered statistically valid.

5.4.3. Comparison with bolted joints

Bolted lap-shear specimens (Figure 5.35) have been produced according to the same test standards in order to compare their mechanical performance with that of the friction riveted lap-shear joints. 5 mm diameter holes have been produced through the AA2198 plates and through the PEI-GF plates as well. Threaded titanium grade 2 M5-threaded bolts were used for the connection, along with stainless steel M5 nuts and washers, analogically to the friction riveted lap-shear specimens. The bolt length was 30mm and the bolt torque applied for on the nuts was the same as in the case of the friction riveted joint, 0,5 Nm.
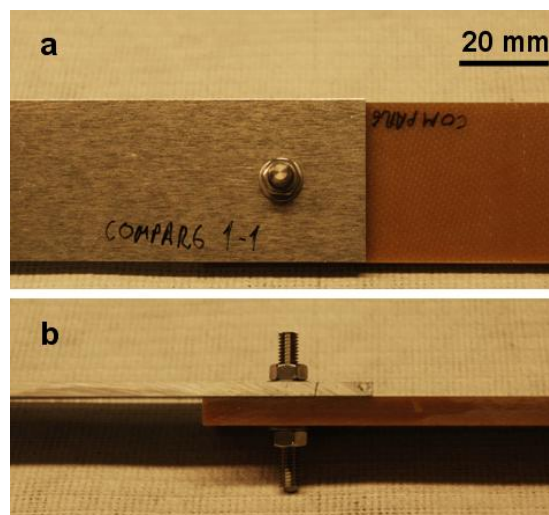

Figure 5.35 – Bolted lap-shear configuration on PEI-GF/AA 2198/Ti gr.2 produced for comparison analysis. a – plane view, b – side view

Three replicates have been tested for comparison, revealing the following results as summarized in Table 5.11:

Table 5.11

Lap shear test – results for bolted lap-shear joints

Sample	Ultimate tensile force [N]	Average ultimate tensile force [N]	Standard deviation [N]
Compare 1	4300		
Compare 2	5000	4360	600
Compare 3	3800		

The force-displacement curves for the bolt comparison lap-shear tests are displayed in Figure 5.36.
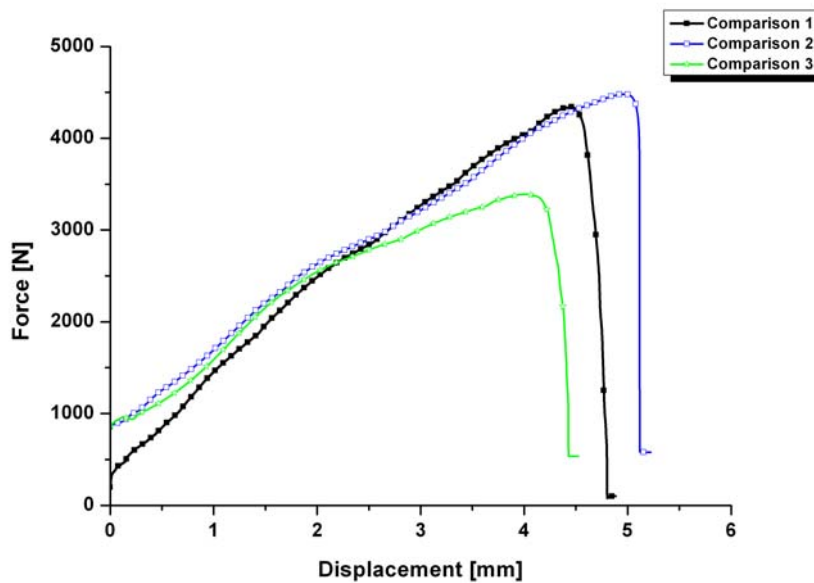
Figure 5.36 – Force-displacement curves for bolt lap-shear comparison experiment

The lap-shear strengths in this case have been calculated according to equation 5.5 with the values listed in table 5.12.

Table 5.12

Lap-shear strength of the bolted joints

Experiment	Avg. ULSF [N]	Avg. ULSS [MPa]	Mean ULSS [MPa]	StD. ULSS [MPa]
Compare 1	4300	139,00		
Compare 2	5000	161,30	141,00	20
Compare 3	3800	122,60		

Comparing the ultimate lap-shear strength mean values of the friction riveted lap-shear specimens with those of the bolted lap joints we can observe that the means for the nominal ULSS values (calculated by Equation 5.5) have nearly similar values (Friction Riveted:147,80 ± 19,7 MPa and Bolted= 141,00 ± 20MPa). This fact is explainable also with the help of the failure modes; the comparison specimens have also all failed through shear of the rivet material, as it can be seen in Figure 5.37. Concluding, One can assume that the friction riveted lap joints investigated in this work have comparable strength as bolted lap joints (under the same circumstances, rivet or and bolt diameters).
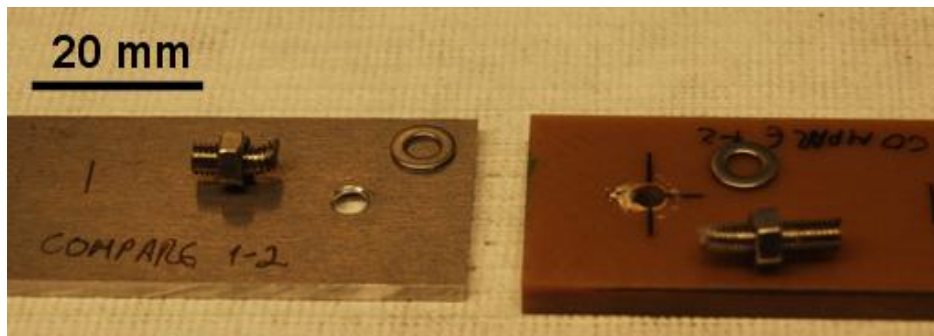

Figure 5.37 – Aspects of the fractured bolted comparison specimen showing rivet shear failure mode.

5.4.4. Temperature measurement of PEI-GF/Ti Gr. 2 for the DOE evaluation

Process temperatures have been measured using the methodology described in chapter 4.2.7 on two replicates from each experimental condition. Point-on-plate on PEI-GF/Ti Gr.2 joints had their surface temperature (temperature of the flash being expelled) without the overlaying of the aluminium AA 2198 plate, in order to increase the accuracy of the data measurement. All DOE conditions were evaluated. Appendix TT presents the thermograms and experimental temperature measurement curves for this parameter study.

It could be observed that the temperature development is close related to the rotational speed; therefore the results will be presented in groups according to the rotational speed of the conditions, with 8000 rpm, 10000 rpm and 12000 rpm. Table 5.13 summarizes the results of the peak temperatures for the specimens under investigation. Figure 5.38 shows an example of a thermogram and the average curve for the temperature measured within the marked area of the thermogram.

Table 5.13

Influence of the rotational speed on the average peak temperatures selected PEI-GF/Ti Gr.2 FricRiveting joints

Experiment	RS [rpm]	Avg. Peak Temp. [°C]
T1	8000	450
T2	10000	550
T3	12000	600

In the case of condition T1 (8000 rpm), temperatures reached peak levels of up to 450°C. With the increasing of the rotational speed to 10000 rpm (condition T2), the peak temperatures raised upon 550 °C while in condition with the rotational speed of 12000 rpm, the temperatures increased until a peak of 600 °C (see Figure 5.38). This increase of temperature can be directly related to the effect of the rotational speed on the heat input (see Chapter 3.5). The larger the rotational speeds the larger the temperatures will be, as reported for the case of unreinforced PEI/AA 2024—T351 joints [35].
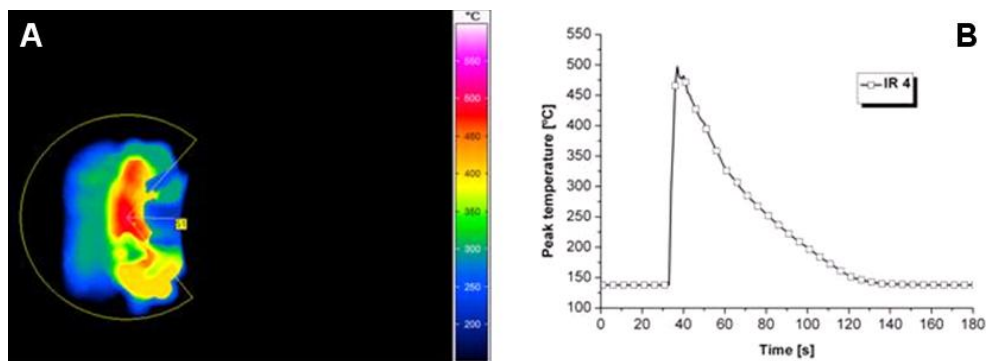
Figure 5.38 - (A) Thermogram showing the temperature of the softened composite flash material being pushed off to the surface. (B) The average peak temperatures measured from the semi-circle area in (A). (a replicate specimen for condition T2).

The thermograms and peak temperatures for the DOE conditions measured with the infrared camera are shown in Appendix 11. The recorded temperatures for all tested specimens were situated at 0,3-0,4 of the titanium grade 2 melting point (1600 °C). In the previous research by Amancio [35], the temperature reached 95% of the melting point of the metal (aluminium 2024-T351). In the current research, the temperature reached as mentioned up to 40% of the melting temperature of the titanium grade 2; despite that, the deformation of the rivet could still be achieved. In the case of titanium, increased temperatures lead to a higher ductility, therefore a higher formability [7]. The temperatures for hot forming of commercially pure titanium range from 480 °C - 705 °C [61]. The measured temperatures of the DOE were in this range, explaining therefore the achieved formation of the rivet anchoring zone.

Nevertheless, exposing titanium alloys at extreme temperatures should be avoided for longer times, due to the possibility of scaling and embrittlement; recommendations from literature [61] limit this time to 20 min, therefore the Fricriveting process should not cause embrittlement of the titanium grade 2, with joining times of less than 20 s. Temperatures above 815 ºC should also be avoided, to avoid deterioration of the mechanical properties [61]. Again, this recommendation was also respected by Fricriveting, as the IR temperature measurements revealed.

Furthermore it was observed in the previous chapters that some specimens presented signs of polymer thermal degradation (e.g. smoke evolution, ashes, darkened regions around the anchoring zone, etc.). Thermal degradation for PEI has been reported to take place by chain-scission (breaking of molecules) between 510-540ºC with an markedly stage above 600ºC [98]. This could explain some of the high heat conditions observed for PEI-GF/Ti Gr.2 specimens, where materials are being possibly degraded. Further investigation is required to allow the evaluation of the real extent and level of thermally degraded material.

5.5. Case study

5.5.1. GFRP lightweight emergency bridge

As already mentioned in the chapter referring to the objectives of the work, the scope of this work is to develop and adapt an innovative joining technique suitable for a GFRP lightweight emergency bridge structure. For the case study, a GFRP Warren truss bridge was calculated using the SAP2000 v14 Computers and Structures software [99]. The calculus was conducted in order to obtain the values of the axial forces in a presumptive real truss bridge structure; in the case of joining the truss elements by Fricriveting, the maximum axial forces should be transmittable through the joints. The calculus of the bridge was not intended for stability verification, only for allowable resistances. Figure 5.39 shows the elevation of the 25 m span truss bridge.
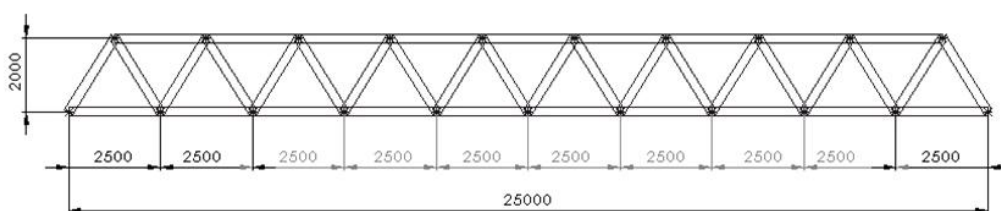

Figure 5.39 – Elevation of the 25 m span lightweight FRP bridge

The choice of materials was based on the previous conducted studies for Fricriveting. Therefore the material of choice in the modelling was PEI-GF. Nevertheless, at this time there, due to costs reason, there are no commercially available structural PEI-GF profiles. The cross section shapes of the truss elements were chosen similar to commercially available structural shaped of structural profiles (Fiberline Composites pultruded structural profiles). For practical reasons in order to

ensure an easy exchange of truss members only three different types of profiles have been proposed to use in the bridge model (Figure 5.40):
- Top chords and lower chords: 2 U 240/72/12
- Diagonals and cross girders: square tubes 240/240/12
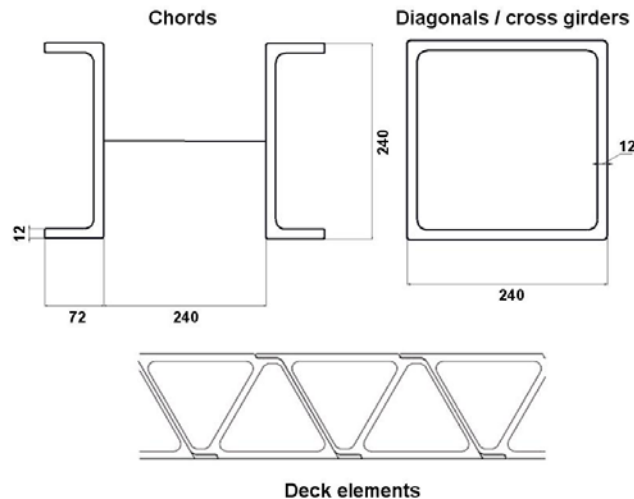- Deck elements: FBD600 ASSET bridge deck, for heavy loads

Figure 5.40 – Structural profiles proposed for GFRP lightweight bridge model

Several researches have been undertaken in the past on deck elements. Therefore, different types of GFRP structural profiles for bridge decks are available. The proposed FBD 600 ASSET bridge deck was specially developed for heavy loads and is ideal for busy road and rail bridges [3]. Different available GFRP bridge decks are further detailed in Appendix 6.

With the proposed profiles, according to the manufacturers' technical data, the whole structure would weight hardly 15 tonnes, from which around 10 tones is the dead load of the bridge deck. The live load of the bridge consists of a single 30 tonnes truck from the standard A30 convoy [62], shown here schematically in Figure 5.41. The crossing speed of the truck is set to 40 km/h, with a dynamic impact factor of 1,2. The width of the bridge carriageway is 3900 mm, assuring a single lane for the vehicle crossing (width of the A30 convoy is 2700 mm).
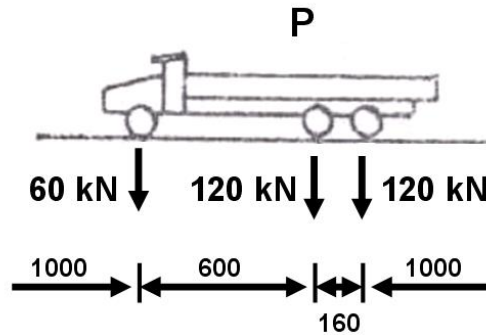
Figure 5.41 – A30 truck specifications

An isometric view of the Warren truss bridge is displayed in Figure 5.42. The truss axial forces for the specified load combination (bridge dead load + A30 vehicle at 40km/h) were determined with the SAP v14 software and are displayed in Figure 5.43.
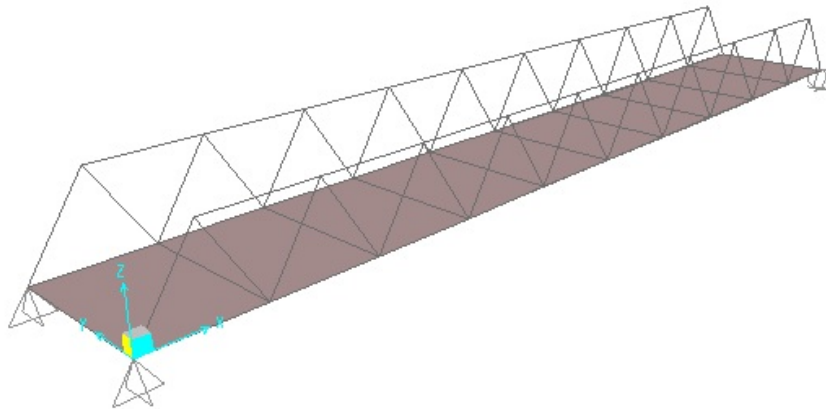

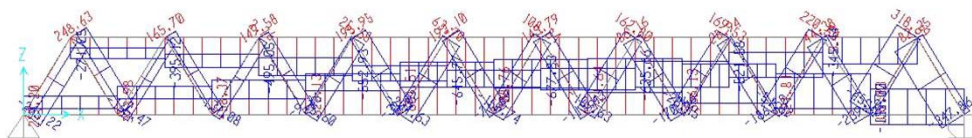Figure 5.42 – Isometric view of the PEI-GF truss bridge

Figure 5.43 – Axial forces diagrams for the dead load + convoy combination

For the load combination (dead load + live load from A30 truck) the maximum axial force was determined in the central members of the lower chords, to be around 800kN. This force was taken as a reference for designing the future friction riveted joints of the GFRP Bridge. As already mentioned this analysis served only for resistance purposes (determining the joint forces that have to be transmitted through the rivets) and not for stability verifications, as it is not the scope of this thesis.

5.5.2. Friction riveted connections for GFRP truss elements

For the connections of the truss elements, friction riveted joints are proposed. The forces to be transferred by the rivets are based on the calculations from the previous chapter (ultimate lap shear strength of 199,20 ± 25,6 MPa), for the determination of the number of rivets necessary for each joint. Adjacent bars were modelled by adding connections joined using threaded titanium grade 2 rivets, joined on the polymeric profiles through Fricriveting, as shown in Figure 5.44.
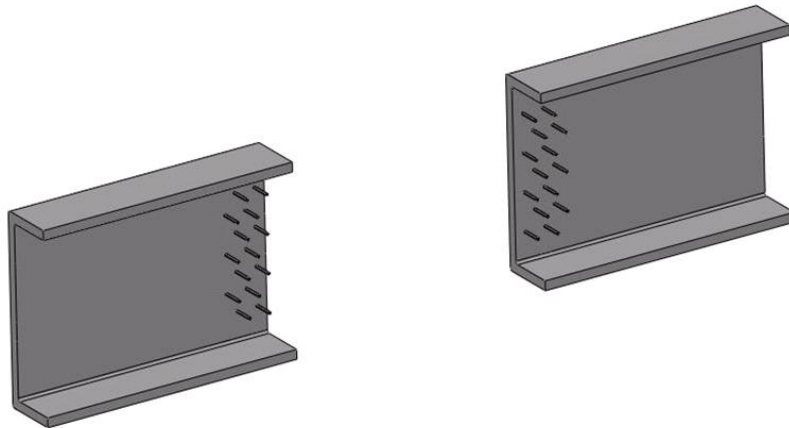
Figure 5.44 – Scheme of the friction riveted GFRP elements.

The load transfer was calculated by using 3 mm thick pre-drilled aluminium gussets, screwed with nuts and washers (Figure 5.45). Figure 5.46 shows the scheme of a assemble GFRP profile connect by the screwed aluminium gusset.
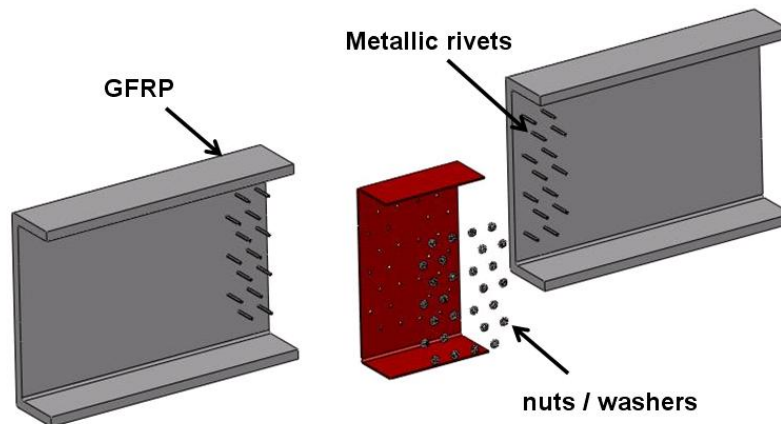
Figure 5.45 – Joining partners used for the structural analysis.
(GFRP structural profiles, metallic rivets, aluminium gusset, metallic nuts and washers)
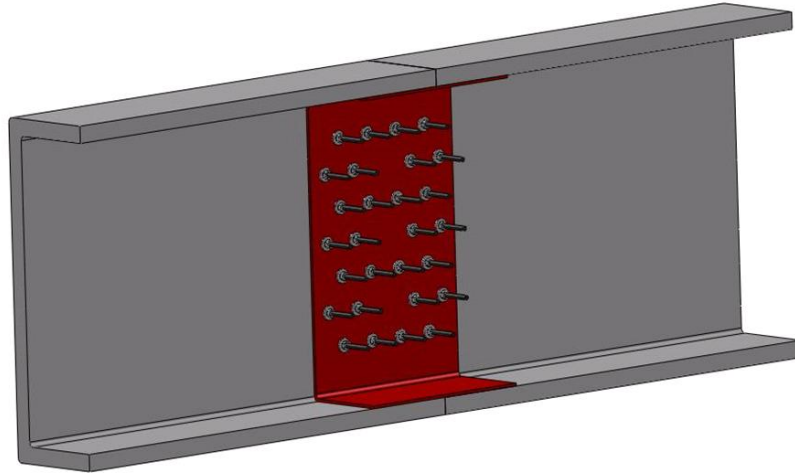
Figure 5.50 – Schematic view of the assembly on GFRP/Ti gr. 2 /AA 2198 friction riveted joints used in the structural bridge model.

The assembly proposed is similar to the one tested in the lap-shear design of experiments in Chapter 5.4.2. Therefore, the joints will be calculated using the resulted lap-shear strength from the DOE with the specified optimized joining conditions, which achieved shear strength of 200 MPa. In the case of the highest joint force to be transmitted (760 kN), the number of rivets necessary was determined, using the following equation [63]:

$$n \geq \frac{F}{\frac{\pi \cdot d^2}{4} \cdot \tau_s} \tag{5.7}$$

With: n – number of rivets

F – force to be transmitted

d – rivet diameter

τ_s - shear strength of the rivet

With the tested rivet diameters of Φ 5 mm, Equation 5.7 specifies a number of 162 rivets necessary for the GFRP/Al/Ti assembly. Increasing the rivet diameter would of course reduce the amount of rivets. Currently the rivet diameter is limited by the welding system used in the process of Fricriveting to Φ 14 mm (Appendix 1). Using this rivet diameter would presumptively reduce the amount of necessary rivets to only 22. Further investigations have to be undertaken on Fricriveting of PEI-GF with larger diameter rivets in order to reduce the amount of rivets; Fricriveting process variables are not linearly dependent to the rivet diameter.

6. CONCLUSIONS AND FINAL REMARKS

6.1. Conclusions of the results in the present work

With regard of the scope of this thesis, stated in chapter 2 (Motivation and Objectives), which is to develop an innovative joining technique and solution for GFRP, the results of the analysis and experiments carried out in this work lead to the following conclusions:

- Aluminum AA 2024-T351 and PEI-GF can be joined through Fricriveting only using proper rivet tip geometries. Rivet anchoring in the case of plain rivets could not be achieved, although deformation of the rivet took place. It was therefore possible to plasticize the rivet inside the polymeric base plate, but the high thermal conductivity of the aluminum alloy led to the uncontrollability of the heat generation and heat dissipation inside the metallic material. The deformation of the rivet tip took place to close to the surface of the polymeric base plate (and causing thereby local damaging of the composite's surface), also as a result of the successive 0°/90 ° stacking lay up of the PEI-GF plies resisting the insertion of the rivet. The unfeasibility of this material combination was doubled by the high smoke, sparks and even fire generation, having a direct result a considerable amount of thermo-mechanically degraded material around the rivet tip.

- By lowering the heat input of the process in the above mentioned material combination, through changing of the cross section geometry of the rivet tip, better joining results and an indirect feasibility could be achieved for PEI-GF / AA 2024-T351 joints. Center holes in the rivet tip resulted in decreased friction surfaces and therefore a lower process heat input while threads provided a drilling effect during the friction phase of Fricriveting, resulting into higher insertion depths. Tensile tests showed that, under the same joining parameters, hollow threaded rivets had a better mechanical performance than plain rivets, with up to 5 times higher ultimate tensile forces. The feasibility study of Fricriveting for PEI-GF / AA 2024-T351 was researched on over 80 test joints.

- The feasibility of Fricriveting for PEI-GF with Titanium grade 2 has been successfully tested and proved. Process parameters have been optimized for a fair level of thermo-mechanically degraded material in the anchoring zone and for mechanical performance. Tensile tests revealed moderate to good mechanical performance, compared to previous research on Fricriveting for unreinforced polymers. Overlap joints have been tested in order to investigate the behavior and lap-shear strength of friction riveted PEI-GF/Ti gr.2. The conducted design of experiments determined the optimal joining parameters for lap-shear strengths at the level of the shear-strength of the titanium alloy, causing in most of the cases failure through shear of the metallic rivet instead of the weaker bearing failure, related to the low shear strength of the composites. Under optimal joining parameters, the achieved lap-

shear strengths reached up to 60% of the tensile strength of the titanium grade 2 rivet material (340 MPa, see Appendix 10)

- Thermographic temperature measurements have shown that generated temperatures ranged between 450 ºC - 600 ºC (30% to 40% of the titanium's melting point), closely dependent to the rotational speed. Comparison tests revealed that friction riveted overlap joints have similar mechanical performance and behavior as bolted joints, using the same diameters of rivets, respectively bolts.
- Numerical modeling of a presumptive lightweight PEI-GF truss bridge showed that, if joined by Fricriveting, elements would take from 22 up to 162 necessary rivets in order to transfer the truss' axial forces in the bars with maximum stresses, depending on rivet diameters (limited to Φ 14 mm in current state of the art). The number of rivets was determined using the lap-shear strengths from the optimal joining parameters (determined in the design of experiments).
- A friction riveted PEI-GF/AA 2198/Ti gr.2 overlap joint assembly has been proposed for joining GFRP structural elements, similar to the one tested in the design of experiments for lap-shear specimens.
- In order to evaluate mechanical performance of the joints using macrographs, a new terminology has been introduced for anchoring efficiency: the volumetric ratio (VR). Hereby, a volumetric approach is being used for predicting the joining efficiency, with the volume of the dislocated polymeric material playing an important role. The volumetric ratio has been evaluated for the PEI-GF/AA 2024-T351 and the PEI-GF/Ti gr. 2 joints used in tensile tests. It has been proven that higher volumetric ratios lead to higher ultimate tensile forces and thereby higher joint strengths. The volumetric ratio approach has been also validated using results from previous research by Amancio [35].
- Although Fricriveting is a friction welding based process and thermosetting polymers are considered un-joinable through welding processes, it has been achieved in course of this work to join thermosetting glass fiber reinforced polyester (P-GF) with titanium grade 3.
- Using the experience of Fricriveting PEI-GF with Titanium grade 2 and P-GF with Titanium grade 3, it has been achieved to join also P-GF with the high strength alloy Titanium grade 5, considered until the present research un-joinable through welding with polymers.

6.2. Contributions of the author

The present work achieved the following original contributions to the state of the art of GFRP joining:

- First joining of a glass fiber reinforced polymer with a metallic rivet, by Fricriveting
- Demonstration of the feasibility of Fricriveting for several material combinations: PEI-GF/AA 2024-T351, PEI-GF/Ti gr. 2, P-GF/Ti gr.5, P-GF/Ti gr. 5
- Introduction and validation of a new concept for the evaluation of anchoring efficiency and mechanical performance of friction riveted joints: volumetric ratio (VR)
- Optimization of the Fricriveting process for lap-shear strength of PEI-GF/Ti gr.2 overlap joints

- Design proposal for an innovative PEI-GF/AA 2198/Ti gr.2 friction riveted overlap joint assembly for structural members, with possible applications in lightweight GFRP bridges (Figure 6.1).
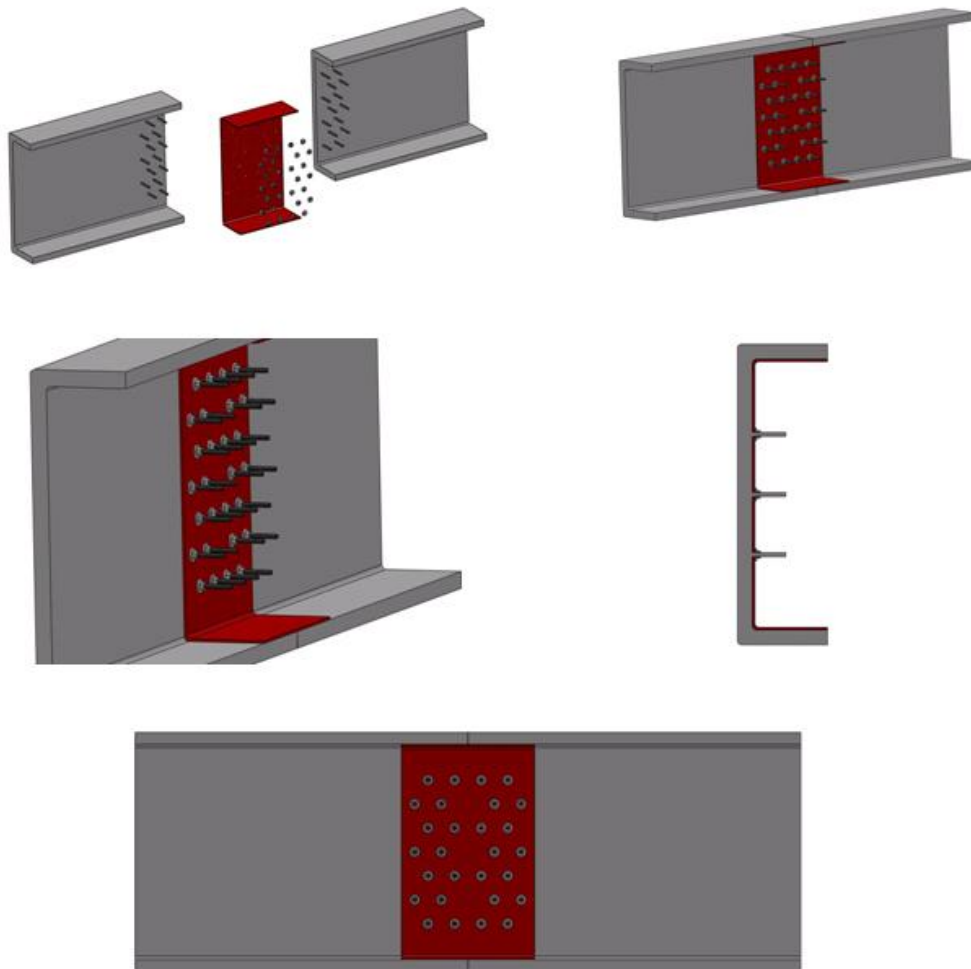

Figure 6.1 – Detailed views of the proposed friction riveted GFRP/AA 2198/Ti gr.2 overlap joint assembly

7. OUTLOOK AND RECOMMENDATIONS FOR FUTURE WORK

Fricriveting is still in its pioneering stage as a potential joining solution of GFRP in industrial applications, especially in civil engineering. Therefore, further research is still necessary in order to obtain a better understanding but also standardization that will make this technology also financial viable. Future work will have to focus on:

- Material choice and feasibility studies for other material combinations
- Fatigue analyses; different industrial applications such as aircraft manufacturing and bridge building require good mechanical performances under cyclic load pattern, therefore a high fatigue strength. Present state of the art provides insufficient information of friction riveted FRP composite-metal joints
- Further development and improving of joint mechanical performance through adequate optimized geometries of joining partners, surface treatments (such as abrasion, surface coating, chemical etching [71, 72])
- For the proposed design of a friction riveted overlap PEI-GF/AA 2198/Ti gr. joint for structural bridge profiles, a safety factor should be developed using the safety concept of the Eurocode 0 [73].

8. BIBLIOGRAPHY

[1] C. E. Bakis, L. C. Bank, V. L. Brown, E. Cosenza, J. F. Davalos, J. J. Lesko, A. Machida, S. H. Rizkalla, T. C. Triantafillou, Fiber-Reinforced Polymer Composites for Construction – State of the Art Review, Journal of Composites for Construction, May 2002, ASCE, ISSN 1090-0268

[2] N. Taranu, Polymeric Composites in Construction, Course notes, Universitatea Politehnica "Gh. Asachi" Iasi, The University of Sheffield Printing Office, UK 2009

[3] J. M. Skinner, A critical analysis of the Aberfeldy Footbridge, Scotland, Proceedings of Bridge Engineering 2 Conference 2009, April 2009, University of Bath, Bath, UK

[4] www.fiberline.com, website from Fiberline Composites A/S, Denmark, date of visit: 01.12.2011

[5] http://www.strongwell.com/, website of Strongwell Composites, 09.09.2011

[6] T. J. Reihard, Overview of Composite Materials, Handbook of Composites, 2nd. Edition, edited by S. T. Peters, Chapman & Hall, 1998 London, UK, ISBN 0 412 54020 7

[7] D. L. Chung, Composite materials – Science and Applications, 2nd edition, Springer, NY, 2010

[8] W.W. Wolf, S. L. Mikesell, Glass Fibres, Encyclopedia of Materials Science and Engineering, 1st Edition, 1986, ISBN 0080221580

[9] F. A. Cassis, R. C. Talbot, Polyester and Vynil Ester Resins, Handbook of Composites, 2nd. Edition, edited by S. T. Peters, Chapman & Hall, 1998 London, UK, ISBN 0 412 54020 7

[10] L. S. Penn, H. Wang, Epoxy Resins, Handbook of Composites, 2nd. Edition, edited by S. T. Peters, Chapman & Hall, 1998 London, UK, ISBN 0 412 54020 7

[11] J. L. Hull, Processing of Thermosets, Modern Plastics Handbook, edited by C. A. Harper, McGraw-Hill, 2000 New York, ISBN 0-07-0267890

[12] J. A. Brydson, Plastics Materials, 7th edition, Butterworth-Heinemann, 1999 Oxford, ISBN 0-7506-4132-0

[13] R. E. Wright, Thermosets. Reinforced Plastics and Composites, Modern Plastics Handbook, edited by C. A. Harper, McGraw-Hill, 2000 New York, ISBN 0-07-0267890

[14] A.-M. Baker, J. Mead, Thermoplastics, Modern Plastics Handbook, edited by C. A. Harper, McGraw-Hill, 2000 New York, ISBN 0-07-0267890

[15] Materials Datasheets PEI-GF composite laminate (CETEX® PEI) www.tencate.com , website of TenCate Advanced Composites BV Company, date of visit 16.08.2011

[16] B. A. Wilson, Pultrusion, Handbook of Composites, 2nd. Edition, edited by S. T. Peters, Chapman & Hall, 1998 London, UK, ISBN 0 412 54020 7

[17] EN 13706:2002. Reinforced plastic composites – Specification for pultruded profiles

[18] L. Fong, S. G. Advani, Resin Transfer Molding, Handbook of Composites, 2nd. Edition, edited by S. T. Peters, Chapman & Hall, 1998 London, UK, ISBN 0 412 54020 7

[19] Y. M. Tarnopolskii, S. T. Peters, A. L. Beil, Filament Winding, Handbook of Composites, 2nd. Edition, edited by S. T. Peters, Chapman & Hall, 1998 London, UK, ISBN 0 412 54020 7

[20] L. Blaga, Advantages and problems regarding the applications of glass-fibre-reinforced-polymers, Proceedings of the Modtech International Conference - New Face of TCMR, Modern Technologies, Quality and Innovation, Iasi, 21-23 May 2009

[21] http://www.bmlv.gv.at , website of the Austrian Armed Forces, date of visit: 23.10.2011

[22] Field Manual No. 5-277, Bailey Bridge, Headquarters Department of the Army, Washington DC, 9 May 1986

[23] M. LaViolette, Bridge Construction Practices using Incremental Launching, report of the Bridge Engineer Center, Center for Transport Research and Education, Iowa State University, Ames, 2007

[24] www.mil.state.or.us , website of the Oregeon Military Department, date of visit, 23.10.2011

[25] G. Sedlacek, M. Oppe, H. Trumpf, Design and testing of an inventive GFRP-truss- bridge for 40 t trucks and 30 m span, Proceedings of the COBRAE Conference 2005 – Bridge Engineering with Polymer Composites, Leusden 2005

[26] G. Sedlacek, H. Trumpf, Innovative developments for bridges using FRP composites, Advanced Polymer Composites, ACIC 2004, University of Surrey, Guildwoford, Woodhead Publishing Ltd., Cambridge, April 2007, ISBN 1855737361

[27] L. Blaga, S. T. Amancio Filho, J. F. dos Santos, R. Bancila, Fricriveting of civil engineering composite laminates for bridge construction

[28] D. Duthinh, Connections of fiber-reinforced polymer (FRP) structural members: a review of the state of the art, NISTIR 6532, National Institute of Standards and Technology, Gaithersburg MD, US 2000

[29] Hart-Smith, Design of adhesively bonded joints, Joining Fiber-Reinforced Plastics, Matthews, F. L. ed, Elsevier, 1987

[30] ASTM D 5573-99: Standard practice for classifying failure modes in fiber-reinforced-plastic (FRP) joints. ASTM International, Pennsylvania US, 2005

[31] J. T. Mottram, Challenges for the design of connections and joints in all-FRP construction, Costruzioni in Materiale Composito – All-FRP Constructions, Universita Iuav di Venezia, Italy, 18th September 2007

[32] L. C. Banks, Composites for Construction. Structural Design with FRP Materials, John Wiley & Sons, NY 2006, ISBN 0-471-68126-1

[33] J. T. Mottram, Y. Zheng, Further tests on beam-to-column connections for pultruded frames, Journal of Composites for Construction, 1999, ISSN 1090-0268

[34] S. T. Amancio Filho, J. F. dos Santos, Fricriveting: a new technique for joining thermoplastics to lightweight alloys, ANTEC 2008, Plastics: Annual Technical Conference Proceedings, Society of Plastic Engineers, Milwaukee WI 2009, ISBN 978-1-6056032-0-9

[35] S. T. Amancio Filho, Friction Riveting: development and analysis of a new joining technique for polymer-metal multi-materials structures, PhD thesis at the Hamburg-Harburg University of Technology, GKSS 2007, ISSN 0344-9629

[36] S. T. Amancio Filho, Friction Riveting: development and analysis of a new joining technique for polymer-metal multi-materials structures, Henry Granjon Prize Competition 2009, Welding in the World Vol. 55, No. 01/02 2011

[37] F. W. Billmeyer Jr., Textbook of polymer science, 2nd. Edition, Willey-Interscience NY, USA, ISBN 0471072966

[38] S. T. Amancio Filho, J. F. dos Santos, Entwicklung des Reibnietens als neues Fügeverfahren für Kunststoff und Leichtbaulegierungen, Materialwissenschaft und Werkstofftechnik Nr. 11, 39, 2008, Willey-VCH Verlag GmbH & Co KGaA, Weinhein 2008

[39] S. T. Amancio Filho, J. F. dos Santos, Influence of processing parameters on microstructure and properties of a polyetherimide joined by FricRiveting: Investigation of rotational speed, ANTEC 2009, Annual Technical Conference Proceedings, ISBN 978-0-9753707-7-3, Society of Plastic Engineers, Chicago II, 2009

[40] S. T. Amancio Filho, J. Roeder, S. P. Nunes, J. F. dos Santos, F. Beckmann, Thermal degradation of polyetherimide joined by friction riveting (FricRiveting). Part I: Influence of rotation speed, Polymer Degradation and Stability 93 (2008), Elsevier Ltd, 2008

[41] R. W. Messler Jr., Joining composite materials and structures: some thought- provoking possibilities, Journal of Thermoplastic Composite Materials, Vol. 17, January 2004, Sage Publications, ISSN 0892-7057/04/01 0051

[42] RSM 400 RK…, Reibschweissköpfe - Technisches Handbuch 24651 4-29433-2, Harms & Wende GmbH & Co. KG, Hamburg, Germany, 2006

[43] G. Petzow, Metallographic etching, techniques for metallography, ceramography and plastography. 2nd ed. ASM International, USA 1999

[44] www.struers.com , website of Struers Company, date of visit: 11.01.2012

[45] ASTM E384-992e1, Standard Test Method for Microindentation Hardness of Material, ASTM International, 2005

[46] F.J.B. Calleja, S. Fakirov, Microhardness of polymers. Cambridge University Press, Cambridge, England, 2000

[47] EN ISO 527-4: Tensile Properties of Isotropic and Orthotropic Fiber-Reinforced Plastic Composites

[48] DIN EN ISO 898-1: Mechanische Eigenschaften von Vergindungselementen aus Kohlenstoffstahl und legierten Stahl – Teil 1: Schrauben, Deutsches Institut für Normung e.V., 1999

[49] DIN EN 10002: Metallische Werskstoffe – Zugversuch, Deutsches Institut für Normung e.V., 2001

[50] ASTM D 5961 M – 08: Standard test method for bearing response of polymer matrix composite laminates, ASTM International, 2010

[51] G. Taguchi, S. Chowdhury, Y. Wu, Taguchi's Quality Engineering Handbook, John Wiley & Sons Inc., Hoboken, New Jersey 2005, ISBN 0-471-41334-8

[52] ASM Materials Handbook Metals, ASM International, USA 2006

[53] CETEX ® PEI data sheet, TenCate Advanced Composites, Netherlands 2011.

[54] E. A. Brandes, G.B. Brook, Smithells Light Metals Handbook, Butterworth-Heinemann, Oxford 1998, ISBN 0-7506-3625-4

[55] S. T. Amancio Filho, J. F. dos Santos, FricRiveting: A new joining technique for thermoplastics-lightweight alloy structures, Materials Science and Technology 2008, Joining of advanced and speciality materials, October 5-9, Pittsburgh, Pennsylvania 2008

[56] D. C. Montgomery, Design and analysis of experiments, 5th Edition, NY, John-Willey & Sons Inc 2006

[57] P. J. Ross, Taguchi techniques for quality engineering, Tata, McGraw-Hill, NY 1988

[58] L. J. Hart-Smith, Mechanically fastened joints for advanced composites – phenomenological considerations and simple analyses, Conference of fibrous composites in structural design, Plenum Press, NY, USA 1978

[59] V. P. Lawlor, W. F. Stanley, M.A. McCarthy, Characterisation of damage development in single-shear bolted composites, Journal of Plastics, Rubber and Composites 31 (3)

[60] M.C.-Y., Composite airframe structures, practical design information and data, 2nd edition, Hong Kong Conmilit Press Ltd. Hong Kong 2000

[61] M. J. Donachie Jr., Titanium. A technical guide. 2nd edition, ASM International, Ohio, USA 2010

[62] STAS 3321-86, Romanian Standard for road bridges, convoys and load classes

[63] P. Tripa, Rezistenta materialelor, Ed. Mirton, Timisoara 2001

[64] L. J. Hart-Smith, Mechanically fastened joints for advanced composites – phenomenological considerations and simple analysis, Douglas Paper 6748, 1972

[65] P.P. Camanho, F.L. Matthews, Stress analysis and strength prediction of mechanically fastened joints in FRP: a review, Composites Part A 28A, Elsevier Science Ltd., 1997

[66] S. Thoppul, J. Finegan, R. F. Gibson, Mechanichs of mechanically fastened joints in polymer-matrix composite structures – A review, Composites Science and Technology 69, Elsevier Science Ltd., 2009

[67] R. R. Schmit,W.J. Horn, Viscoelastic relaxation in bolted thermoplastic composite joints, 35th International SAMPE Symposium and Exhibition 1990

[68] W. J. Horn, R. R. Schmit, Relaxation in bolted thermoplastic composite joints, AIAA J 1993; 32(3)

[69] H. Zhao, R.F. Gibson, Influence of clamping force relaxation on vibration damping measurements for polymer composite cantilever beams. Proc SEM Spring Conf 1995; Grand Rapids, MI

[70] M. F. Ashby, D. R. H. Jones, Engineering Materials 1. An introduction to their properties and applications, 2nd edition, Butterworth Heinemann, Jordan Hill, Oxford, UK 2002

[71] R. F. Wegman, Surface preparation techniques for adhesive bonding, Noyes Publications, New Jersey, USA 1989

[72] J. Rotheiser, Joining of Plastics- Handbook for designers and engineers, Carl Hanser Verlag, Munchen, Germany 1999

[73] Eurocode 0. EN 1990 Basis of Structural Design

[74] http://www.kockums.se, official website of the Kockums company, part of ThyssenKrupp Marine Systems, date of visit: 21.01.2012

[75] www.arcaspace.com , official website of Aeronautics and Cosmonautics Romanian Association (ARCA), date of visit 01.12.2011

[76] http://pinktentacle.com/2010/03/photos-expo-70/, collection of photographs from the Shanghai Expo 70, date of visit: 09.01.2012

[77] C. Tuakta, Use of FRP in bridge structures, MSc. Thesis in civil and environmental engineering at the Massachusetts Institute of Technology, June 2005

[78] G. Sedlacek, H. Trumpf, Mobile Leichtbau-Festbrücke aus pultrudierten faserverstärkten Polymerprofilen, Bauingenieur, Springer VDI Verlag, Düsseldorf, Germany, 2005

[79] K.F. Koch, Hilfsbrücken. Grundlagen, Planung, Konstruktion, Ausführung, Werner Verlag, 1998

[80] S. T. Amancio Filho, M. Beyer, J.F. dos Santos, DE 10 2005 056 606 A1, Verfahren zum Verbinden eines metallischen Bolzens mit einem Kunststoff-Werkstück, Deutsches Patent- und Markenamt, München 2007

[81] R. A. Daniel, Environmental considerations to structural material selection for a bridge, European Bridge Engineering Conference, Lightweight Bridge Decks, Rotterdam, March 2003

[82] http://pultruders.com, official website of the European Pultrusion Technology Association, date of visit: 11.09.2011

[83] www.fibre-reinforced-plastics.com, The Fiber Reinforced Plastic & Composite Technology Resource Center, date of visit: 01.12.2011

[84] OSHA Technical Manual (OTM), Occupational Safety & Health Administration, United States Department of Labor, Directive Number: TED 01-00-105, Office of science and technology assessment, Washington D.C. 1999

[85] EUROCOMP Design Code and Handbook: Structural design of polymer composites, The European Structural Polymeric Group, E & FN Spon, 1996

[86] Fiberline Design Manual, Fiberline Composites A/S, Denmark, 2003

[87] H. Trumpf, Stabilitätsverhalten ebener Trafwerke aus pultrudierten faserverstärkten Polymerprofilen, PhD Thesis, Schriftenreihe Stahlbau, RWTH Aachen, Heft 59, Schaker Verlag, Aachen 2006

[88] Extern Design Manual, Strongwell Corporation, Bristol, Virginia 1998

[89] ASCE Manuals and Reports on Engineering Practice No. 63: Structural Plastics Design Manual, American Society of Civil Engineers, 1984

[90] BÜV Empfehlungen: Tragende Kunststoffbauteile im Bauwesen (TKB) – Entwurf, Bemessung und Konstruktion, October 2002

[91] DIN 18820: Laminate aus textilfaserverstärkten ungesättigten Polyester- und Phenacrylharzen für tragende Bauteile, Beuth Verlag, Berlin 1991

[92] Snaplock fiber reinforced composites technology applied to overhead sign structures: Design, construct and test a fiber reinforced composite overhead sign truss, Final report, No CA07-0246, Composite Support & Solutions Inc., San Pedro, CA 2008

[93] S.T. Amancio Filho, J. F. dos Santos, V. Ventzke, Determination of fracture mechanisms under tensile loading in a commercial available engineering thermoplastic material joined by Fricriveting, 5th International Conference on Fracture of Polymers, Composites and Adhesives, 7-11 September 2008, Les Diablerets, Switzerland 2008

[94] C. F. Rodrigues, FricRiveting of polycarbonate and aluminum AA 2024-T351, Graduation work, Universidade Federal de Sao Carlos, Sao Carlos 2011

[95] S.T. Amancio Filho, J.F. dos Santos, Joining of polymers and polymer-metal hybrid structures: recent developments and trends, Polymer Engineering and Science, Wiley & Sons, NY 2009

[96] AASHTO, Standard specifications for highway bridges

[97] M.F. Borges, Análise numérica e experimental do comportamento mecânico de juntas híbridas polímero-metal obtidas através de processo de união por fricção, Graduation work, Universidade Federal do Rio Grande do Sul, Escola de Engenharia, Department of mechanical engineering, Porto Alegre 2009

[98] S.-I. Kuroda et al., Degradation of aromatic polymers – I. rates of crosslinking and chain scission during thermal degradation of several soluble aromatic polymers, European Polymer Journal, 20(1), 1989

[99] www.csiberkeley.com, official website of Computers & Structures Inc., Structural and Earthquake Engineering Software, date of visit: 11.01.2012

[100] ASTM E8 / E8M – 11, Standard test methods for tension testing of metallic materials, ASTM International

[101] DIN EN ISO 527-4: Plastics – Determination of tensile properties, part 4: Test conditions for isotropic and anisotropic fiber-reinforced plastic composites

9. APPENDIXES

Appendix 1:

RSM 400 high-speed friction welding machine , Harms & Wende GmbH.

The sumarized data sheet of the friction welding equipment used in this work consisted of:

Type	RSM 400
Manufacture	Harms & Wende GmbH & Co. KG
Weight	45 kg
Drive type	Induction motor
Power	Asynchronic 1,85 kW or 3,0 kW
Supply voltage	3 x 400 V/N/PE 50 Hz
Ambient temperature	+10ºC to +40ºC
Control voltage	24 VDC
Speed	6000 rpm to 24000 rpm
Pneumatic force	11 kN at p = 6 bar
Supply	Max p = 10 bar
Feed	Pneumatic, stroke 50 mm
Dimensions	Diameter = 280 mm Length = 550 mm
Spindle	Triple row angular contact ball bearing mount encapsulated on separate carriage
Holding capacity	Φ = 5 mm to 14 mm Length = 10-100 mm

Appendix 2:

Influence of process parameters on the aspect of PEI-GF / AA 2024 joints (one-fact-at-a-time approach, OFAT) in terms of aspect ratio
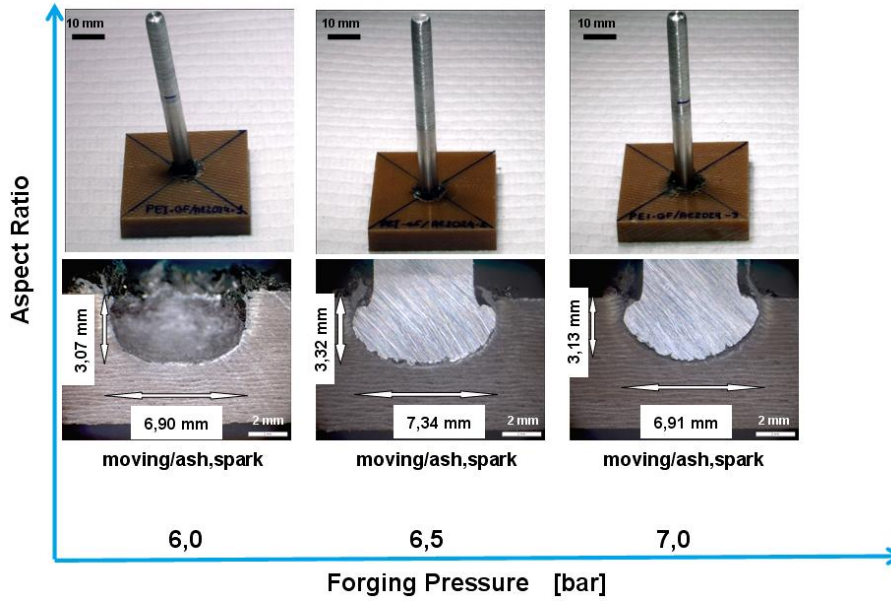
Figure A.1 – Influence of forging pressure on PEI-GF / AA 2024 joints under constant parameters: RS 12000 rpm, FT 1500 ms, FOT 1200 ms, FP 4,0 bar
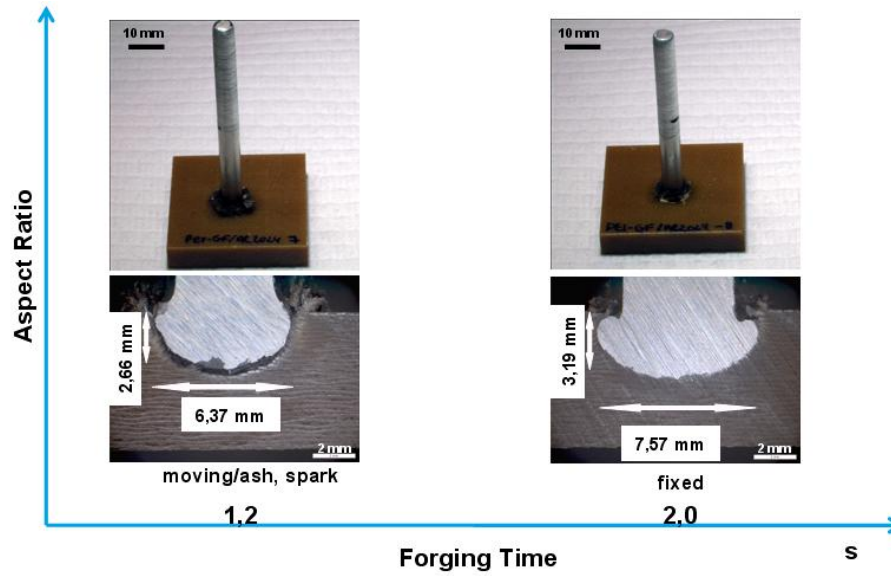
Figure A.2 – Influence of forging time on PEI-GF / AA 2024 joints under constant parameters: RS 12000 rpm, FT 1500 ms, FP 3,5 bar, FOP 6 bar
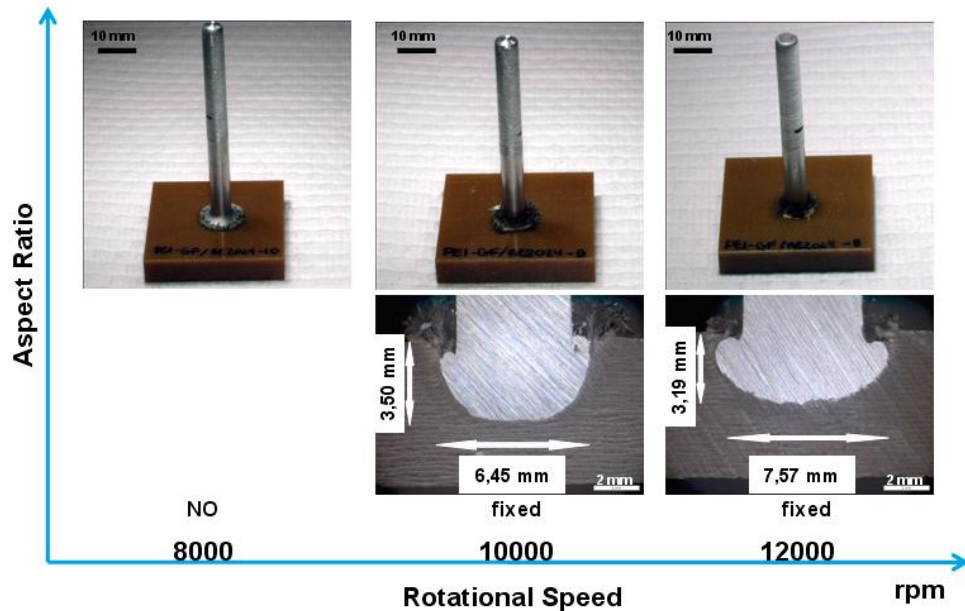
Figure A.3 – Influence of rotational speed on PEI-GF / AA 2024 joints under constant parameters: FT 1500 ms, FOT 2000 ms, FP 3,5 bar, FOP 6 bar
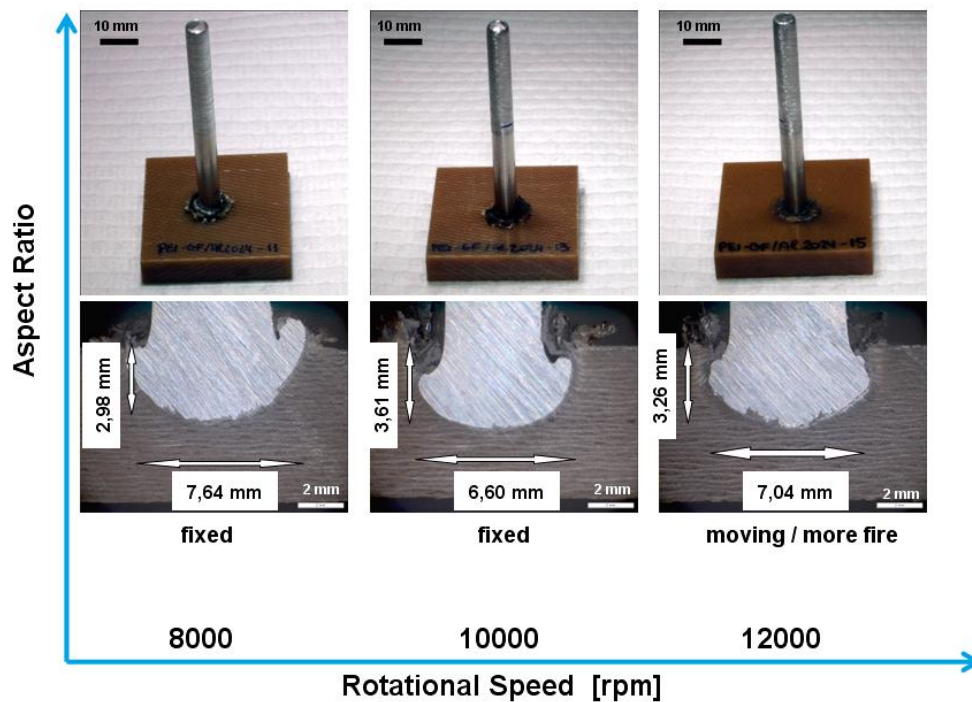
Figure A.4 – Influence of rotational speed on PEI-GF / AA 2024 joints under constant parameters: FT 2000 ms, FOT 2000 ms, FP 3,5 bar, FOP 6 bar
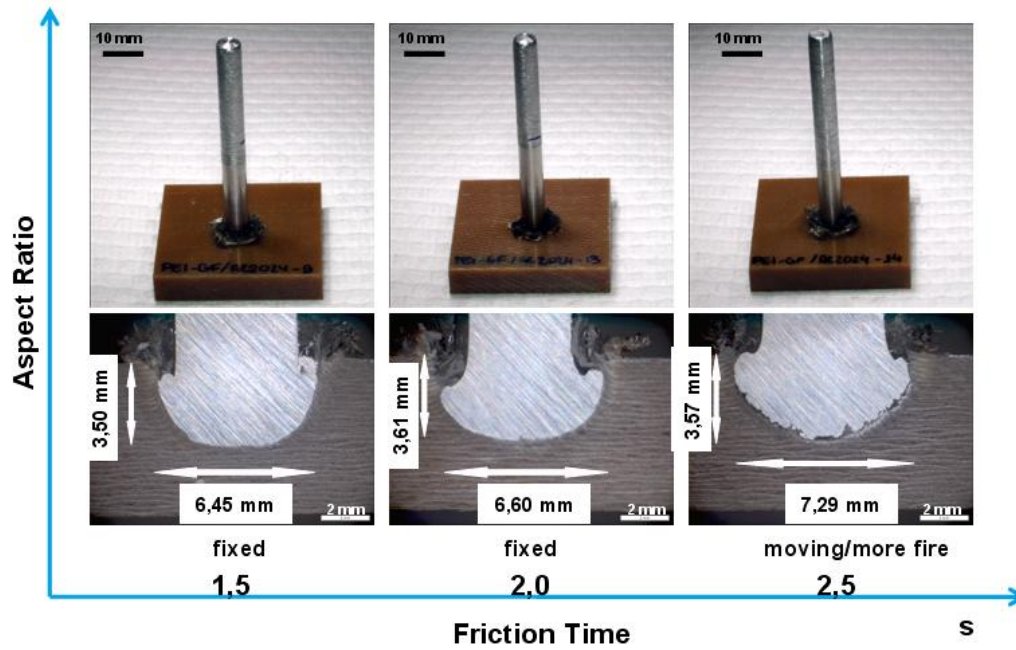
Figure A.5 - Influence of friction time on PEI-GF / AA 2024 joints under constant parameters: RS 10000 rpm, FOT 2000 ms, FP 3,5 bar, FOP 6 bar

Appendix 3:

Macrographs of the PEI-GF / Ti gr. 2 conditions from the feasibility study
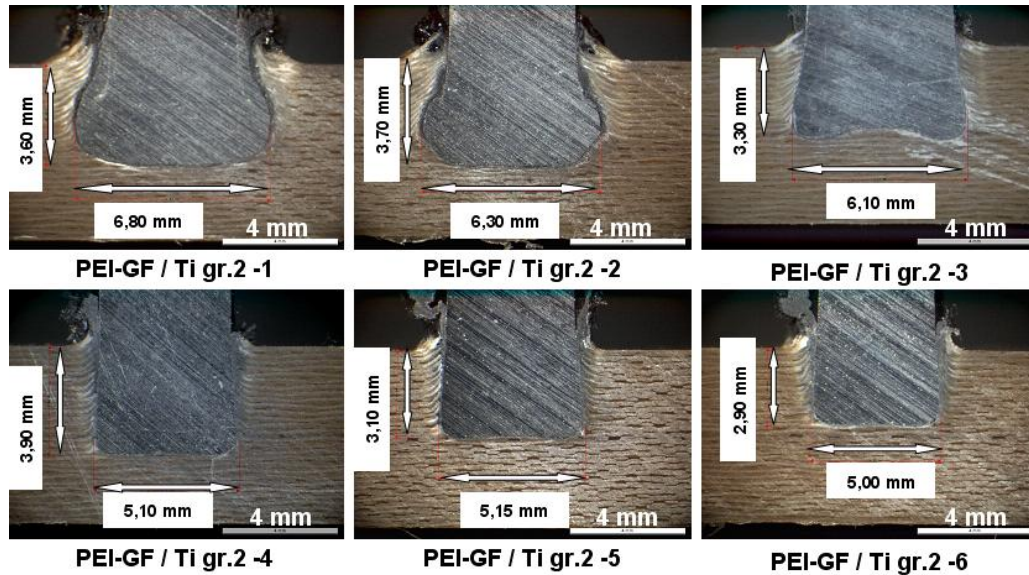
Figure A.6 – Friction riveted PEI-GF/Ti gr. 2 specimens 1-6
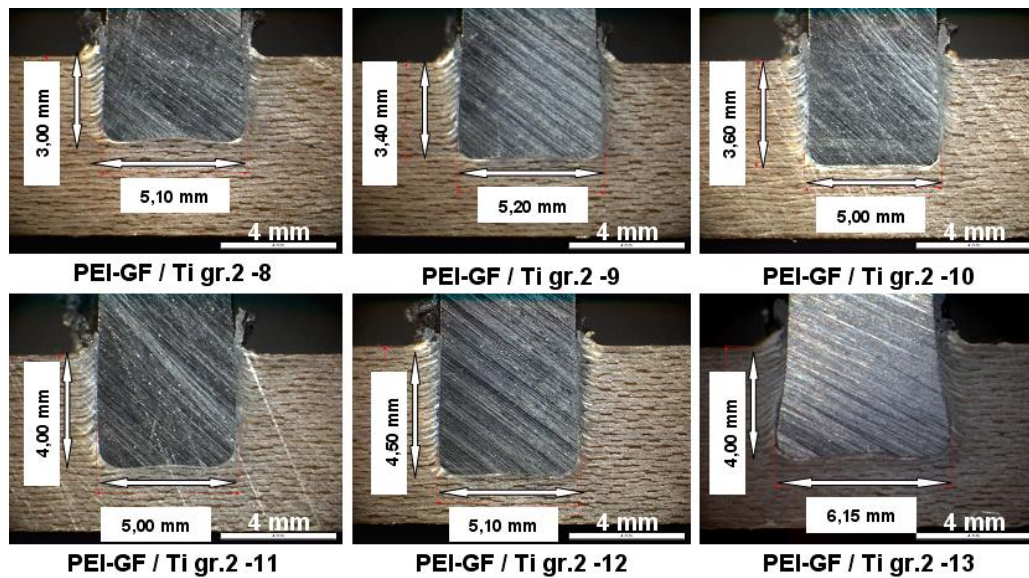
Figure A.7 – Friction riveted PEI-GF/Ti gr. 2 specimens 8-13
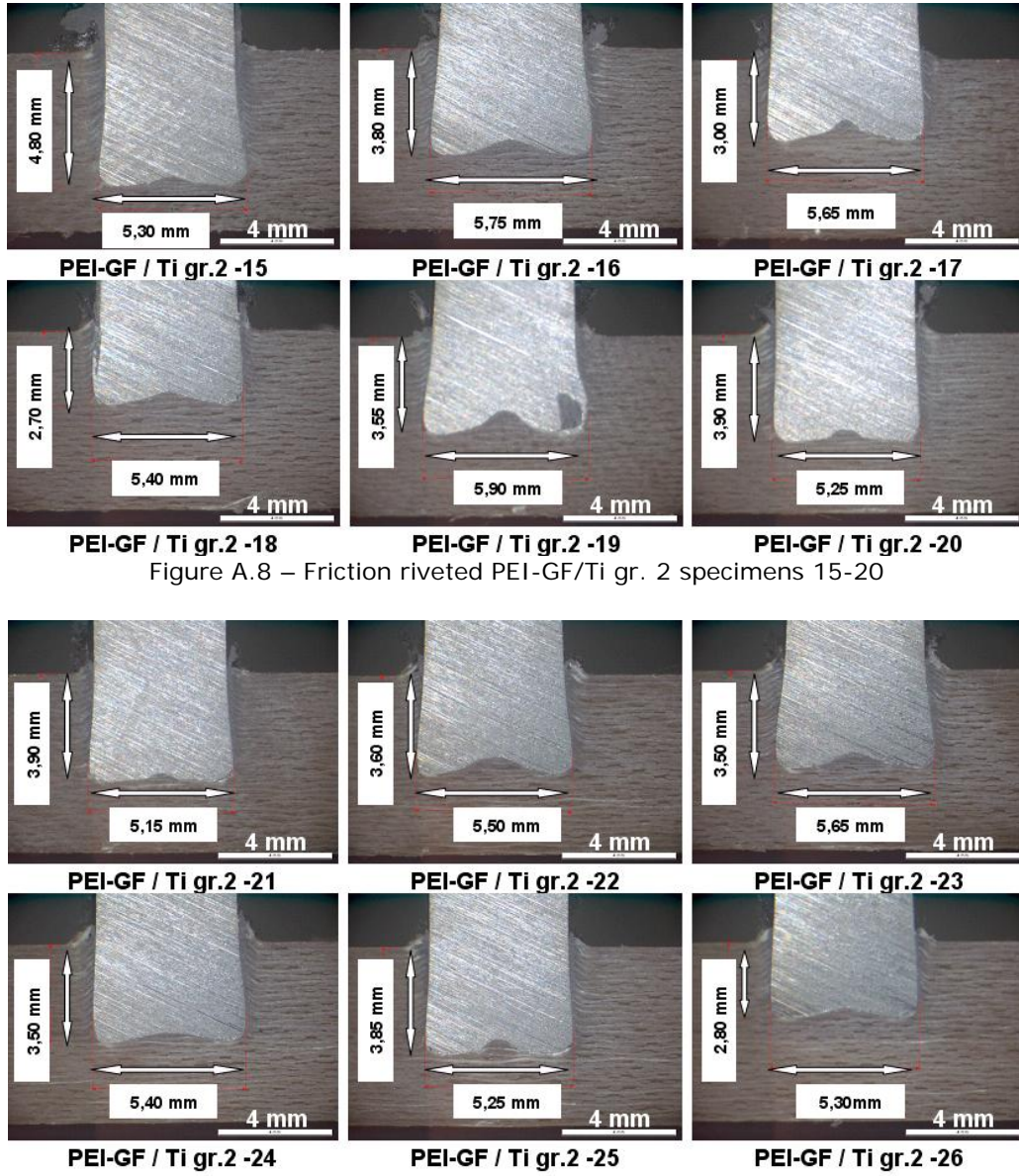
Figure A.8 – Friction riveted PEI-GF/Ti gr. 2 specimens 15-20

Figure A.8 – Friction riveted PEI-GF/Ti gr. 2 specimens 21-26

Appendix 4:

Results of the lap-shear design of experiments. Typical force-displacement curves and failure modes.
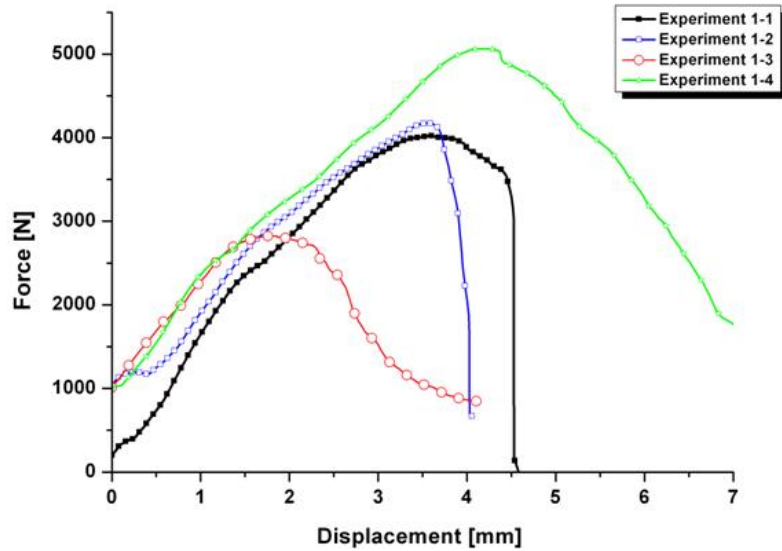
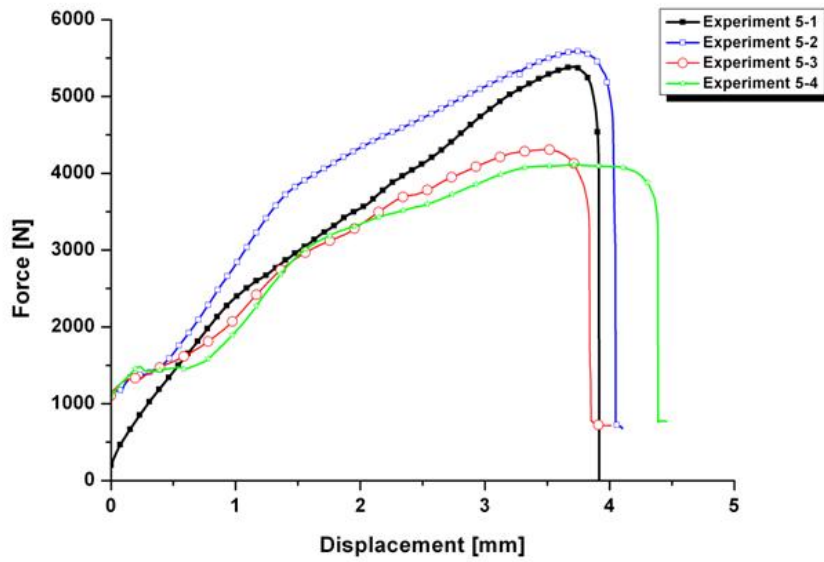Figure A.9 – Results of Experiment 1
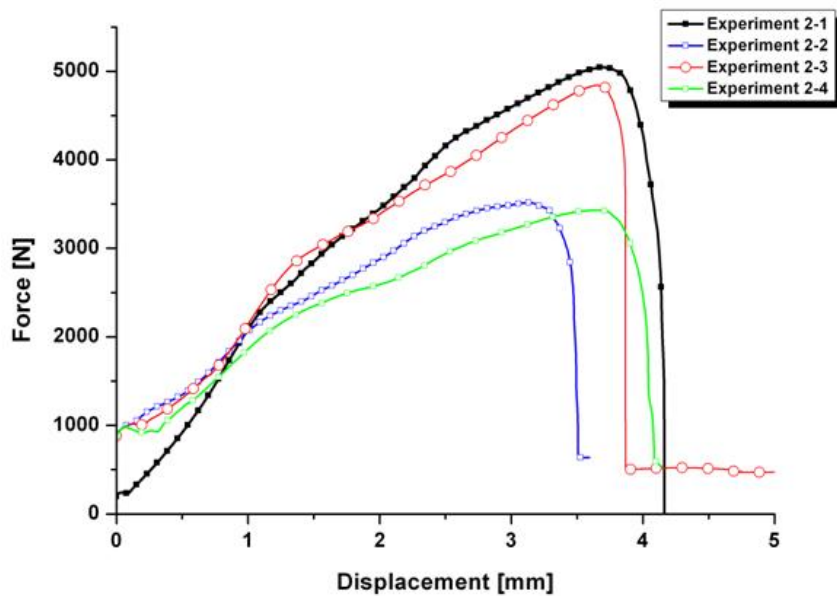
Figure A.10 – Results of Experiment 2
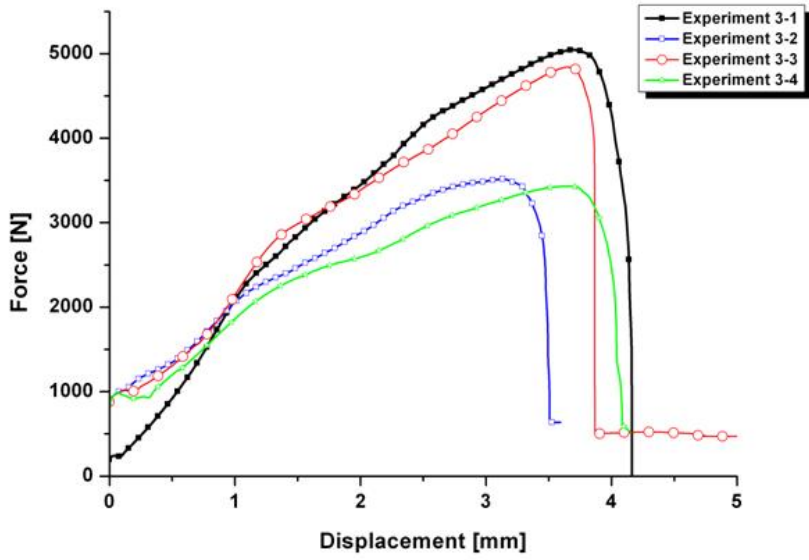
Figure A.11 – Results of Experiment 3
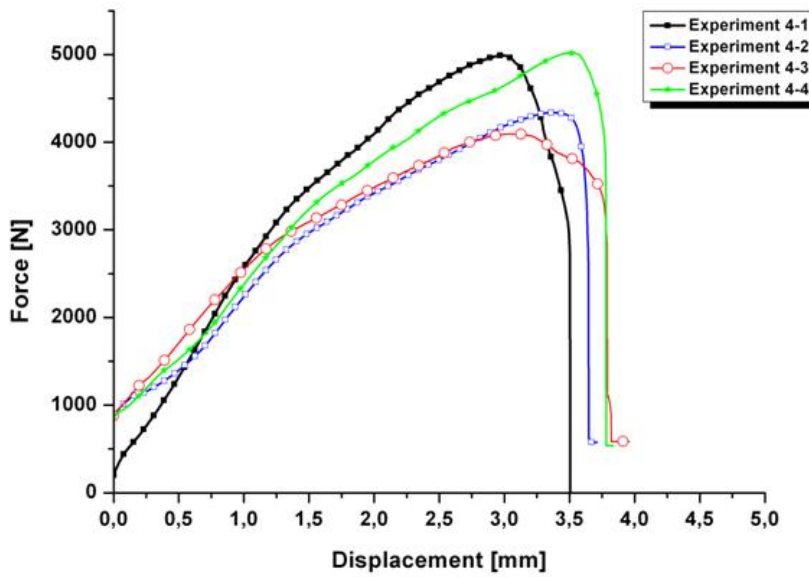
Figure A.12 – Results of Experiment 4

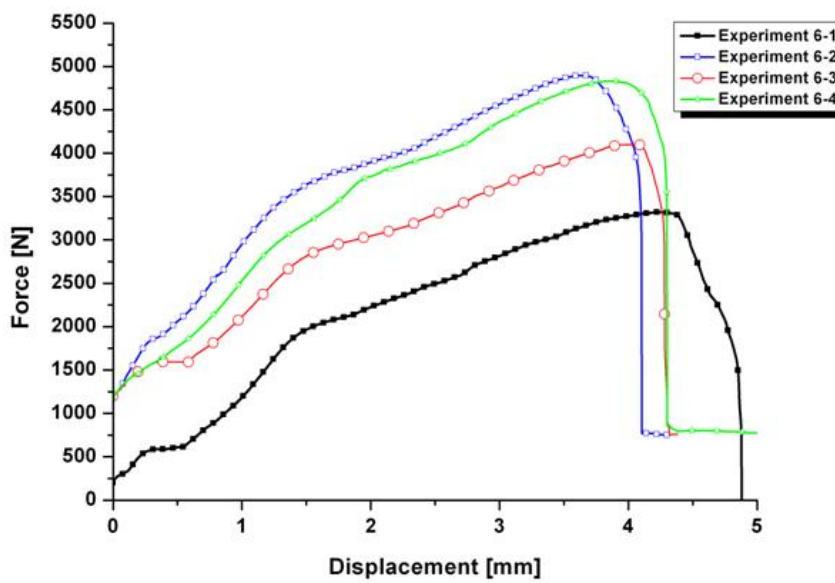Figure A.13 – Results of Experiment 5

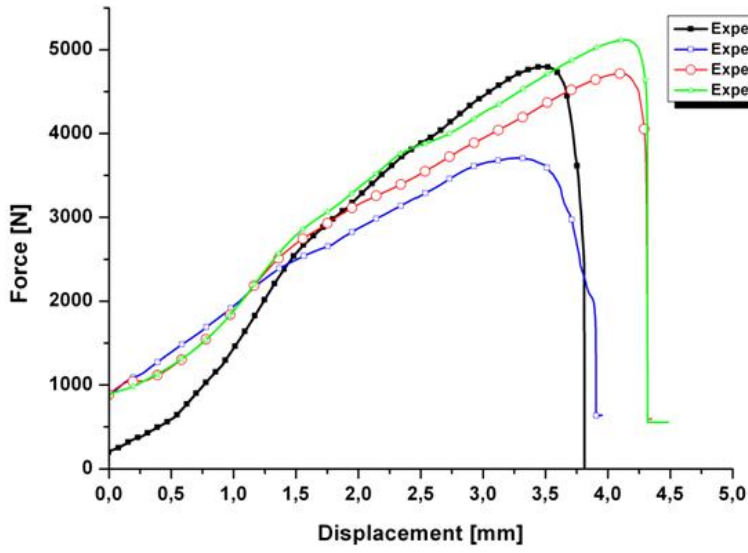Figure A.14 – Results of Experiment 6
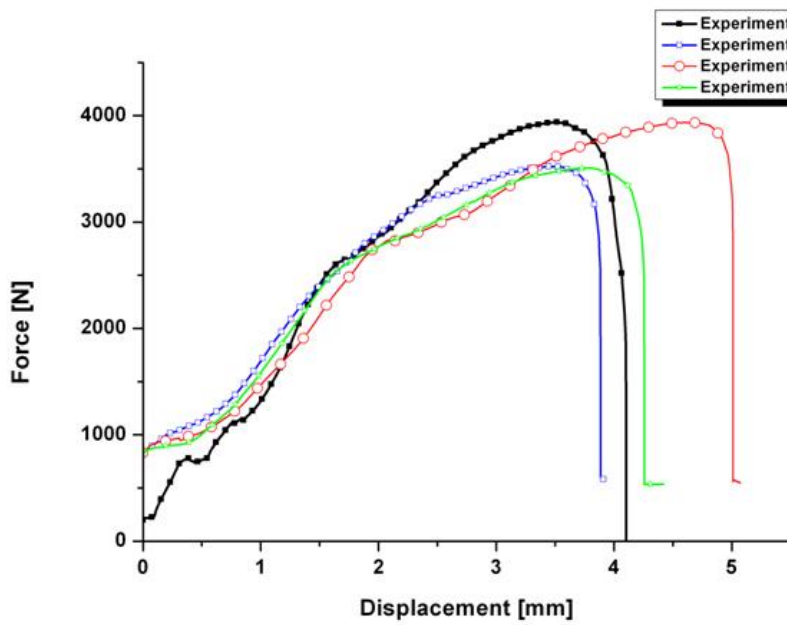
Figure A.15 – Results of Experiment 7

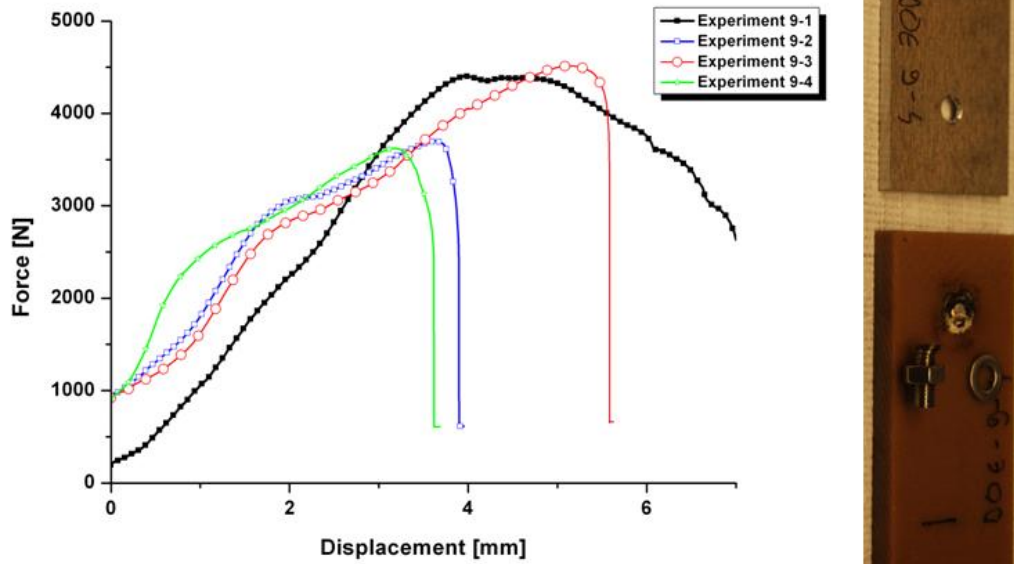Figure A.16 – Results of Experiment 8

Figure A.17 – Results of Experiment 9

Appendix 5:

Taguchi design of experiments. Analysis of variance (ANOVA) using MINITAB 15 software

————— 12.12.2011 18:33:33 ——————————————————

Welcome to Minitab, press F1 for help.
Executing from file: C:\Program Files\Minitab 15\English\Macros\Startup.mac

This Software was purchased for academic use only.
Commercial use of the Software is prohibited.

Taguchi Design

Taguchi Orthogonal Array Design

L9(3**4)

Factors: 4
Runs: 9

Columns of L9(3**4) Array

1 2 3 4

————— **22.12.2011 10:07:04** ———————————————————

Welcome to Minitab, press F1 for help.
Retrieving project from file: 'D:\LUCIAN\WORK HZG\DOE LAP SHEAR\EXPERIMENTS
LAP SHEAR.MPJ'

Taguchi Analysis: result 1; result 2; result 3; mean versus RS; FT; FOT; FOP

Linear Model Analysis: Means versus RS; FT; FOT; FOP

Estimated Model Coefficients for Means

```
Term       Coef
Constant  4227,08
RS 8000   -337,08
RS 10000   90,83
FT 700     174,17
FT 1200    298,75
FOT 1200  -500,42
FOT 1850   425,83
FOP 6      -56,25
FOP 7       97,92
```

S = *

Analysis of Variance for Means

Source	DF	Seq SS	Adj SS	Adj MS	F	P
RS	2	547545	547545	273772	*	*
FT	2	1029707	1029707	514854	*	*
FOT	2	1311941	1311941	655970	*	*
FOP	2	43464	43464	21732	*	*
Residual Error	0	*	*	*		
Total	8	2932656				

Response Table for Signal to Noise Ratios
Nominal is best (10*Log10(Ybar**2/s**2))

Level	RS	FT	FOT	FOP
1	14,77	19,82	18,65	16,23
2	21,63	18,19	21,50	18,44
3	20,34	18,72	16,58	22,06
Delta	6,86	1,63	4,92	5,83
Rank	1	4	3	2

Response Table for Means

```
Level   RS    FT   FOT   FOP
1      3890  4401  3727  4171
2      4318  4526  4653  4325
3      4473  3754  4302  4185
Delta   583   772   926   154
Rank     3     2     1     4
```

Response Table for Standard Deviations

```
Level    RS     FT    FOT    FOP
1      709,4  524,7  481,1  662,3
2      416,3  597,9  451,7  542,3
3      442,6  445,7  635,4  363,7
Delta  293,2  152,1  183,7  298,7
Rank     2      4      3      1
```

Main Effects Plot for Means

 Main Effects Plot for StDevs

Main Effects Plot for SN ratios

 Taguchi Analysis: result 1; result 2; result 3; mean versus RS; FT; FOT; FOP

Predicted values

```
S/N Ratio    Mean    StDev   Ln(StDev)
 12,7383   3507,50  809,254   6,69611
 16,1629   4712,50  733,002   6,59715
 15,3984   3450,00  586,003   6,37333
 28,2771   4876,25  188,033   5,23662
 15,8940   4635,00  743,617   6,61153
 20,7133   3442,50  317,109   5,75925
 18,4417   4820,00  576,715   6,35735
 22,5066   4230,00  316,965   5,75879
 20,0573   4370,00  434,127   6,07334
```

Factor levels for predictions

```
  RS     FT   FOT  FOP
 8000   700  1200   6
 8000  1200  1850   7
 8000  1700  2500   8
10000   700  1850   8
10000  1200  2500   6
10000  1700  1200   7
12000   700  2500   7
12000  1200  1200   8
12000  1700  1850   6
```

Taguchi Analysis: result 1; result 2; result 3; mean versus RS; FT; FOT; FOP

Predicted values

S/N Ratio   Mean   StDev Ln(StDev)
 16,1629 4712,5 733,002   6,59715

Factor levels for predictions

  RS   FT   FOT FOP
8000 1200 1850   7

Taguchi Analysis: result 1; result 2; result 3; mean versus RS; FT; FOT; FOP

Predicted values

S/N Ratio   Mean   StDev Ln(StDev)
 11,6422 2860,42 730,333   6,66806

Factor levels for predictions

  RS   FT   FOT FOP
8000 1700 1200   6

Taguchi Analysis: result 1; result 2; result 3; mean versus RS; FT; FOT; FOP

Predicted values

S/N Ratio   Mean   StDev Ln(StDev)
 9,03241 4207,08 1036,78   7,29793

Factor levels for predictions

  RS   FT   FOT FOP
8000 1200 2500   6

 Taguchi Analysis: result 1; result 2; result 3; mean versus RS; FT; FOT; FOP

Predicted values

S/N Ratio   Mean   StDev Ln(StDev)
 27,1810 4229,17 109,112   5,20856

Factor levels for predictions

  RS   FT   FOT FOP
10000 1700 1850   8

Taguchi Analysis: result 1; result 2; result 3; mean versus RS; FT; FOT; FOP

Predicted values

S/N Ratio   Mean   StDev Ln(StDev)
 28,2771 4876,25 188,033   5,23662

Factor levels for predictions

   RS   FT   FOT FOP
10000 700 1850   8

 Taguchi Analysis: result 1; result 2; result 3; mean versus RS; FT; FOT; FOP

Predicted values

S/N Ratio   Mean   StDev Ln(StDev)
 28,2771 4876,25 188,033   5,23662

Factor levels for predictions

   RS   FT   FOT FOP
10000 700 1850   8

 Taguchi Analysis: result 1; result 2; result 3; mean versus RS; FT; FOT; FOP

Predicted values

S/N Ratio   Mean   StDev Ln(StDev)
 9,03241 4207,08 1036,78   7,29793

Factor levels for predictions

  RS   FT   FOT FOP
8000 1200 2500   6

 ————— **1/15/2012 8:28:11 PM** ——————————————————

Welcome to Minitab, press F1 for help.
Retrieving project from file: 'C:\USERS\LUCKYLUKE\DESKTOP\TAGUCHI\TAGUCHI
EXPORT\EXPERIMENTS LAP SHEAR.MPJ'

Taguchi Analysis: mean versus RS, FT, FOT, FOP

Linear Model Analysis: Means versus RS, FT, FOT, FOP

Estimated Model Coefficients for Means

Term   Coef

Constant 4255.56
RS 8000   -322.22
RS 10000   44.44
FT 700   344.44
FT 1200   111.11
FOT 1200 -422.22
FOT 1850   377.78
FOP 6   -55.56
FOP 7   77.78

S = *

Analysis of Variance for Means

Source	DF	Seq SS	Adj SS	Adj MS	F	P
RS	2	548889	548889	274444	*	*
FT	2	1015556	1015556	507778	*	*
FOT	2	968889	968889	484444	*	*
FOP	2	28889	28889	14444	*	*
Residual Error	0	*	*	*		
Total	8	2562222				

Response Table for Signal to Noise Ratios
Larger is better

Level	RS	FT	FOT	FOP
1	71.85	73.18	71.65	72.44
2	72.58	72.80	73.30	72.64
3	73.10	71.54	72.58	72.44
Delta	1.26	1.64	1.66	0.20
Rank	3	2	1	4

Response Table for Means

Level	RS	FT	FOT	FOP
1	3933	4600	3833	4200
2	4300	4367	4633	4333
3	4533	3800	4300	4233
Delta	600	800	800	133
Rank	3	1	2	4

Main Effects Plot for Means

Main Effects Plot for SN ratios

* NOTE * Could not graph the specified residual type because MSE = 0 or the
       degrees of freedom for error = 0.

Appendix 6:

Pultruded GFRP bridge decks

FBD600 ASSET bridge deck (produced by Fiberline Composites A/S [3])

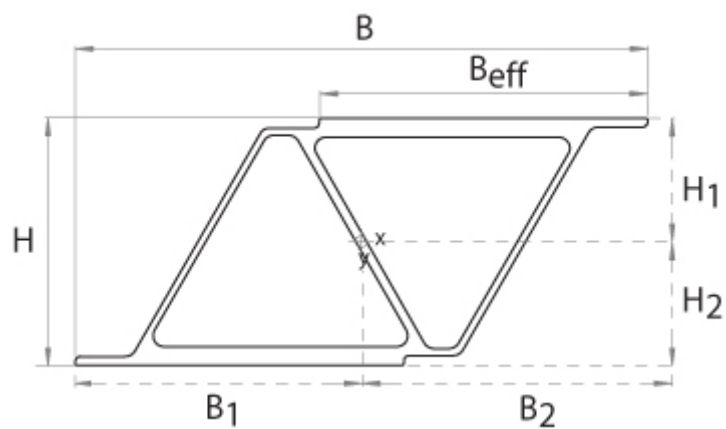Figure A.18 – unit of the ASSET bridge deck

H	225 mm
B	521 mm
B_{eff}	299 mm
B_1	260,5 mm
B_2	260,5 mm
H_1	112,5 mm
H_2	112,5 mm
A	15644 mm²

I_x	$125,4 \cdot 10^6 \, mm^4$
W_x	$1114 \cdot 10^3 \, mm^3$
I_y	$228,8 \cdot 10^6 \, mm^4$
W_y	$87 \cdot 10^3 \, mm^3$
$E_{0°}$	$20 \cdot 10^3 \, MPa$
Weight	103690 g/m²

The ASSET bridge deck profile is typically for bridges subjected to heavy loads and is conform to the Eurocode 1, EN 1991-2-1 and can be used in accordance to the standard's load classes [3].

Appendix 7:

Testing curves for the conducted T-pull tests
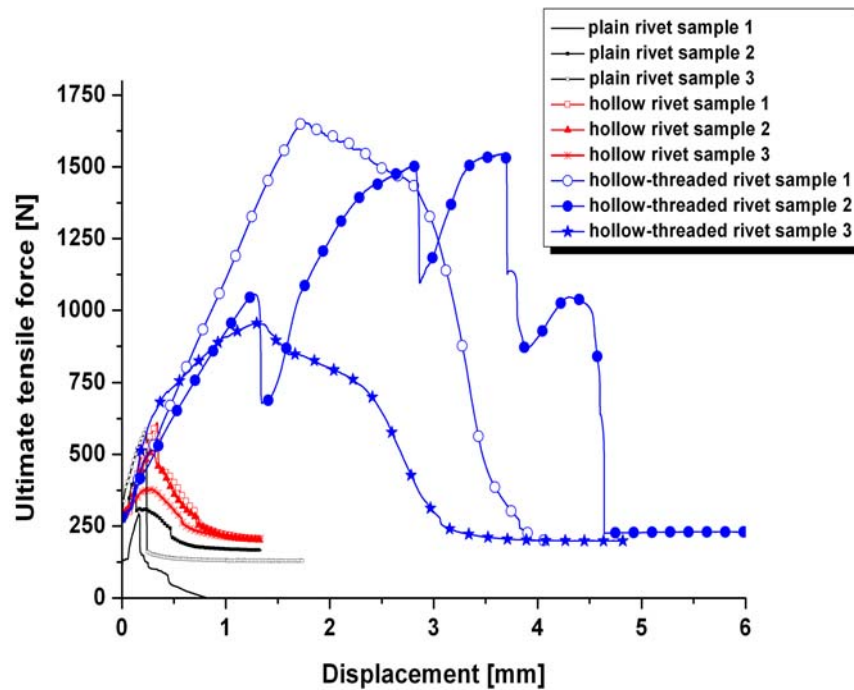
Figure A.19 – Tensile force-displacement curves for the T-pull specimens tested on PEI-GF/AA 2024
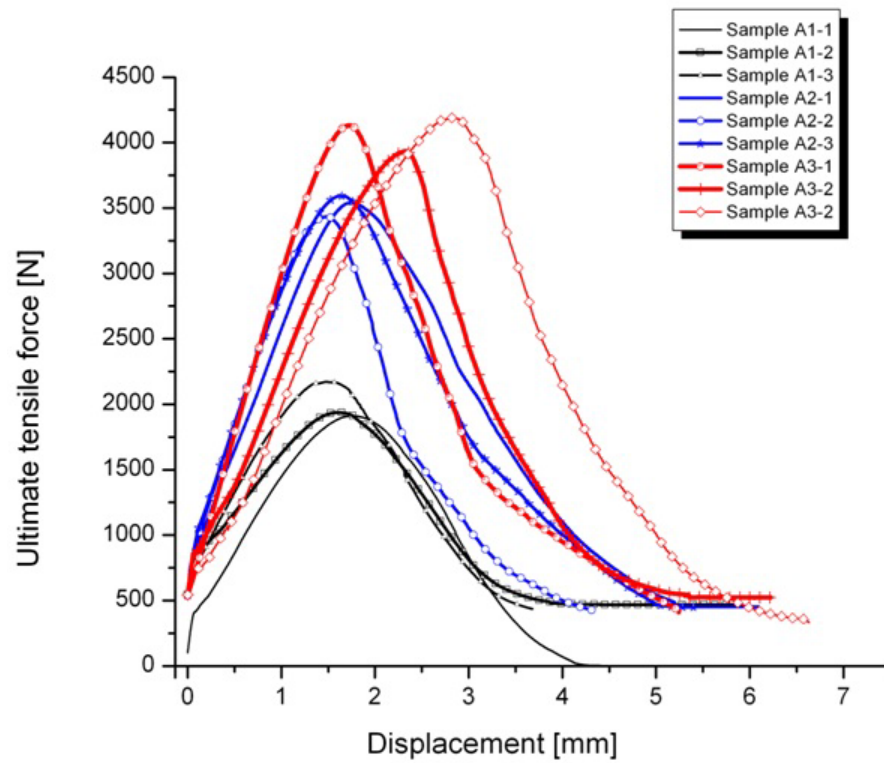
Figure A.20 – Tensile force-displacement curves for the T-pull specimens
tested on PEI-GF/Ti gr.2

Appendix 8:

Calculated values for Aspect Ratios (AR) and Volumetric Ratios (VR)

Specimen	H [mm]	W [mm]	AR [a.u.]	VR [a.u.]
PEI-GF/AA 2024 plain rivet	2,85	7,81	0,36	0,20
PEI-GF/AA 2024 hollow rivet	2,78	9,50	0,29	0,25
PEI-GF/AA 2024 hollow-threaded rivet	4,21	7,89	0,53	0,50
PEI-GF/Ti gr.2 A1	3,90	5,15	0,75	0,04
PEI-GF/Ti gr.2 A2	3,80	5,75	0,66	0,19
PEI-GF/Ti gr.2 A3	3,30	6,00	0,55	0,26

Appendix 9:

Microstructure and geometry of the PEI-GF/Ti Gr.2 M5-threaded rivet specimens
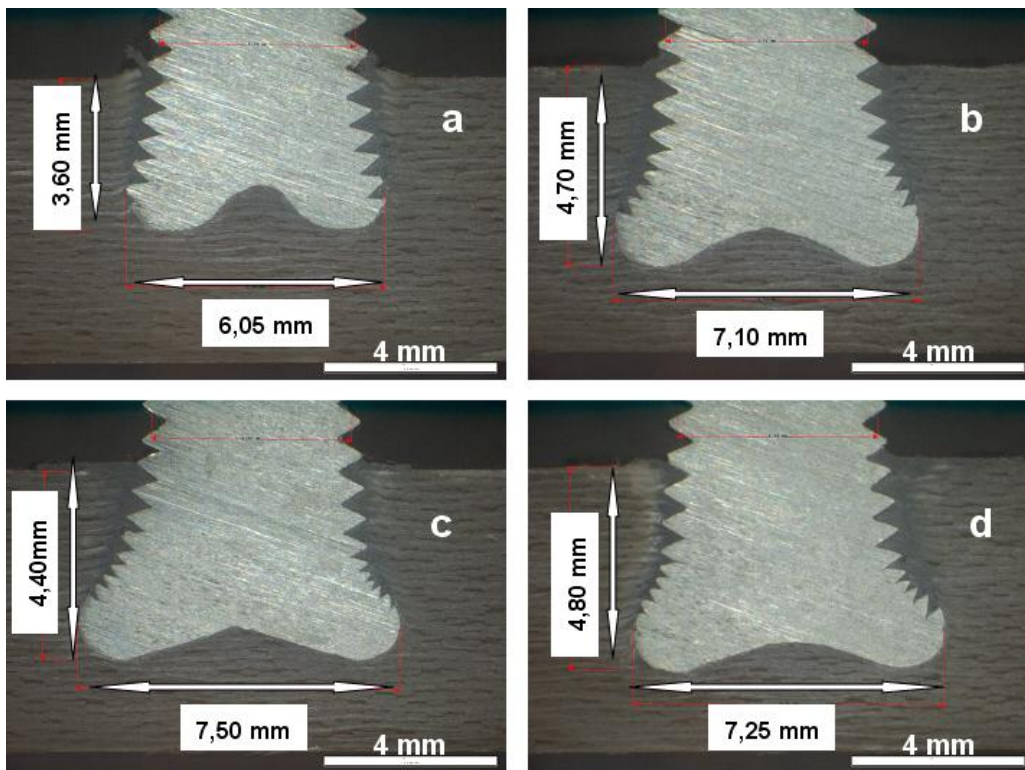
Figure A.21 – Microstructures and anchoring zones for PEI-GF/Ti gr.2 M5 threaded rivets. Conditions with constant RS=10000 rpm, FT=700 ms, FOT=1200 ms, FP=6 bar and variable FOP (a – 6 bar, b – 7 bar, c – 8 bar, d – 9 bar)

Appendix 10:

Tensile test curves for the base materials used in this work
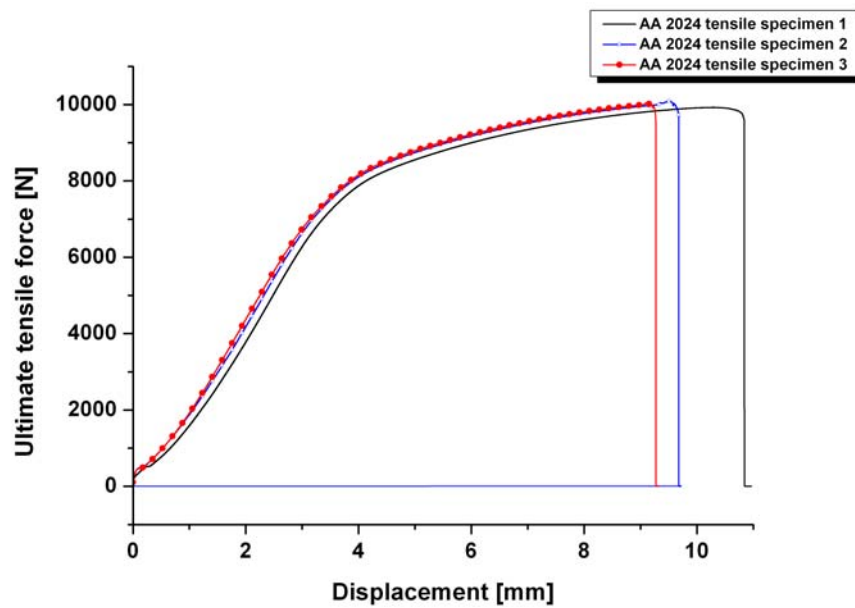
Figure A.22 – Tensile force-displacement curves for AA 2024 rods, tested
according to ASTM E8 / E8M – 11 [100]
(Average ultimate tensile strength 458 MPa ± 12 MPa)
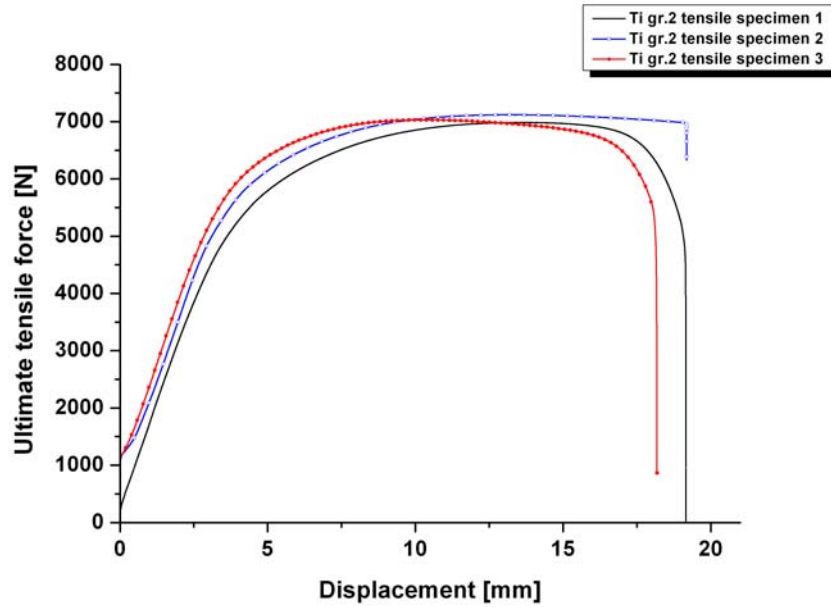
Figure A.23 – Tensile force-displacement curves for Ti gr. 2 rods, tested
according to ASTM E8 / E8M – 11 [100]
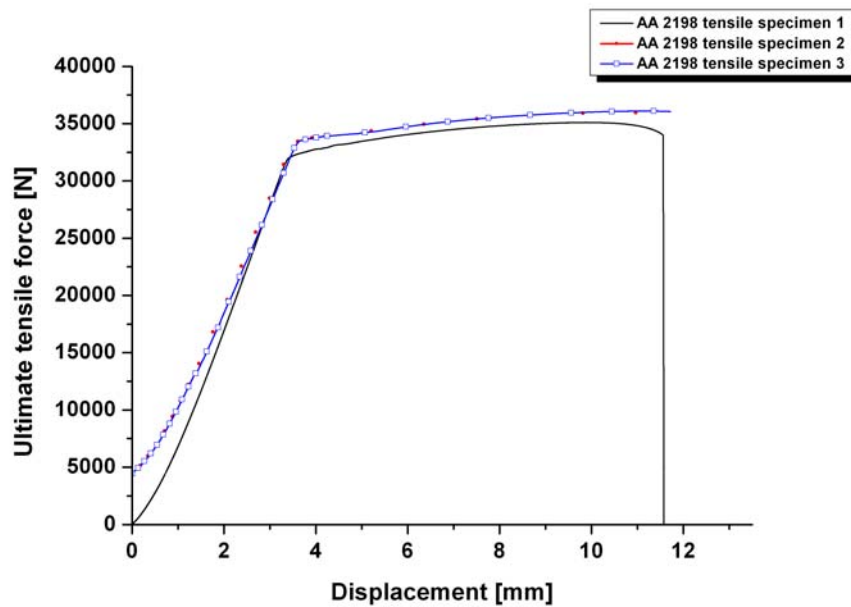(Average ultimate tensile strength 340 MPa ± 14 MPa)

Figure A.24 – Tensile force-displacement curves for AA 2198 plates, tested
according to ASTM E8 / E8M – 11 [100]
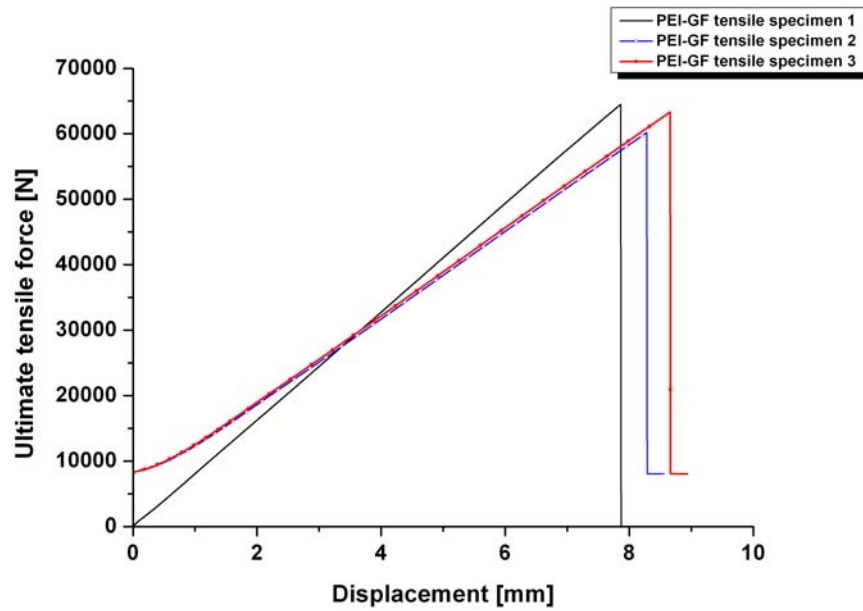(Average ultimate tensile strength 491 MPa ± 3,6 MPa)

Figure A.25 – Tensile force-displacement curves for PEI-GF plates, tested
according to DIN ISO 527-4 [101]
(Average ultimate tensile strength 420 MPa ± 12,1 MPa)

Appendix 11:

Thermograms and peak temperatures of replicated from the DOE conditions
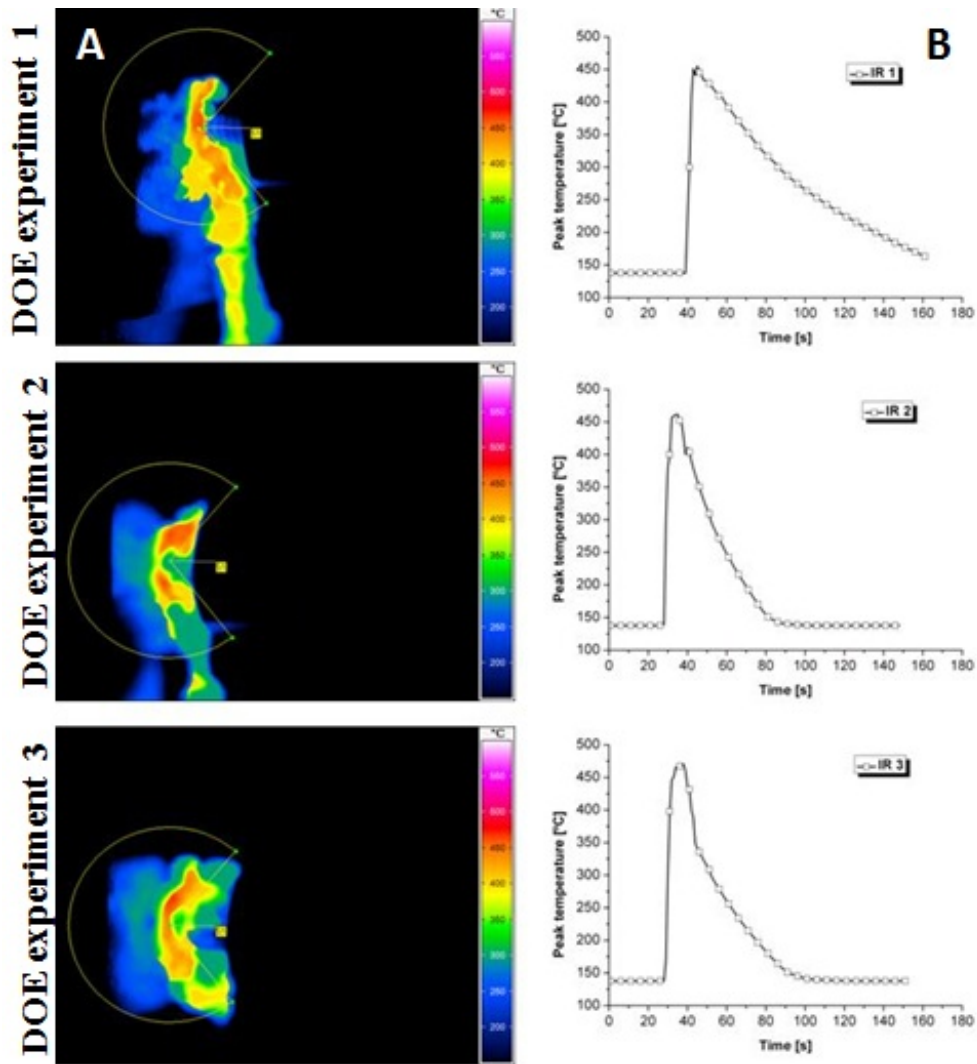

Fig A.26 – Thermograms (A) and showing the temperature of the softened composite flash material being pushed off to the surface and average peak temperatures (B) measured from the semi-circle areas in (A) (replicates of experiments 1-3)
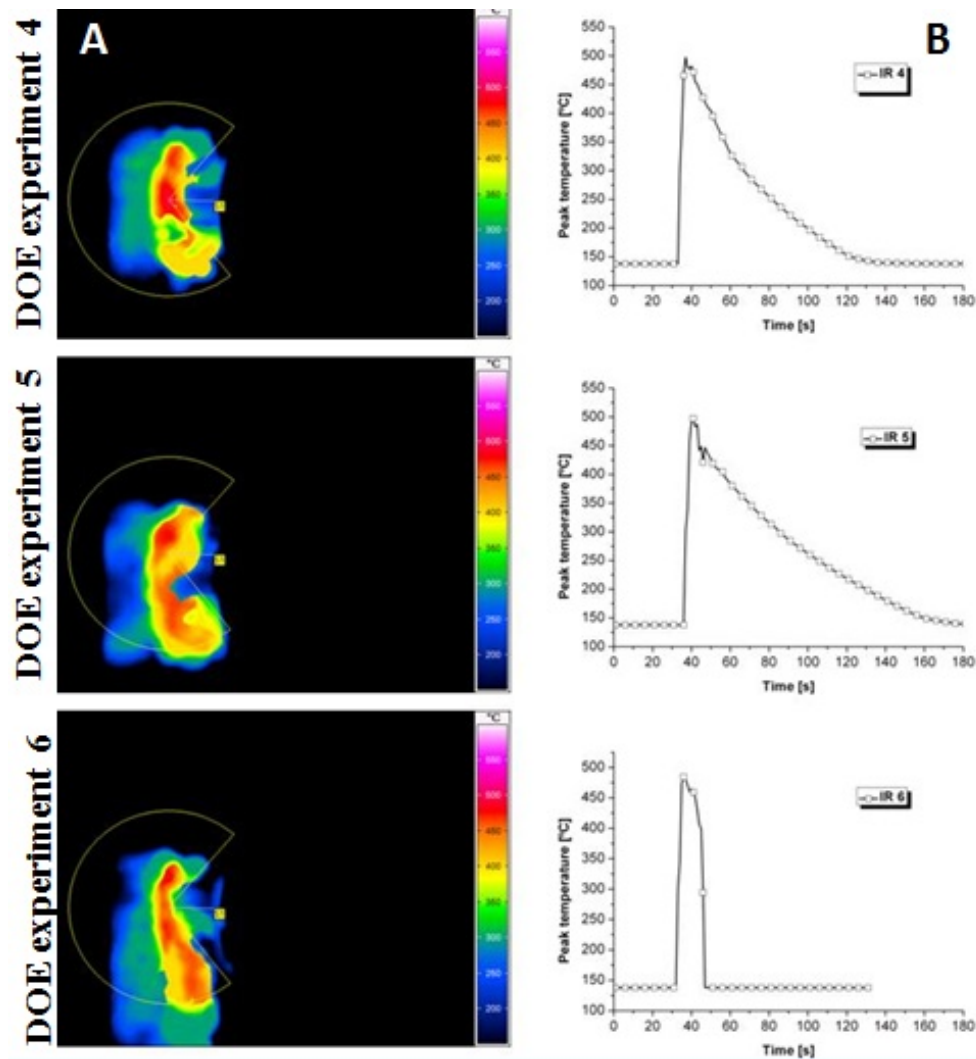
Fig A.27 – Thermograms (A) and showing the temperature of the softened
composite flash material being pushed off to the surface and average peak
temperatures (B) measured from the semi-circle areas in (A)
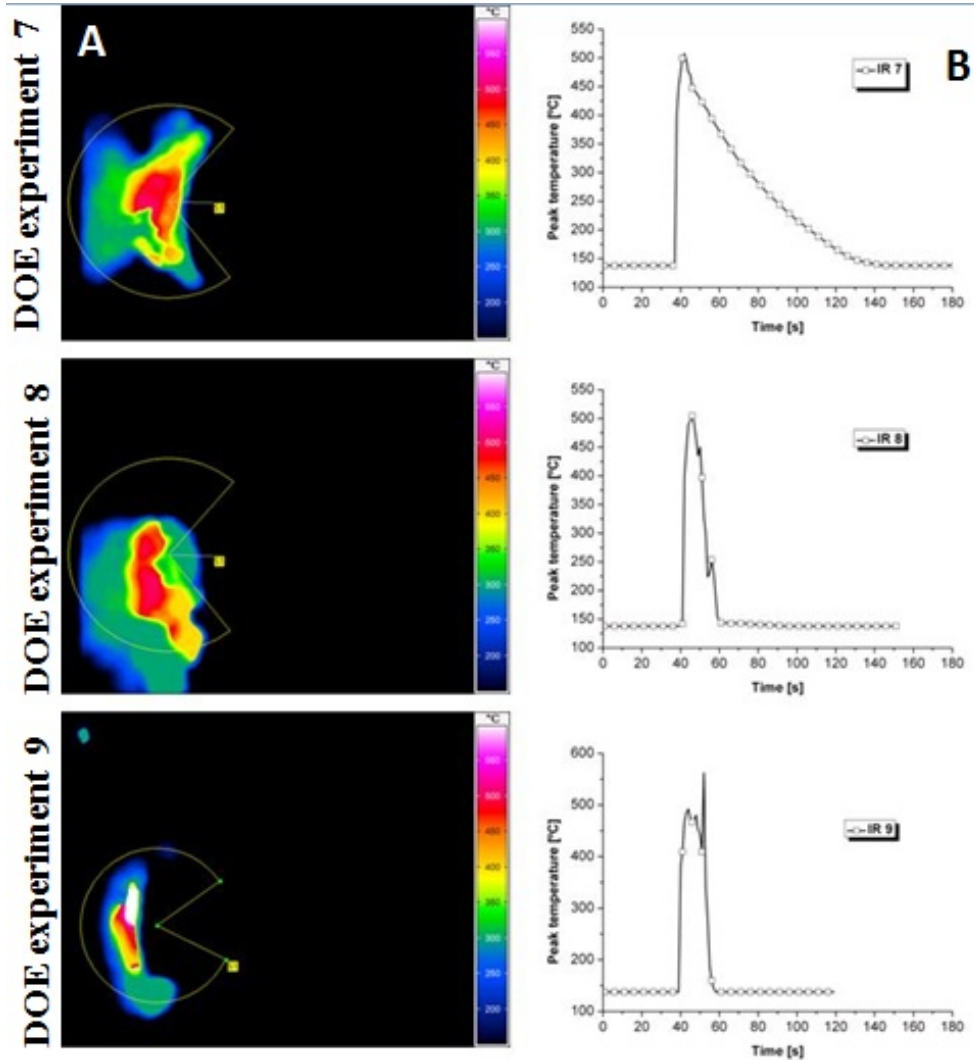(replicates of experiments 4-6)

Fig A.28 – Thermograms (A) and showing the temperature of the softened composite flash material being pushed off to the surface and average peak temperatures (B) measured from the semi-circle areas in (A) (replicates of experiments 7-9)